Journal of Sustainable Bulit Environment

ISSN 2759-7318

Volume 2
Number 2
March 2025

press

https://press.jandoo.ac/journals/jsbe

Journal Statement

1. The opinions expressed in articles published in the *Journal of Sustainable Built Environment (JSBE)* are solely those of the authors and do not necessarily reflect the views of the editorial board or the editorial office.
2. The journal reserves the right to edit and revise submitted manuscripts as necessary. Authors with specific requirements should state them upon submission.
3. *JSBE* supports an Open Access policy, making all articles freely accessible to the public. Users are permitted to read and use the content provided the original authors and source are properly credited, and the content is not used for commercial purposes.
4. The journal holds the exclusive right to publish all accepted articles online. Authors are required to ensure that their submissions are original and not under consideration elsewhere. Any objections to online publication must be stated at the time of submission.
5. *JSBE* is indexed in CrossRef and Google Scholar. All published articles are assigned a unique DOI to facilitate citation and academic dissemination. Authors who do not wish their articles to be indexed should notify the editorial office upon submission.
6. All articles published in the journal require prior authorization from the authors. Reproduction, translation, or compilation of any published content must obtain written permission from both the editorial office and the authors.
7. The journal accepts submissions exclusively through its official website: https://press.jandoo.ac/journal/jsbe. Due to resource constraints, submitted manuscripts will not be returned. If no decision is communicated within three months, authors are free to submit their work elsewhere.
8. *JSBE* promotes academic integrity. Authors are responsible for ensuring the originality and accuracy of their work. Any detected plagiarism or academic misconduct will result in retraction and potential legal consequences.

Volume 2, Number 2 (March 2025)

Contents

Journal of Sustainable Built Environment

https://doi.org/10.70731/rr1d0y93

Differences and Evaluation of the Development of Urban Rail Transit Interchanges in the Perspective of Multi-source Data

Jiahao Wan [a,*], Xiaoyang Guo [a,]

[a] *College of Architecture and Urban Planning, Suzhou University of Science and Technology, Suzhou, China*

KEYWORDS

Multi-Source Data,
Interchanges,
Service Facilities,
Real-Time Population Data

ABSTRACT

With the rapid development of urban rail transport, regional functional differences result in significant variations in service facilities and population growth around stations. A scientific assessment of station development can enhance the comprehensive benefits and sustainability of rail transit systems. Using Suzhou as a case study, this research analyzes the correlation between variables such as service facilities and population distribution utilizing POI data and Baidu heat map data. Interchanges were classified using clustering methods, and specific differences in service facilities among these stations were identified through analysis of variance (ANOVA).

1. Introduction

With the growing demand for convenient transportation and rapid urbanization, urban rail transit (URT) has become increasingly vital in urban development. URT facilitates population movement and regional growth. Despite China's late start in URT development, national policies and large-scale investments have led to significant achievements, with passenger flow surpassing other countries for years. However, high costs and challenges in achieving operational profitability remain. Nonetheless, URT's external benefits drive local economic growth and land use. Scholars have explored ways to balance URT losses through value capture and diversified business models. Classifying URT stations and aligning service facilities with population changes can support effective transit-oriented development (TOD).

Studies confirm URT's strong influence on population concentration and service facility development. A rich variety of service facilities attracts residents, businesses, and enterprises, driving local economic prosperity and enhancing property value. This concentration of services fosters urban expansion and population growth. The rise of urban multi-source data has enabled more precise research on urban environments at finer scales, facilitating real-time studies of URT stations. Research highlights URT's role in urban growth, with population as a key factor reflecting station characteristics. Comprehensive vitality assessments of station areas using multi-source data are essential for optimizing resource allocation and promoting spatial synergy.

This study uses multi-source data (Amap POI and Baidu Heat Maps) to analyze service facilities and real-time population data around Suzhou's URT interchange stations. By exploring the development characteristics and typological differences of these stations, the research aims to support urban development and improve transportation and citizens' quality of life.

2. Research Scope and Data Presentation

2.1. Research Scope

* Corresponding author. E-mail address: 359834709@qq.com

Received 20 November 2024; Received in revised form 14 February 2025; Accepted 14 March 2025; Available online 31 March 2025.

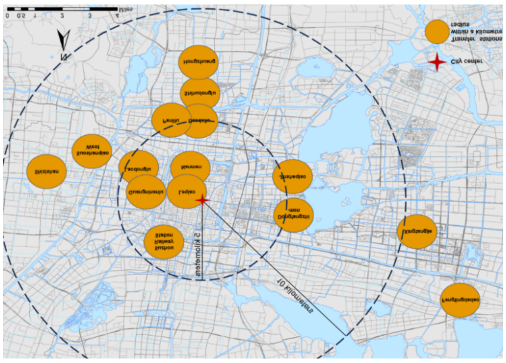

Figure 1 | Diagram of Suzhou Railway Interchanges

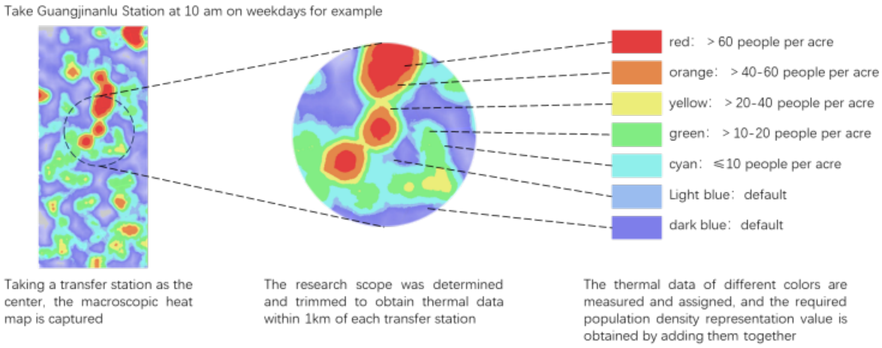

Figure 2 | Heat data extraction process

Suzhou is the first prefecture-level city in China to build and open a URT system. The first rail transit line, Suzhou Rail Transit Line 1, commenced operations on April 28, 2012. By 2023, Suzhou has a total of 7 lines in operation, with 197 stations, including 16 interchange stations. This study focuses on the 1km radius around these interchange stations, representing a 15-minute living circle. The research scope includes 15 interchanges (Figure 1). Huaqiao Station on Line 11 is excluded from the study as it is not under the city's jurisdiction.

2.2. Data Acquisition and Processing

There are three main types of data included in the study to represent the development of interchanges: service facility data, demographic data, and locational planning (Table 1).

The population data were sourced from Baidu Heat Maps and acquired in March and April 2024. Real-time heat maps for each interchange were regularly captured using a mobile phone, and the specific heat data within a 1-kilometer radius were cropped out. The number of pixels in different color classes was then calculated separately, and population values were assigned based on these color classes (Figure 2). The population data were categorized into two types: weekdays and weekends, covering the period from 6:00 to 23:00. By averaging the data from multiple weekdays and weekends, the specific population changes for each period were determined (Figure 3).

The service facility data were obtained from amap POIs on April 9, 2024. Based on the Urban Residential Code Design Standards and considering the availability and practicality of the data, the POI data were classified into 10 categories of facilities: automobile repair-related services, food and beverage services, shopping services, living services, sports and recreation, health care, governmental

Table 1 | Specific variables and data acquisition methods

Typology	Specific variables	Sources of data
Population data	Total population (S_A)	Sum of real-time headcount by time period
	Real-time population peaks (S_{MAX})	Maximum real-time headcount from 6-23 p.m.
	Population fluctuation (σ_n)	Standard deviation of real-time population
Planning condition	Interchange completion time (T)	Official operating time of the line
	Entrances and exits (W)	Number of entrances/exits in amap
	Distance from the city center (D)	Straight-line distance from the interchange site to the city center
Service facilities	Auto Service (K_1), Food & Beverages (K_2), Shopping (K_3), Daily Life Service (K_4), Sports & Recreation (K_5), Medical Service (K_6), Governmental Organization & Social Group (K_7), Science/Culture & Education Service (K_8), Transportation Service (K_9), Finance & Insurance Service (K_{10}), Total Services and Facilities (K_A)	Number of pois within 1km of the interchange
	Service facility imbalance (H)	Information entropy of different services in the vicinity of the interchange

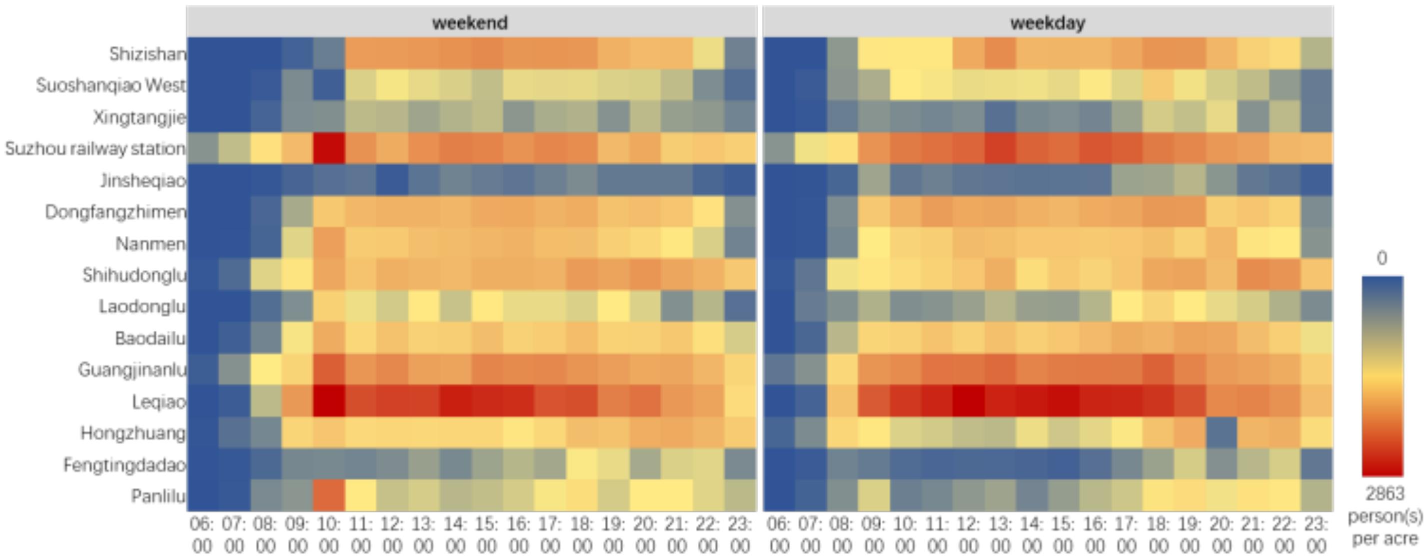

Figure 3 | Real-time population of the interchanges at different times of the day

institutions, science, education and culture, transportation, and financial and insurance services. The KEY was acquired through the amap Open Platform's WEB service, and the POI data within a 1km radius of each interchange were further retrieved using Python, resulting in a total of 32,037 nodes.

2.3. Research Indicators

Several specific variables are selected for this study. S_A represents the total population in one day at the interchange, which is obtained by summing up the real-time population (S_i) ross the 18 study periods at the interchange. S_i is derived by multiplying the number of color pixels (A_{color}) in different study periods by the weights of the corresponding colors. This study focuses on a relatively active population, so only the color range from red to cyan is selected, and the minimum weight value is used:

$$S_i = 60A_{red} + 40A_{orange} + 20A_{yellow} + 10A_{green} + A_{cyan}$$

The population fluctuation (σ_n) is used to measure the daily population activity at different interchanges. A larger value indicates a higher level of population vitality at the interchange on that day. σ_n is the standard deviation of the real-time population (S_i), where $\bar{S}$ is the average real-time population at the interchange for a single day. The calculation formula is as follows:

$$\sigma_n = \sqrt{\frac{\sum_{i=6}^{23}\left(S_i - \bar{S}\right)^2}{18}}$$

Service facility imbalance (H) represents the degree of disarray in the number of various service facilities around the interchange. A higher value indicates a greater imbalance among different types of service facilities. H is the information entropy of different types of service facilities, where P_{K_i} represents the overall proportion of a certain type of service facility. The calculation formula is as follows:

$$H = -\sum_{i=1}^{10} P_{K_i} \log_2 P_{K_i}$$

3. Analysis of Data Results

The study first used SPSS to process and analyze the data, explored the correlation relationship between various variables through correlation analysis, found a more stable and conducive to explaining the developmental differences in the variable groups, and then further carried out clustering and analysis of variance (ANOVA). On this basis, the data were imported into ArcMap, and the spatial distribution of the variables was combined to obtain the developmental differences of each site.

3.1. Correlation Analysis

Correlating the specific variables of the interchange (Table 2), it can be observed that the total service facilities (K_A) show a highly stable positive correlation with the total population (S_A), the real-time population peak (K_{MAX}), and the population fluctuation (σ_n), (p-values$<$0.1). This suggests that an abundance of service facilities positively impacts the mobility of the population around the interchange. Simultaneously, active demographic changes prompt the presence of a considerable number of service facilities. Although further research is needed to analyze the influence mechanism between these two factors, their relationship is notably close at the macro level.

Additionally, the total population (S_A), the real-time population peak (S_{MAX}), and the population fluctuation (σ_n) on weekdays and weekends are all negatively correlated with

Table 2 I Correlation and significance between different variables

r \ p	Total Services and Facilities (K_A)	Service facility imbalance (H)	Weekday: Total population (S_A)	Weekday: Real-time population peaks (S_{MAX})	Weekday: Population fluctuation (σ_n)	Weekend: Total population (S_A)	Weekend: Real-time population peaks (S_{MAX})	Weekend: Population fluctuation (σ_n)	Distance from the city center (D)	Interchange completion time (T)	Entrances and exits (W)
Total Services and Facilities (K_A)		0.889**	0.760**	0.802**	0.747**	0.777**	0.787**	0.690**	-0.703**	0.565*	0.5
Service facility imbalance (H)	0		0.600*	0.564*	0.561*	0.579*	0.566*	0.569*	-0.750**	0.499	0.575*
weekday: Total population (S_A)	0.001	0.018							-0.658**	0.549*	0.246
weekday: Real-time population peaks (S_{MAX})	0	0.028							-0.586*	0.518*	0.323
weekday: Population fluctuation (σ_n)	0.001	0.03							-0.629*	0.535*	0.21
weekend: Total population (S_A)	0.001	0.024							-0.592*	0.556*	0.255
weekend: Real-time population peaks (S_{MAX})	0	0.028							-0.582*	0.572*	0.49
weekend: Population fluctuation (σ_n)	0.004	0.027							-0.628*	0.556*	0.408
Distance from the city center (D)	0.003	0.001	0.008	0.022	0.012	0.02	0.023	0.012		-0.336	-0.34
Interchange completion time (T)	0.028	0.058	0.034	0.048	0.04	0.031	0.026	0.031	0.221		0.397
Entrances and exits (W)	0.058	0.025	0.377	0.24	0.453	0.359	0.063	0.131	0.215	0.142	

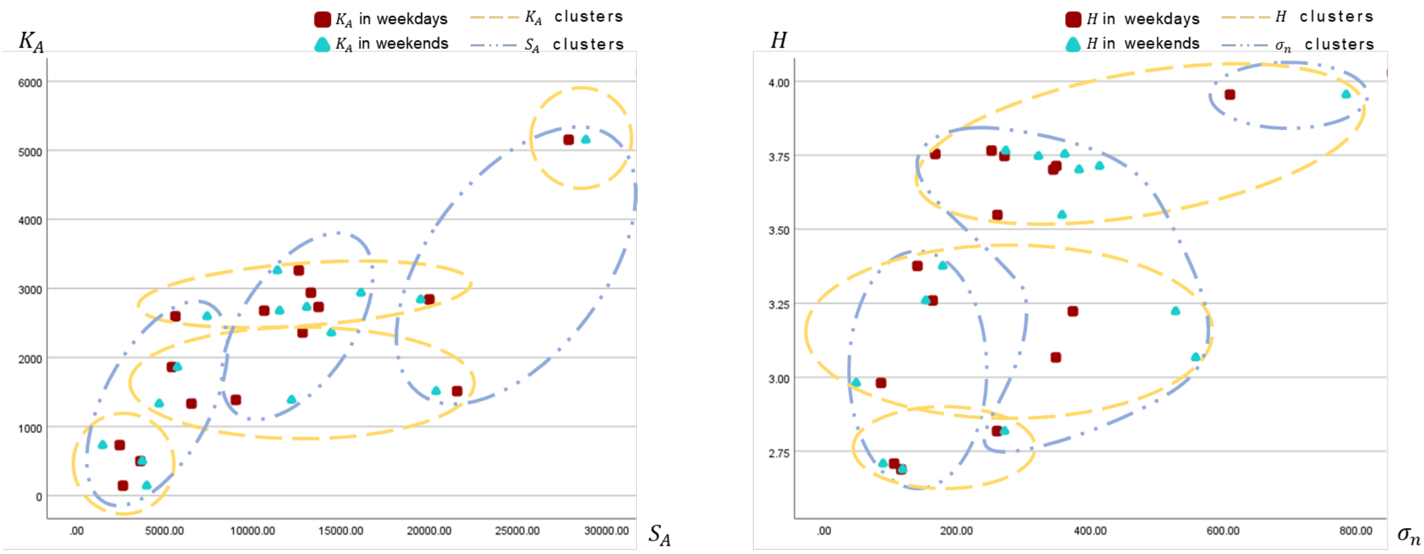

Figure 4

the distance from the city center (D). This partly reflects that interchanges farther from the city center have lower total population, less vigorous surrounding populations, and lower single-day real-time headcount maxima. The imbalance of service facilities (H) and the distance (D) from the interchange to the city center show a high negative correlation, indicating that the closer the interchange is to the city center, the more imbalanced the distribution of various types of service facilities. Conversely, the further the station is from the city center, the more balanced the distribution of service facilities.

It is worth noting that there is a strong positive correlation between the total service facilities (K_A) and the imbalance of service facilities (H) (p=0.000009 < 0.01). This also indicates that the higher the total number of service facilities around the interchange, the more serious the imbalance in service facility types. Combined with the distance to the city center (D), the closer the station is to the city center, the greater the number of service facilities, and consequently, the greater the imbalance in the types.

By transforming the above variables into scatterplots (Figure 4), it can be observed that the points display a basic linear distribution. However, due to the scattered nature of the distribution, it is difficult to draw clear and intuitive conclusions from the scatterplots alone. To more accurately and visually interpret their correlations, further cluster analysis is necessary to identify the specific differences among the relevant variables.

3.2. Cluster Analysis

Given that this study is based on big data, it continues to examine population dynamics and service facilities. Four

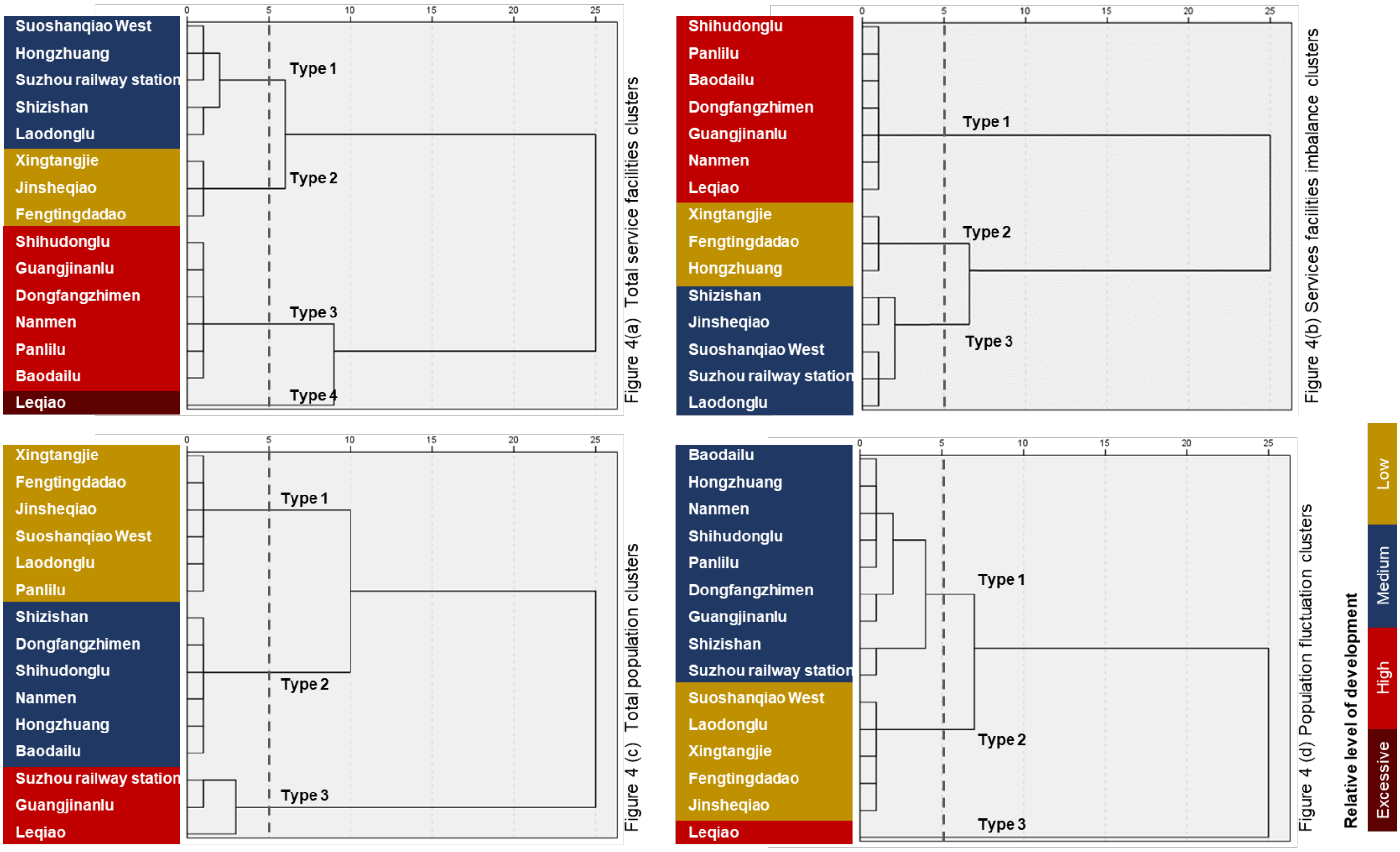

Figure 5 | Cluster analysis of S_A, σ_n, K_A and H

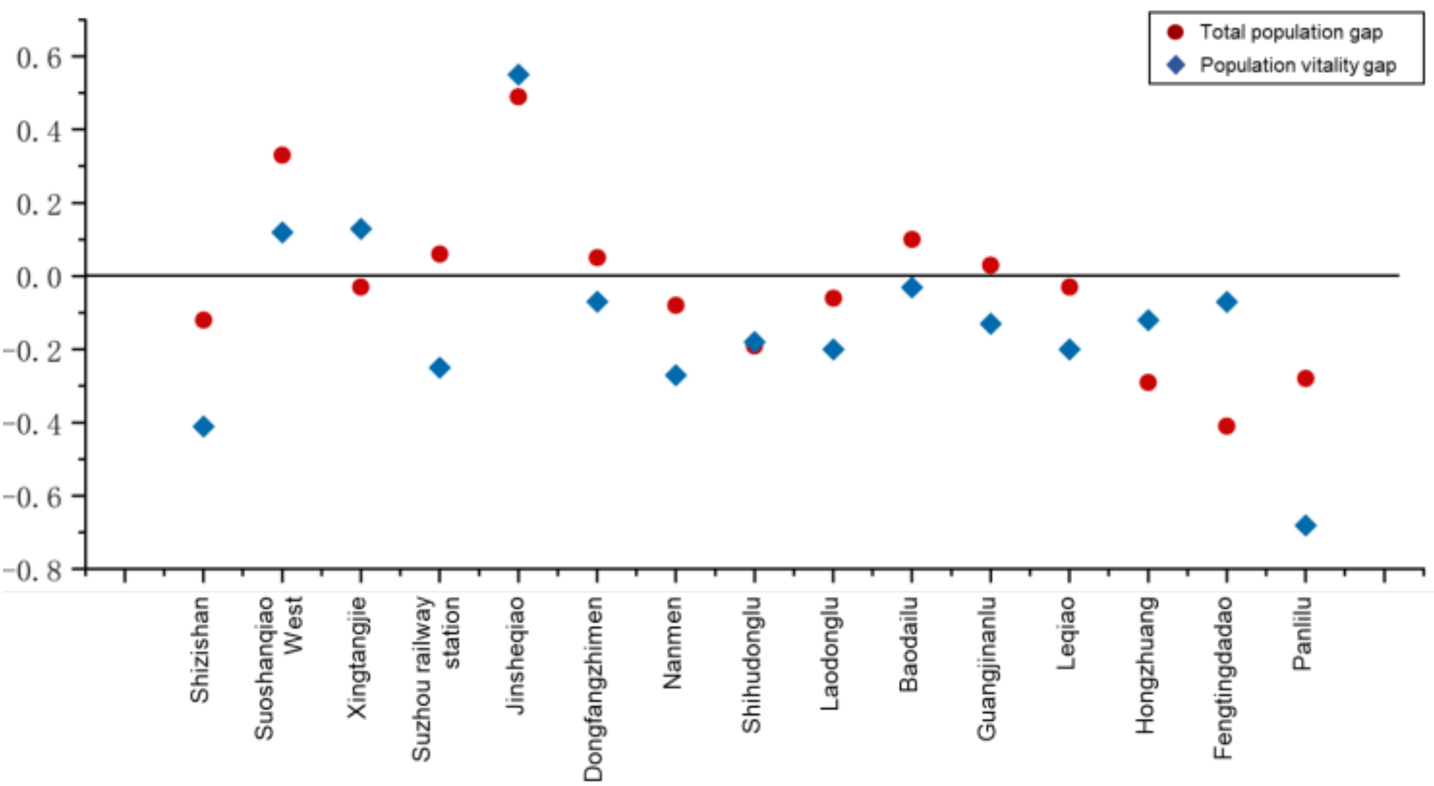

Figure 6 | Gap in total population and population vitality on weekdays and weekends

variables S_A, σ_n, K_A and H —are categorized and summarized to reveal the basic characteristics and differences in the development of interchanges. Using systematic clustering in SPSS, 15 interchanges were analyzed based on these 4 variables. The clustering method used was Wald's method, with the measurement interval being the squared Euclidean distance. Based on the clustering results, the different interchanges were classified into 2 to 8 categories. To compare the relative levels of these interchanges, the results of 3-4 categories were selected for comparative analysis (Figure 5).

Since the total population clusters on weekdays and weekends are similar, but considering the differences in their specific conditions, the gap situation is further plotted (Figure 6) to analyze the population characteristics of the interchanges in more detail. The specific calculation method for the gap situation involves the difference between weekday and weekend data. A positive difference indicates stronger population data on weekdays than on weekends, and vice versa. This difference is then divided by the average population data of the two periods to get the specific fallout of the total population at various interchanges. The circle represents the total population gap, and the diamond represents the difference in the population vitality gap.

In terms of K_A clusters, Type 3 has the largest share, with the total service facilities around its interchanges ranging between 2500 and 3500, symbolizing that these interchanges are at a relatively mature level of development, marked High. Additionally, since the total number of service facilities in Type 4 (Leqiao station) is significantly higher than the other types, it is classified as a separate category, indicating that its service facility situation is at an over-saturated development level compared to other interchanges, marked Excessive. Regarding H clusters, Type 1 > Type 3 > Type 2, are characterized as severe imbalance, moderate imbalance, and slight imbalance respectively. Most interchanges experience severe imbalance and combined with the total number of service facilities, there are significant developmental differences in service facilities among different interchange stations. The reasons for this imbalance will be further analyzed in the following section.

In terms of S_A clusters, Type 1 and Type 2 have the same number and both account for the largest proportion of the clusters. This indicates that the total population at most of the interchanges is small-sized (1469-7383) and medium-sized (9011-16093), with only three interchanges having a large-sized population (20345-28824). Figure 6 shows that the number of positive and negative values in the total population gap is approximately the same, and most of the absolute values of the gap are between 0 and 0.2. This indicates that the total population at these interchanges is relatively stable on weekdays and weekends. However, there are also cases with significant differences, such as Fengtingdadao station and Jinsheqiao station, which are -0.41 and 0.49 respectively. It shows that the difference in total population between weekdays and weekends is prominent, with people tending to gather at Fengtingdadao station on weekends and at Jinsheqiao station on weekdays. Combined with the real-time population data in Fig. 2, most of the interchanges in Type 1 show a high concentration of population during weekdays only during commuting hours, indicating that the main function of these interchanges is oriented towards daily commuting. Type 2 and Type 3 have significant population concentration throughout the day, indicating that these interchanges not only serve daily commuting but also accommodate various functions such as commerce and culture.

In terms of S_A clusters, Type 2 has the lowest population volatility, suggesting that these interchanges have a less vibrant population profile. Type 1, which is the most numerous, has moderate population volatility, indicating

Table 3 | Relative development and characteristics of different interchanges

Interchange \ Level \ Factor	Total service facilities K_A	Service facility imbalance H	Total population S_A	Total population gap ΔS_A	Population fluctuation σ_n	Population fluctuation gap $\Delta\sigma_n$	Distance from the city center D
Xingtangjie	Low	Low	Low	Negative	Low	Positive	11.3
Fengtingdadao	Low	Low	Low	Negative	Low	Negative	14.4
Jinsheqiao	Low	Medium	Low	Positive	Low	Positive	5.2
Laodonglu	Medium	Medium	Low	Negative	Low	Negative	3.7
Suoshanqiao west	Medium	Medium	Low	Positive	Low	Positive	6.1
Hongzhuang	Medium	Low	Medium	Negative	Medium	Negative	8.4
Shizishan	Medium	Medium	Medium	Negative	Medium	Negative	7.6
Suzhou railway station	Medium	Medium	High	Positive	Medium	Negative	2.5
Panlilu	High	High	Low	Negative	Medium	Positive	5.3
Dongfangzhimen	High	High	Medium	Positive	Medium	Negative	5
Nanmen	High	High	Medium	Negative	Medium	Negative	2.3
Shihudonglu	High	High	Medium	Negative	Medium	Negative	6.5
Baodailu	High	High	Medium	Positive	Medium	Negative	5
Guangjinanlu	High	High	High	Positive	Medium	Negative	2.6
Leqiao	Excessive	High	High	Negative	High	Negative	0.7

more distinct changes in real-time headcount. Additionally, there is only one interchange in Type 3, Leqiao station, which has the highest population volatility and the most dramatic population fluctuations. Combined with the data in Figure 2, it can be seen that the population build-up at Leqiao station becomes progressively more pronounced from 9:00 a.m. to 11:00 p.m. This suggests that Leqiao station is the most prominent in terms of demographic factors. It not only has high-intensity population activity values but also a stable continuation of population activity. This, to some extent, explains the excessive level of development in terms of the number of service facilities. The data in Figure 6 reflects the difference in population volatility between weekdays and weekends. Most interchanges have negative population gap values, indicating a higher intensity of population activity on weekends than on weekdays. For example, at Panlilu station, population activity from 10 a.m. to 10 p.m. on weekends is consistently high, while on weekdays from 10 a.m. to 3 p.m., there is less activity around the site, suggesting that people are more inclined to visit this interchange on weekends.

The above analysis provides the specific development differences for each interchange site (Table 3).

3.3. One-Way Analysis of Variance Analysis

The total service facilities and the total population can summarize the basic reasons for the differences in the development of interchanges, so the one-way analysis of variance analysis (ANOVA) was continued based on these two clusters to analyze the specific reasons for each of them to cause significant differences in the occurrence of interchanges (Table 4).

No significant between-group differences were shown between each of the above variables. In K_A clusters, 7 variables—Food & Beverages (K_2), Shopping (K_3), Daily Life Service (K_4), Sports & Recreation (K_5), Medical Service (K_6), Transportation Service (K_9) and Distance from the city center (D) —showed high significance. These factors are likely crucial in determining the differences in service facilities at interchange sites. Governmental Organization & Social Group (K_7), Science/Culture & Education Service (K_8), and Finance & Insurance Service (K_{10}) also contribute to the classification of the total development type of service facilities. The histogram of facility types (Figure 7) reveals a certain regularity in the proportion of each type of K_A: $K_3 > K_2$ or $K_4 > K_9$. This indicates that differences between various development types are concentrated in these four types of service facilities.

In S_A clusters, only K_2 showed high significance, indicating that Food & Beverages are the most critical among the various service facilities and are the key factor influencing population size changes. Following K_2, K_4, K_5 K_8 and K_9 also impact population growth. However, the surprisingly low significance of shopping services suggests the grow-

Table 4 | One-way ANOVA for K_A and S_A

ANOVA	K_A		S_A	
	F	***P***	***F***	***P***
Auto Service (K_1)	0.980	0.404	0.235	0.794
Food & Beverages (K_2)	8.823	0.004	7.315	0.008
Shopping (K_3)	9.445	0.003	3.050	0.085
Daily Life Service (K_4)	13.513	0.001	4.626	0.032
Sports & Recreation (K_5)	7.840	0.007	5.151	0.024
Medical Service (K_6)	9.615	0.003	1.625	0.237
Governmental Organization & Social Group (K_7)	5.357	0.022	1.579	0.246
Science/Culture & Education Service (K_8)	4.990	0.026	4.838	0.029
Transportation Service (K_9)	23.080	0.000	4.842	0.029
Finance & Insurance Service (K_{10})	4.938	0.027	1.806	0.206
Distance from the city center (D)	12.173	0.001	3.439	0.066
Interchange completion time (T)	1.406	0.283	1.750	0.215
Entrances and exits (W)	3.699	0.056	0.162	0.852

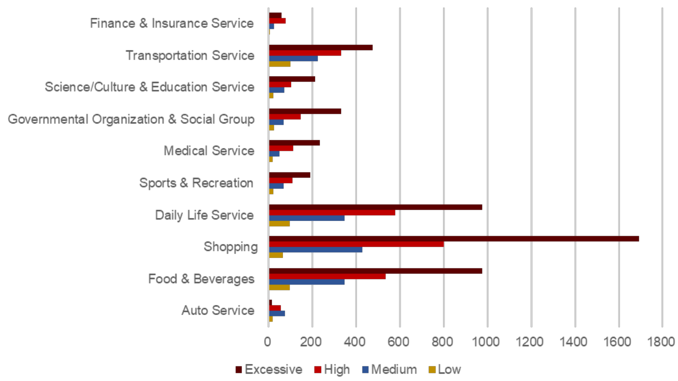

Figure 7 | Number of service facilities in K_A clusters

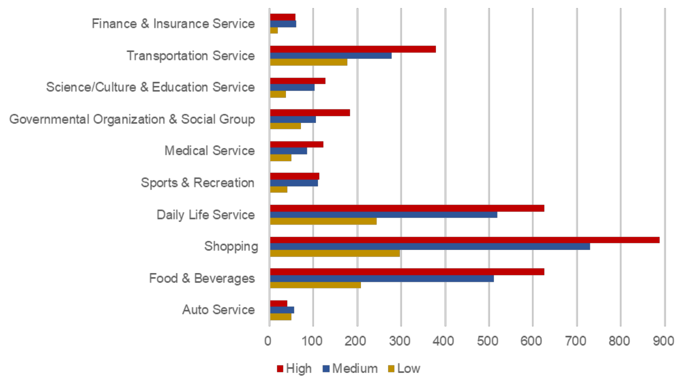

Figure 8 | Number of service facilities in K_A clusters

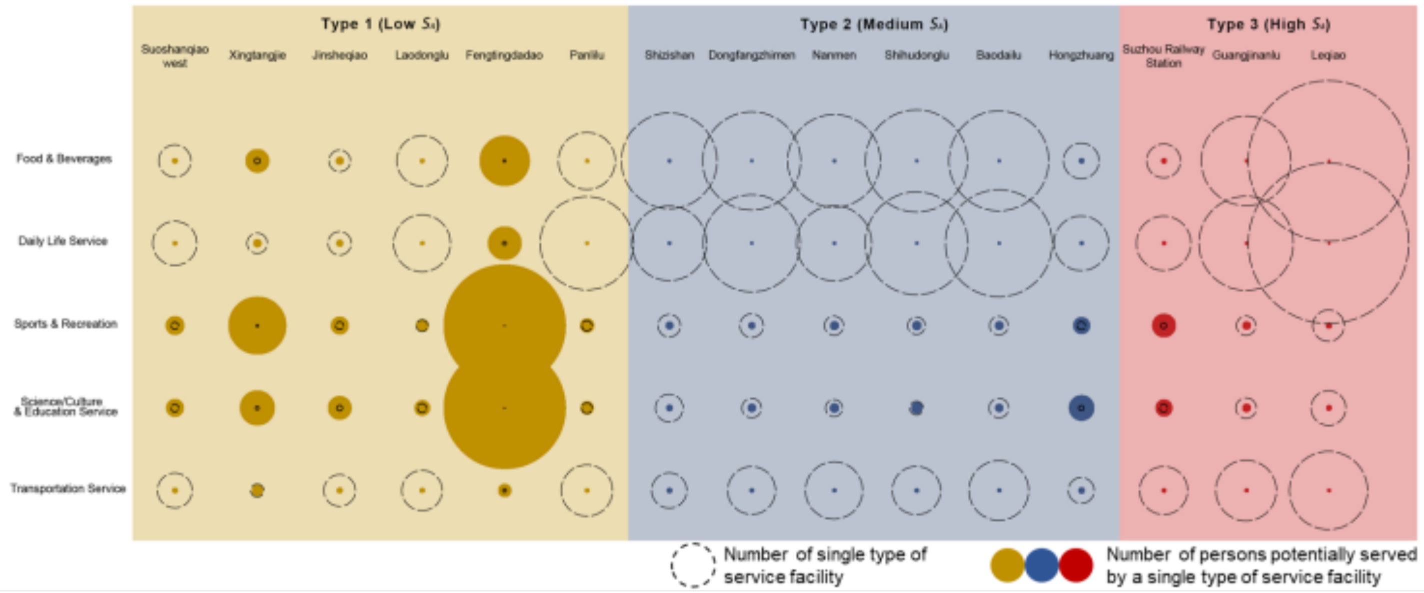

Figure 9 | Number of persons potentially served by a single type of service facility

ing popularity and convenience of online shopping, which reduces people's reliance on physical shopping places. The histogram of facility types (Figure 8) shows a consistent pattern with the previous section: $K_3 > K_2$ or $K_4 > K_9$.

The five service facilities with higher significance in the clusters were further analyzed and combined with the real-time S_{MAX} at their respective interchanges (Figure 2) to determine the specific number of people potentially oriented towards different service facilities at each interchange (Figure 9). In Figure 9, the coil size represents the number of each service facility, while the solid circle size reflects the number of potential users for each facility. Most coils surround the solid circle, indicating that the overall trend of the two is similar. However, in a few cases, the coils are smaller than the solid circles, suggesting that the configuration of the service facilities at these interchange stations is inadequate to meet the needs of the surrounding population, leaving room for further development and utilization. Conversely, if the solid circle is too small within the same type of service facility, it indicates that these facilities are under significant pressure and require better planning to enhance their comprehensive utilization rate.

4. Discussion

This study investigates the differences in development among Suzhou metro interchanges by examining service facilities and population data through multiple data sources. The findings highlight several patterns and relationships.

From the perspective of interrelationships, except for Suzhou Railway Station, there is a clear correlation between S_A and K_A. According to the relative development levels indicated in this study: low S_A - low/mid/high K_A, mid S_A- mid/high K_A, high S_A- high/very high K_A, the relative development level of service facilities is always greater than or equal to the total population. This indicates that the provision of service facilities is generally designed to meet or exceed the needs of the surrounding population, ensuring the functionality and service quality of the interchanges. It also reflects the foresight and redundancy in urban planning and service facility configuration to handle surges in population during holidays. The situation at Suzhou Railway Station is unique due to its dual function as a railway station, leading to an imbalance between service facilities and total pedestrian flow, and hence it is discussed separately.

Regarding σ_n and S_A, interchanges with mediumσ_n typically have medium to high S_A. This suggests that interchanges with medium S_A tend to attract more people. When considering the distance from the city center, Nanmen Station, which is relatively close to the city center, shows a trend of increasing to a high S_A. Similarly, Panlilu Station also exhibits a trend of rising to a medium S_A. In contrast, interchanges with low population volatility may need to develop multi-functional uses to enhance their overall attractiveness and utilization, thereby promoting population gathering and mobility, and driving the overall development of these interchange stations.

Moreover, there is a significant relationship among K_A, H and D. The closer an interchange is to the city center, the more service facilities it has, but also the more imbalanced the distribution of these facilities. In the city center, high population density and demand drive the development of commercial service facilities such as shopping, dining, and living services, while the quantity of other service facilities remains relatively stable, leading to resource over-concentration and supply-demand imbalance. The most typical example is Leqiao Station, where the excessive K_A

results in serious imbalance, leading to high pressure and competitive intensity among service facilities. To address this, government intervention is necessary to guide businesses and investors to build service facilities in peripheral areas, thereby alleviating the high-pressure environment of the city center.

5. Conclusion and Outlook

The development of URT interchanges is influenced by a multitude of factors, and cannot be inferred solely from service facilities and population factors. Land use types, local development policies, and per capita income levels all contribute to the comprehensive development of communities, creating a complex web of influencing factors. However, by combining pedestrian flow and service facility data, it is possible to monitor and track the development status and differences of interchanges in real-time. The study preliminarily demonstrates the potential for establishing a real-time development monitoring system for interchanges through this approach.

In the long run, the sustainable development of URT sites primarily depends on population density and the density of service facilities. High population density areas drive increased demand for commercial, educational, and medical facilities, which in turn fosters the clustering and development of these service facilities. This positive correlation ensures that the area surrounding a rail transit station is well-supported and functional. Adequate and diverse service facilities meet residents' daily needs, enhance the convenience and comfort of life, and attract more people, creating a virtuous cycle of "attracting population with service facilities." Moreover, the availability and quality of service facilities directly impact the attractiveness and utilization rate of the rail transit station. The richer and more evenly distributed the facilities around the station, the better they can meet diverse needs, increase passenger flow, and enhance the overall efficiency of the rail transit system. This interaction and synergistic development have a far-reaching impact on the sustainable development of cities, maximizing comprehensive benefits.

1. Quan Liu (2018) Indicator control in TOD planning and management. Planners 34(01): 48-58.
2. Wanting Xu, Hongtao Ma, Yi Chen, et al (2018) Exploring the Influencing Factors of Beijing Subway Station Vitality. Beijing Planning Review 3: 40-46.
3. Baoming Han, Yiran Yu, Zhe Xi et al (2024) Statistical Analysis of Urban Rail Transit Operations Worldwide in 2023: A Review. Urban Rapid Rail Transit 37(01), 1-9.
4. Qiannan Wu, Qianwen Li, Sumin Zhang (2023) Analysis of Operating Revenue of Typical Chinese and Foreign Urban Rail Transit Companies. Urban Mass Transit 26(08):123-128. DOI:10.16037/j.1007-869x.2023.08.022.
5. Iseki H (2016) Equity in Regional Public Transit Finance: Tradeoffs Between Social and Geographic Equity. Journal of Urban Planning and Development 142(4):04016010.
6. Meyer J. R., Kain J. F., Wohl M (2013) The Urban Transportation Problem. Harvard University Press, Cambridge, MA.
7. Keeler T. E., Small K (1975) The Full Costs of Urban Tranport, Part III: Automobile Costs and Final Intermodal Cost Comparisons. University of California, Berkeley.
8. Merewitz L. A (1975) The Full Costs of Urban Transport, Part II: Marginal Costs of Fixed-Rail Rapid Transit Service in the San Francisco Bay Area. Monograph No. 20. Institute of Urban and Regional Development, University of California, Berkeley.
9. Chomitz K. M., Lave C. A (1984) Part Time Labour, Work Rules, and Urban Transit Costs. Journal of Transport Economics and Policy 18(1):63–73.
10. Anupriya, Daniel J. Graham, Jose M. Carbo, Richard J. Anderson, Prateek Bansal (2020) Understanding the costs of urban rail transport operations. Transportation Research Part B: Methodological 138:292–316.
11. Hong Zhang, Yong Liu, Sanxi Dong (2007) Experiences of Investment/Financing on Metro in Seven World Cities. Urban Mass Transit 10:6-10.
12. David Z.W. Wang, Hong K. L (2016) Financial sustainability of rail transit service: The effect of urban development pattern. Transport Policy 48:23–33
13. Jeffrey R Kenworthy, Felix B Laube (1999) Patterns of automobile dependence in cities: an international overview of key physical and economic dimensions with some implications for urban policy. Transportation Research Part A: Policy and Practice 33(7-8):691–723.
14. Mathur S (2020) Impact of transit stations on house prices across entire price spectrum: a quantile regression approach. Land Use Poicy 99:104828
15. Chao Wang, Hanzhong Zheng, Rui Zhi et al (2021) A Comparative Study on the Diversified Development of Urban Tail Transit Enterprises in China. China Transportation Review 43(01):122-126.
16. Luning Li (2011) On Group Control Mode of Urban Mass Transit Enterprises. Urban Mass Transit 14(07):1-5. DOI:10.16037/j.1007-869x.2011.07.003.
17. Soliz, A., Rodrigue, L., Peaker, C., Bernard, I., El-Geneidy, A (2023) Zoning In on Transit-Oriented Development: Understanding Bylaw Reform as Critical Policy Groundwork. Journal of the American Planning Association 90(2):318–335.
18. Cervero R, Duncan M (2006) Which reduces vehicle travel more: jobs-housing balance or retail-housing mixing. Journal of American Planning Association 72(4):475-490.
19. Isabelle N, Elizabeth C D (2020) Impact of new rail transit stations on neighborhood destination choices and income segregation. Cities 102:102737.
20. Bothe K, Kalsø Hansen H, Winther L (2018) Spatial restructuring and uneven intraurban employment growth in metro- and non-metro-served areas in Copenhagen. Journal of transport geography 70: 21-30.
21. Bhattacharjee S, Goetz A R (2016) The rail transit system and land use change in the Denver metro region. Journal of transport geography 54:440-450.
22. MONHEIM R (1992) Town and transport planning and the development of retail trade in metropolitan areas of West Germany. Landscape and urban planning 22(2-4):121-136.
23. Bollinger C R, Ihlanfeldt K R (1997) The impact of rapid rail transit on economic development: the case of Atlanta's MARTA. Journal of urban economics 42(2):179-204.
24. Hicks M (2006) Transportation and infrastructure, retail clustering, and local public finance: evidence from Wal-Mart's expansion. Regional economic development 2(2):100-114.
25. Buch T, Hamann S, Niebuhr A, et al (2014) What makes cities attractive? The determinants of urban labour migration in Germany. Urban studies 51(9):1960-1978.
26. Jooseok Oh (2020) Residential mobility and quality of life between metropolitan areas: the case of South Korea. Sustainability 12(20):8611.
27. Dongsheng Zhan, Wenzhong Zhang, Li Chen et al (2019) Research progress and its enlightenment of urban public service facilities allocation. Progress in Geography 38(4):506-519.
28. Jian Feng, Yichun Zhong (2020) The spatial structure of urban residents' quality of life in Changzhou based on residential envi-

ronment. Acta Geographica Sinica 75(6):1237-1255.
29. Pengjun Zhao, Nanhui Li, Shengxiao Li (2016) The Impacts of the Built Environment on Residents' Acitivities and Travel Behavior in TOD Areas: A Case Study of Beijing. Urban Development Studies 23(6):45-51.
30. Haixiao Pan, Guowei Chen (2009) Rail Transit and Residential Location Choice. Urban Planning Forum 5:71-76.
31. Ki Chan Chun, Jiwon Bahk, Heeju Kim, Hyeong-Chai Jeong, Gunn Kim (2023) Classification of the metropolitan subway stations and spheres of influence of main commercial areas in Seoul. Physica A: Statistical Mechanics and its Applications 609:128387.
32. Sara Ishaq Mohammad, Daniel J. Graham, Patricia C. Melo (2017) The effect of the Dubai Metro on the value of residential and commercial properties. Journal of Transport and Land Use 10(1):263-290
33. Haixiao Pan, Jing Li, Qing Shen, Cheng Shi (2017) What determines rail transit passenger volume? Implications for transit oriented development planning. Transportation Research Part D: Transport and Environment 57:52-63
34. Curtis C (2008) Evolution of the transit-oriented development model for low-density cities: a case study of perth's new railway corridor. Planning practice & research 23(3):285-302.
35. Long Y (2019) Measuring Human-Scale Urban Form and Its Performance. Landscape and Urban Planning 191(C):103612-103612.
36. Zhongqi Wang, Penglin Li (2023) Study on the relationship between urban rail transit and urban space based on POI data. Journal of Xi'an University of Architecture & Technology (Natural Science Edition) 55(06):834-839. DOI:10.15986/j.1006-7930.2023.06.006.
37. Yuping Cai, Juan Huang, Bingyang Chang et al (2023) Reflections on the Interaction Between Nanjing Rail Transit and Urban Space Development. Urban Rapid Rail Transit 36(04):6-12.
38. Chong Ye, Zhenxiang Ye (2023) New structuring of urban space based on the TOD mode of rail transit. Science & Technology Review 41(24):66-73.
39. Zhou Yufei, Yang Jiawen, Zhou Jiangping et al (2020) Evaluating Vitality of Metro Station Service Area with Heat Map: A Case Study on Shenzhen Subway. Acta Scientiarum Naturalium Universitatis Pekinensis 56(05):875-883. DOI:10.13209/j.0479-8023.2020.054.
40. Xuejun Liu, Tong Wang, Hua Liu et al (2023) Evaluation of TOD Effectiveness in Metro Station Areas Based on Multi-source Data: A Case Study of Wuhan Metro Line 2. Journal of Geomatics 48(02):32-37. DOI:10.14188/j.2095-6045.2022772.
41. Li Wang, Lingling Hu, Xiaoqi Tian (2023) Multidimensional evaluation and spatiotemporal characteristics of metro station domain vitality based on big data: A case study of Xi'an City. Progress in Geography 42(06):1112-1123.
42. Shouhong Xie, Yuemin Ning (2006) Modeling the Spatial Distribution of Urban Population Density and Its Evolution in Guangzhou. Journal of Applied Statistics and Management 5:518-522.
43. Xin Tan, Daquan Huang, Xingshuo Zhao et al (2016) Jobs housing balance based on Baidu thermodynamic diagram. Journal of Beijing Normal University (Natural Science) 52(05):622-627+534. DOI:10.16360/j.cnki.jbnuns.2016.05.015.
44. Hongru He (2023) Research on the innovation spillover effect of industry involution from the perspective of internal circulation-Take scenic spot tourism and hotel business as an example. Journal of Commercial Economics 11:163-166.

Conflicts of Interest The authors declare no conflict of interest.

Journal of Sustainable Built Environment

https://doi.org/10.70731/x28qjg16

Distribution Characteristics and Disaster Risks of Ancient Opera Stages in Hunan Province

Jing Chen [a], Ran Peng [a,*]

[a] *School of Civil Engineering and Architecture, Wuhan Institute of Technology, Wuhan 430074, China.*

KEYWORDS

Ancestral Halls;
Revival;
China;
Eastern Hubei;
Rural Areas

ABSTRACT

Focusing on 219 existing ancient opera stages in Hunan Province, this study integrates GIS spatial analysis with the AHP-entropy model to examine their spatial distribution and disaster risk characteristics. The findings reveal a generally discrete distribution pattern (R=1.86), with high-density clusters in southern and western Hunan. Spatial evolution follows a temporal sequence, shifting from a southern concentration during the Ming and Qing dynasties to multi-directional expansion in the late Qing and Republic periods. A total of 72 stages are located in key geologic hazard zones, and 169 are threatened by floods, particularly in mountainous and low-lying areas. Based on disaster risk zoning, a hierarchical protection strategy is proposed—emphasizing structural reinforcement and digital monitoring in high-risk areas, and drainage improvements with community participation in secondary zones. The study establishes a “distribution–risk–response” framework, providing a scientific basis for the preventive conservation of traditional opera heritage under climate change.

1. Introduction

The traditional Chinese opera art and its material carrier, the ancient stage, coexist and co- prosperity, forming a unique cultural system of "performance space". Ancient stage is not only a physical place for opera performance, but also an important social space carrier for clan rituals, trade exchanges and folk activities[1]. Its architectural form since the Song and Yuan hook rail tile house to the Ming and Qing ancestral hall playhouse gradually stereotypes, showing a blend of north and south of the regional characteristics[2]. Hunan Province, as the "ancient sound of Jingchu, the source of the southern opera" cultural town, the number of existing ancient stage among the forefront of the country, Xiang Opera, Qiqu Opera, Yang Opera and other local theater and Dong Nuo opera and other ethnic minorities intertwined here, giving birth to the footstool type, wind and rain bridges, and other very characteristic of the regional architectural types of the stage. However, under the double pressure of accelerated urbanization and frequent occurrence of extreme weather, the ancient stage in Hunan is facing multiple threats such as flooding, termite infestation, improper repair, etc., and its protection has become imminent.

Currently, domestic scholars on the study of the ancient theater mostly focus on the architectural form and cultural functions. For example, Zhou Hua bin[3] systematically sorted out the logic of the spatial evolution of theater buildings, and Chen Zhihua[4] revealed the interaction between Huizhou theater and clan society through field research. At the level of regional studies, Xiao Min[5] conducted a typological analysis of the construction techniques of ancient stage in southern Hunan, while Wu Weiguang[6] paid attention to the cultural symbolism of minority stage in western Hunan. While foreign countries pay relatively less attention to folk architecture such as ancient stage, with the globalization trend of cultural heritage protection and disaster risk management, foreign scholars have made some progress

* Corresponding author. E-mail address: pengran@wit.edu.cn

Received 26 February 2025; Received in revised form 18 March 2025; Accepted 24 March 2025; Available online 31 March 2025.

in the protection of traditional architecture, disaster risk assessment and application of spatial information technology, etc. Smith and Brown[7] emphasized the vulnerability of traditional architecture and disaster risk through case studies of traditional architecture in Asia and suggested spatial analysis and risk assessment through GIS technology. Lee and Kim[8] systematically analyzed the spatial distribution characteristics of traditional theaters in East Asia. Johnson and Thompson[9] proposed to realize the dynamic monitoring of disaster risk of traditional buildings through the combination of 3D modeling and GIS, while Chen and Liu[10] evaluated the disaster vulnerability of traditional timber-framed buildings, and Rossi and Bianchi[11] evaluated the disaster vulnerability of traditional wooden buildings. Rossi and Bianchi proposed an integrated assessment method for flood and earthquake disaster risk of cultural heritage, combining historical data with geographic information system (GIS) for disaster vulnerability analysis. it is worth noting that there is a gap in the existing results in the study of the use of spatial information technology to analyze the distribution pattern of the playhouse, and most of the studies are confined to the protection of single building, and lack of a systematic assessment of disaster risk perspective. GIS technology has shown significant advantages in the field of cultural heritage protection in recent years. In recent years, GIS technology has demonstrated significant advantages in the field of cultural heritage protection, such as Zhang Ying [12] revealing the fire risk pattern of ancient buildings in Shanxi through spatial superposition analysis, which is an important reference value for the comprehensive risk assessment of ancient stage.

Hunan Province, the spatial and temporal distribution of the ancient theater profoundly reflects the "by the mountains, along the water, along the stage" of the wisdom of the camp. The Qing Dynasty "Hunan Tongzhi"[13] in "where the town wharf, there must be a theater to gather popularity", Yueyang Zhang Guying village "sunny not exposed to the sun, the rain does not wet shoes" of the gable-type stage, the passage of the Dong village "to sing instead of fighting" drum tower stage, all reflecting the environmental adaptation. The drum tower stage of Dong Village, where songs are sung instead of fighting, reflects the deep integration of environmental adaptability and ethnic culture. However, previous studies have mostly used case descriptions or qualitative generalizations, and have not yet established a quantitative analysis framework based on geographic big data, and even less interdisciplinary exploration of the association between spatial distribution characteristics and disaster vulnerability. In this study, we propose to reveal the spatial clustering pattern of ancient opera houses and their disaster risk classification through GIS spatial analysis and AHP-entropy combination model, aiming to provide a scientific basis for the construction of a "preventive protection" system, which is of double practical significance for the continuation of the cultural genes of Hunan opera houses and meeting the new challenges of cultural heritage protection in the face of climate change. This is of double significance for the continuation of the cultural gene of Hunan opera and the new challenges of cultural heritage protection under climate change.

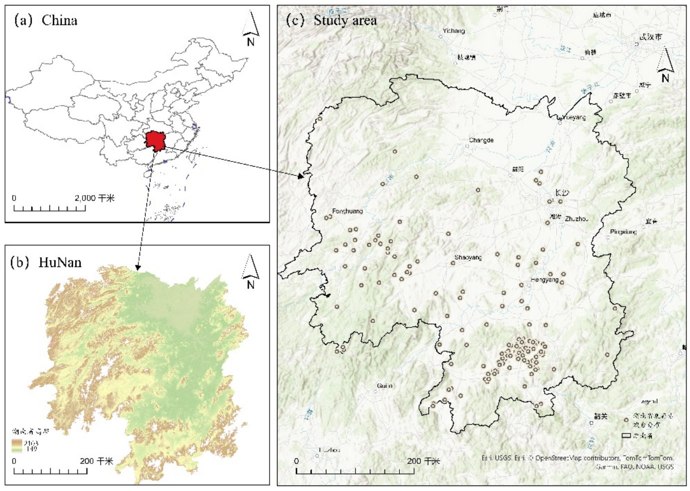

Figure 1 | Overview of the study area

2. Study Area and Data Sources

2.1. Study Area

Hunan Province is located in south-central China, on the south bank of the middle reaches of the Yangtze River, with geographic coordinates between 108°47′ and 114°15′ east longitude and 24°38′ and 30°08′ north latitude, and a total area of 211,800 square kilometers. The province has 13 prefecture-level cities and one autonomous prefecture, with a resident population of about 66 million (2020). Hunan Province is one of the important birthplaces of Chinese opera culture, Xiang Opera, Qi Opera, Yang Opera and other local operas and Dong Nuo Opera, Miao Drum Dance and other ethnic minority operas mingled here, forming a unique "Hunan Opera Cultural Circle"; ancient opera stage as the material carrier of opera performance, widely distributed throughout the province. Meanwhile, Hunan Province has a variety of landforms, with mountains, hills and plains accounting for 51.2%, 29.3% and 13.1% of the total area respectively. Western Hunan and southern Hunan are mainly mountainous and steep, which is the area where the ancient theaters are concentrated; the hills in central Hunan are undulating, and the ancient theaters are mostly built in the center of villages or ancestral halls; the plains of Dong ting Lake in northern Hunan are low and flat, with well-developed water systems, and the ancient theaters are often distributed along the rivers, but they also face a high risk of flooding. The climate is subtropical monsoon climate, with an average annual precipitation of 1200-1700 millimeters, uneven spatial and temporal distribution of precipitation, and heavy rainfall in summer, which is easy to cause flash floods, mudslides and other disasters.

2.2. Data Sources

The data sources mainly contain two parts: the data of ancient theater in Hunan Province and the geographic base data of geology and flooding in Hunan Province. The ancient theater data in this study mainly comes from cultural heritage list, local literature and field research data. The cultural heritage list is derived from the information on ancient theaters in national and provincial cultural protection units in Hunan Province provided by the National Bureau of Cultural Heritage's "List of National Key Cultural Relics Protection Units" (2021) and the Hunan Provincial Department of Culture and Tourism's "List of Provincial

Cultural Relics Protection Units in Hunan Province" (2020), while the local records and related literature are mainly from the "Journal of Hunan Theatre and Opera"[14], Hunan Traditional Architecture Journal, as well as Xue Linping's[15] Study of Traditional Theater Architecture in Hunan, and Hong Xuemei's[16] Study of Existing Ancient Theater Stages in Hunan South; the team conducted field surveys in some areas of Hunan Province in 2022, and supplemented some of the information on ancient theater stages through GPS positioning, photographs taking, and interview records. By the end of 2022, after removing duplicates, there were a total of 219 extant ancient stage in Hunan Province, including 151 ancestral halls, 20 guild halls, 15 temples, and 33 houses and pueblos.

The basic geographic data mainly include topography and geomorphology, hydrology and climate, and disaster risk information. Among them, the DEM digital elevation model of Hunan Province (30-meter resolution) comes from the Geospatial Data Cloud Platform (http://www.gscloud.cn); the geological map of Hunan Province (1:500,000 scale) is provided by the China Geological Survey (http://www.cgs.gov.cn), which covers the geological structure and lithological distribution information of Hunan Province; the River system data (1:250,000 scale) from the National Center for Basic Geographic Information (http://www.ngcc.cn); and Hunan Province precipitation and extreme weather data (1981-2020) from the China Meteorological Data Network (http://data.cma.cn).

2.3. Research Methodology

For the spatial distribution characteristics of the existing ancient opera stages in Hunan Province, this study adopts GIS technology and spatial analysis methods, combined with ArcGIS software, using the spatial statistical methods of kernel density analysis, nearest-neighbor analysis, and standard deviation ellipse analysis (see Table 1), to quantitatively analyze the spatial distribution characteristics and evolutionary trends from the perspective of spatial distribution characteristics and evolutionary trends. Among them, kernel density analysis can intuitively and quantitatively analyze the spatial trend of statistical points, and objectively and accurately express the spatial distribution status of ancient theaters by strengthening the pattern of displaying spatial distribution[17]; standard deviation ellipse analysis can observe geometric parameters such as ellipse's area, long and short semiaxes, and oblateness to intuitively reflect spatial features such as the scope of distribution of the performance venues, directionality, and the degree of discrete; Mean nearest-neighbor analysis can be used to evaluate the degree of agglomeration of elements, and the nearest-neighbor index can be used to determine whether the global distribution pattern of ancient performance venues in Hunan Province is agglomerated, discrete, or stochastic[18].

On the other hand, in the study of disaster risk in Hunan Province, the informativeness method, the weighted comprehensive evaluation method and the geohazard risk index have been used to assess the risk of different types of disasters (see Table 1). The informativeness method is used to study the susceptibility of geohazards, and its basic principle is to measure the potential risk of geohazards in different regions by calculating the ratio of the number of units known to occur geohazards to the total number of units in the region. For the study of flood hazard susceptibility, the weighted comprehensive evaluation method was used, and the corresponding risk model was constructed by evaluating the factors affecting flood hazard susceptibility. The geohazard risk index model is used to comprehensively assess the risk of geohazards by combining the susceptibility and risk coefficients, and this method further refines the assessment of disaster risk through the calculation of the risk index. The flood hazard risk index is used to assess the comprehensive risk of flood hazards and provide a scientific basis for regional disaster risk zoning. Finally, based on the results of the calculation of the susceptibility and danger of geology and flooding, three risk zones were divided into high, medium and low, respectively.

3. Distributional Characterization

3.1. Types of Spatial Distribution

By comparing the average distance of the actual observation with the theoretically expected average distance, the nearest neighbor index R can be calculated to infer the distribution pattern of spatial points. When the index value is small, it means that the spatial point distribution presents a more irregular or discontinuous state. In order to assess the statistical significance of this distribution pattern, the nearest-neighbor index and P-value can be applied to calculate and draw conclusions. When the index of the calculation result is less than 1, it indicates that the point elements present an agglomeration pattern, i.e., there is an obvious aggregation effect; if it is greater than 1, it indicates that the point elements present a dispersed tendency, which is not in line with the characteristics of aggregation. When the index is close to 1, it indicates that the distribution of point elements is close to the random distribution mode.

Previous studies have found that the distribution of ancient theaters in certain areas can be of different types such as aggregated, uniform or random. The nearest neighbor index, as a geographic indicator, is often used to describe the relative proximity between point elements and is widely used in the analysis of spatial distribution characteristics. In the study of ancient theaters, due to the influence of geographic and cultural factors, their distribution usually shows strong clustering characteristics. Using ArcGIS spatial analysis tools, the distribution of existing ancient opera stages in Hunan Province was measured, and the spatial distribution types of ancient opera stages in Hunan Province at different scales were finally identified by calculating the theoretical closest proximity distance and the closest point index R. The spatial distribution of ancient opera stages at different scales in Hunan Province is shown in the following table.

The distribution of the existing ancient stage in Hunan Province is analyzed, and the results are shown in Table 2. The actual nearest point distance of ancient stage in Hunan Province is much larger than the theoretical distance of the average neighboring point, and the actual nearest point distance is 9093 m. The nearest point index is $1.8 > 1$, and the z-value is 24.50, and the significance level p-value < 0.01, which indicates that the ancient stage in Hunan Province has a strong discrete characteristic. Among the 14 cities in Hunan Province, the actual nearest neighbor distance of the urban areas with a larger number of ancient theaters does not reach the theoretical nearest neighbor distance, indicating that the spatial distribution of ancient theaters in these areas shows aggregation characteristics; on the contrary, in the urban areas with a smaller

Table 1 | Statistical analysis model and implications [19]

Exponents	Mould	Model Implications
nuclear density index (NDI)	$f(x) = \frac{1}{nh}\sum_{i=1}^{n} k\left(\frac{x - xi}{h}\right)$	k is the kernel density function; h is the bandwidth; n is the number of points in the threshold range; $x - xi$ denotes the distance from the valuation point x to the event at xi
nearest neighbor index (NMI)	$R = \frac{\bar{r}_i}{r_e} \quad r_e = \frac{1}{2\sqrt{\frac{m}{A}}} = \frac{1}{2\sqrt{D}}$	$\bar{r}_i$ represents the average of the distances between each point and its nearest neighbor; r_e is the theoretical nearest neighbor distance when point elements are randomly distributed; m represents the number of point elements; A represents the study area and Drepresents the number of point elements per unit area.
standard deviation elliptic index (SDEI)	$\mathrm{SDE_x} = \sqrt{\frac{\sum_{i=1}^{n}\left(x_i - \bar{p}_x\right)^2}{n}}$ $\mathrm{SDE_y} = \sqrt{\frac{\sum_{i=1}^{n}\left(y_i - \bar{p}_y\right)^2}{n}}$	x_i and y_i are the coordinates of the spatial position of each element; $\bar{p}_x$ and $\bar{p}_y$ are the arithmetic mean centers; and the variation of the ellipse calculated by $\mathrm{SDE_x}$ and $\mathrm{SDE_y}$.
information quantity method	$I_{A_{j\to B}} = ln\frac{N_j/N}{S_j/S}$	N is the total number of units in the study area where geologic hazards are known to occur, and S is the total number of units in the survey area.
Weighted Comprehensive Evaluation Method (WCEM)	$K_{cz} = \sum_{i=1}^{n} M_{czi}Q_i$	$\mathrm{K_{cz}}$ denotes the total value of susceptibility; n is the number of evaluation indicators; $\mathrm{M_{czi}}$ is the normalized value of the i indicator of factor z; $\mathrm{Q_i}$ denotes the weight of the ith indicator.
Geologic Hazard Risk Index (GHRI)	$H_i = S_i \times e_{h_i}$	$\mathrm{H_i}$ denotes the hazard index of the grid cell; $\mathrm{S_i}$ is the normalized susceptibility index of the grid cell, and e_{h_i} is the hazard coefficient
Flood hazard index	$L = \sum H_i D_i$	L is the hazard index, H_i and D_i correspond to the number of occurrences of each evaluation factor and their corresponding weights.
riskiness index	$V = U \times Y$	V represents the result of the risk evaluation of the disaster; U represents the result of the hazard evaluation of the disaster; and Y is the result of the vulnerability evaluation of the disaster.

number of ancient theaters, such as Changde City, Yiyang City, Loudi City, etc., the spatial distribution of ancient theaters tends to be randomly distributed or discrete distribution.

From a comprehensive point of view, the distribution of the existing ancient stage in Hunan Province has significant regional differences. In southern Hunan and western Hunan, the distribution of ancient theaters shows an obvious aggregation, especially in Xiangxi Tujia and Miao Autonomous Prefecture and Chenzhou City, where the distribution of ancient theaters is dense, reflecting strong cultural inheritance characteristics. The distribution of ancient stage in central and northern Hunan is relatively decentralized, with central Hunan showing a random spatial distribution pattern. Overall, the spatial distribution of ancient opera stages in Hunan Province is discrete, showing local aggregation, but most areas still show discrete or random distribution.

3.2. Degree of Spatial Aggregation

The density of spatial point elements can be estimated using the kernel density analysis method. The method evaluates the spatial density around each point by weighting and summing the spatial point elements, thereby revealing the distribution characteristics of the point elements. Specifically, kernel density analysis obtains the density value of each point by setting a window, calculating the influence of each point within that window and sum-

Table 2 | Spatial distribution types of ancient theater in Hunan Province cities

Shore	City	Number of Ancient Theaters	Theoretical distance	Actual distance	Nearest neighbor index	z-value	Distribution type
South Hunan	Yongzhou	41	9502	5548	0.58	-10.00	Aggregate Distribution
	Chenzhou	103					
	Hengyang	14					
Western Hunan	Huaihua	27	19382	14470	0.75	-2.86	Aggregate Distribution
	Xiangxi Autonomous Prefecture	8					
	Zhangjiajie	——					
North Hunan	Changde	——	75295	98963	1.31	0.85	Discrete Distribution
	yueyang	1					
	Yiyang	1					
Central Hunan	Xiangtan	4	24367	26170	1.07	0.69	Randomized Distribution
	Loudi	2					
	Shaoyang	12					
	Changsha	4					
	Zhuzhou	2					
Hunan Province		219	4878	9093	1.86	24.50	Discrete Distribution

ming it up. Compared with the traditional assumption of uniform distribution, kernel density analysis can more accurately reflect the clustering or dispersion trend of point elements in space.

Through the kernel density analysis, we are able to identify the spatial aggregation area of the ancient theaters more clearly. The spatial distribution density of the ancient theaters in Hunan Province is analyzed in detail by using the spatial analysis tool in the ArcGIS-Pro software, and its distribution pattern is revealed. As shown in Fig. 2, the ancient opera houses in Hunan Province are mainly concentrated in western Hunan and southern Hunan, which show the strongest spatial aggregation. The distribution of ancient opera houses in the eastern and northern Hunan regions is relatively sparse, and the overall distribution shows a pattern of "one center and many belts", specifically, the western part of Chenzhou and the eastern part of Yongzhou serve as the core area for the distribution of traditional ancient opera houses, while the central part of Huaihua City and the central parts of Hengyang and Changsha form a number of important belts for the distribution of ancient opera houses.

Among them, the core of distribution in southern Hunan is located in the western Chenzhou and eastern Yongzhou areas, especially in the western Chenzhou area, where the kernel density value is significantly higher, with 12 to 20 ancient theaters per 100 square kilometers, concentrated in Guiyang County. This is closely followed by the eastern parts of Xintian and Ningyuan counties, which have a kernel density of 8 to 12 per 100 square kilometers. The distribution in other areas is sparser, and the distribution of ancient theaters in southern Hunan is characterized by obvious spatial heterogeneity. Western Hunan also shows a more concentrated distribution of ancient opera tages, especially in Huaihua City, along the belt of the Xuefeng Mountain Range. The geographical conditions of western Hunan provide a favorable natural and cultural environment for the formation of ancient stage, and the lofty mountains, abundant water resources, and unique geographic location make this area an important concentration of ancient stage.

In contrast, the distribution of ancient theaters is sparse in the central and northern Hunan regions because of the relatively flat topography and convenient transportation, and the rapid urbanization process that these regions have experienced. The number of ancient opera houses in central and northern Hunan is significantly lower than that in western and southern Hunan. In conclusion, the distribution of ancient opera houses in Hunan Province shows obvious regional differences, with western Hunan and southern Hunan being the main gathering areas, especially in the western part of Chenzhou and the Xuefeng Mountain Range, while central Hunan and northern Hunan have a relatively small number of existing ancient opera houses due to the rapid modernization process and the relatively flat terrain.

3.3. Trends in Spatial Distribution

In spatial statistical analysis, Standard Deviation Ellipse (SDE) is a commonly used method to analyze the spatial distribution trend of point elements. This method is able to measure the spatial characteristics of geographic ele-

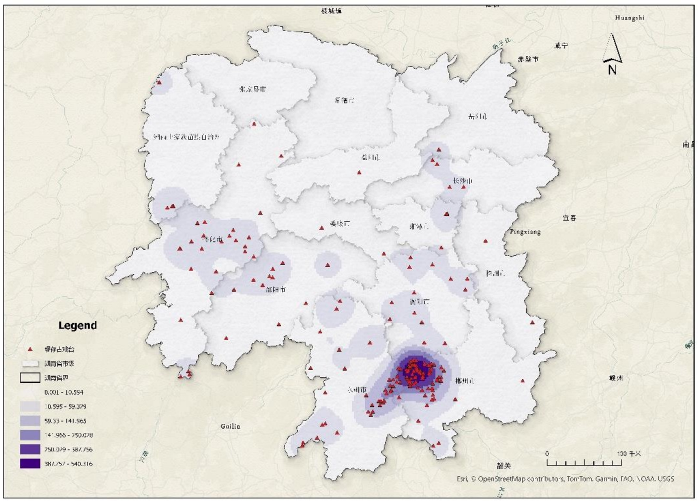

Figure 2 I Kernel density analysis of ancient theaters in Hunan Province

ments, specifically including the center trend, distribution dispersion and directional trend. In the SDE method, the mean center represents the concentrated area of the distribution of geographic elements; while the dominant direction of the distribution can be reflected by rotating the azimuth angle; and the offset is used to measure the change of geographic lements within the region. In addition, the direction and extent of the distribution of geographic elements can be described by the standard distances of the long and short axes. Applying this method to analyze the spatial distribution of the extant ancient theaters in Hunan Province can effectively assess their changes in different time periods.

By utilizing the standard deviation ellipse tool in ArcGIS Pro, the spatial analysis of the existing ancient theaters of different construction periods in Hunan Province was carried out, and their evolution patterns in various historical stages were studied. Taking the earliest construction time mentioned in the traditional documentary records as the benchmark, the 141 ancient stages of the known period are divided into three periods: the early Ming and Qing dynasties (1507-1735), the mid-Qing dynasty (1736-1850), and the late Qing and Republic of China (1851-1949). Through this division, the geospatial development trend of the existing ancient stage in Hunan Province is explored from a temporal perspective (see Figure 3).

According to the standard deviation ellipse analysis in GISPro, the spatial distribution of the ancient stage built from the Ming and Qing Dynasties to the Republic of China (1507~1949) in Hunan Province shows obvious regional characteristics. The results obtained from the standard deviation ellipse analysis show that the distribution of ancient stage has a strong spatial concentration trend, and the distribution trend is mainly concentrated in the south-central part of Hunan Province and part of western Hunan Province. From the results of the analysis in the figure, the ancient stage built in the early period (1507-1735) was mainly concentrated in the south of Hunan, and the distribution showed a long-axis trend in the north-south direction; and into the middle of the Qing Dynasty and the Republic of China (1736-1949), the distribution of the ancient stage was gradually extended to the central and western Hunan areas. Especially in the late Qing and Republican period, the distribution of the ancient theater appeared to have a wider expansion trend, and the western and central Hunan regions became the emerging distribution areas. The results of standard deviation ellipse analysis also reveal the aggregation of distribution. The analysis shows that, although the number of ancient stages gradually increased in all periods, the dense areas of distribution were still concentrated in the southern and western Hunan regions, and this trend persisted throughout the time span. Overall, the distribution trend of ancient stage in Hunan Province from the Ming and Qing Dynasties to the Republic of China is characterized by a gradual expansion from southern Hunan to central and western Hunan. With the advance of time, the construction of ancient theaters was not only concentrated in the traditional southern Hunan area, but also gradually expanded to other regions, especially the number of ancient theaters in the western and central Hunan areas increased, which shows the gradual expansion and development of the spatial distribution of ancient theaters in this period.

3.4. Continuous Regional Distribution

According to the statistical analysis, the county average distribution density of the existing ancient stage in Hunan Province is 1.14 per thousand square kilometers. Through the use of ArcGIS Pro software to screen out the counties where the distribution density of ancient stage is higher than the average value of the province, a total of 23 counties have a distribution density of ancient stage exceeding the average level of the province. Among them, the top three counties with the highest density of ancient stage are Guiyang County, Shuangqing District and Xintian County, while three of the top five counties belong to the southern Hunan region (see Table 3).

From a spatial distribution point of view (see Figure 4), among the counties with a high density of ancient theaters, there are 11 counties in the southern Hunan region, 6 counties in the central and western Hunan respectively,

Table 3 I Top five contiguous areas at the county level in Hunan Province

County	Number of Ancient Opera Stages	Area	Area (square kilometers)	Density (pcs/thousand square kilometers)
Guiyang county	95	South Hunan	2958.17	32.11
Shuangqing District	2	Central Hunan	135.87	14.71
Xintian County	12	South Hunan	999.58	12.00
Steamboat District	1	South Hunan	110.99	9.00
Yuhu District	3	Central Hunan	450.44	6.66

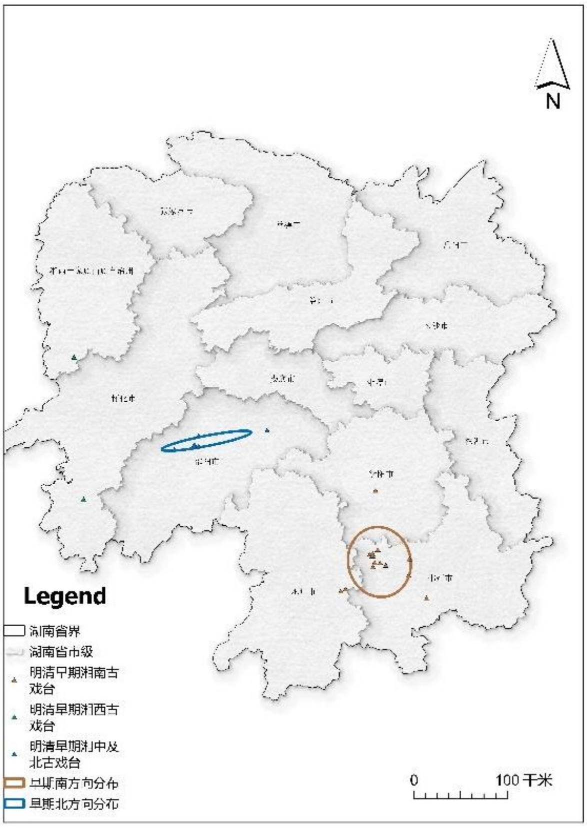

a. Trends in the Distribution of Ancient Opera Stages Built in the Early Ming and Qing Dynasties (1507-1735)

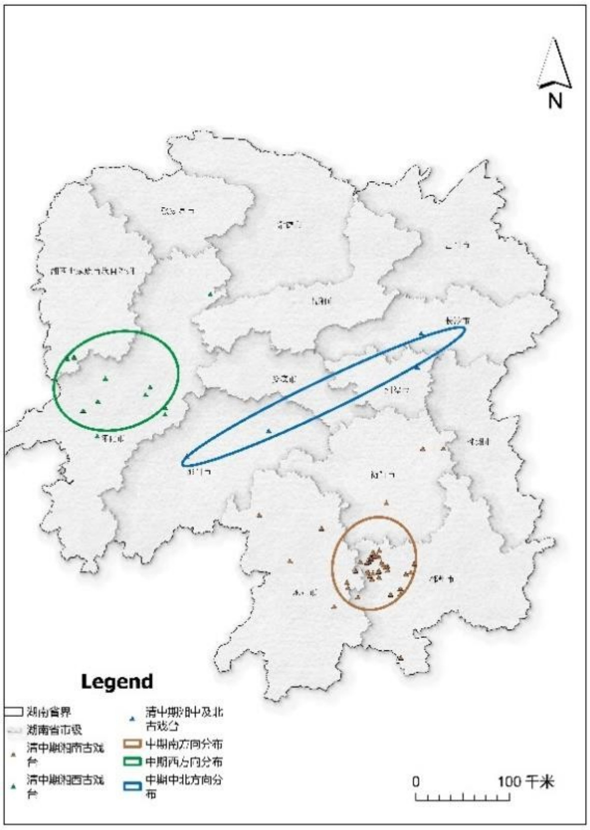

b. Trends in the Distribution of Ancient Opera Stages Built in the Mid-Qing Period (1736-1850)

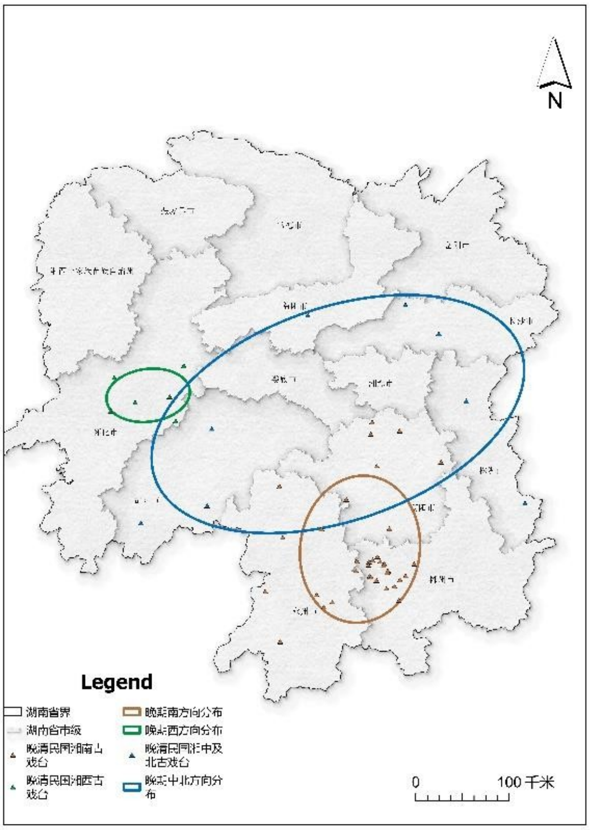

c. Trends in the Distribution of Old Opera Stages Built in the Late Qing and Republic of China (1851-1949)

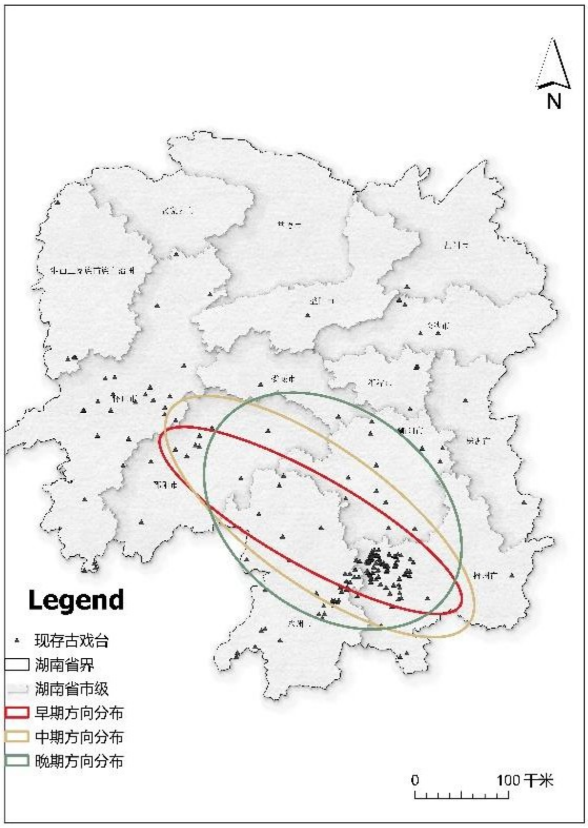

d. Trends in the distribution of ancient theaters built in the Ming and Qing Dynasties-Republic of China (1507-1949)

Figure 3 l Distribution of the direction of ancient theaters in each period (1507-1949)

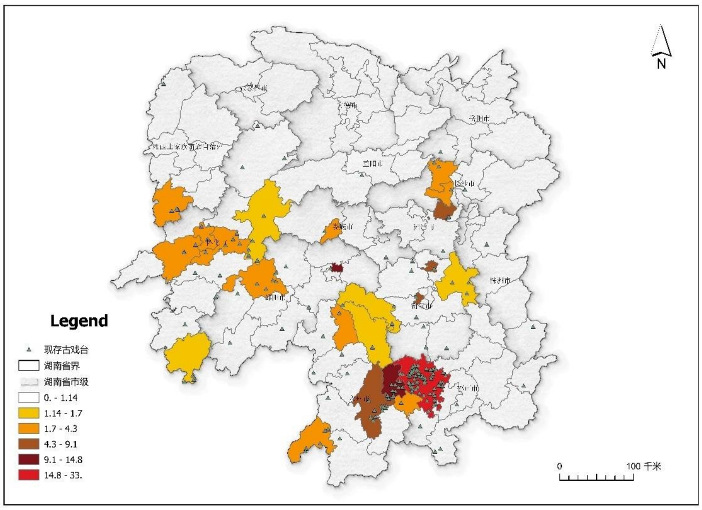

Figure 4 l County-level centralized area of existing ancient theatres

while the northern Hunan region fails to find any counties with a density exceeding the provincial average. According to the statistics, Nanyue District of Hengyang City, Ningyuan County and Jiangyong County of Yongzhou City, Jiahe County of Chenzhou City, Fenghuang County of Xiangxi Autonomous Prefecture, and Zhongfang County of Huaihua City, together with the five contiguous areas in the table below, the distribution densities of the ancient theaters in a total of 11 districts and counties are all higher than 3 per 1,000 km2, which are areas of high potential for centralized and contiguous conservation and utilization.

4. Geologic Hazard Risk Zoning

4.1. Evaluation of Susceptibility

Geological disaster susceptibility refers to the possibility of geological disasters occurring in a specific area due to geological conditions. When carrying out the vulnerability assessment, it mainly analyzes the occurrence of existing geohazards in the area and predicts the trend of possible disasters in the future, which lays the foundation for further hazard and risk assessment. In this paper, the information quantity method is used to assess the susceptibility to geological hazards, and the information quantity model measures the degree of influence of various disaster-causing factors on geological hazards with the help of probabilistic statistical methods.

According to the relevant requirements for the evaluation of the susceptibility of geologic disasters in Hunan Province, this study carried out a comprehensive assessment of the susceptibility of geologic disasters by combin-

Table 4 l Geologic Hazard Vulnerability Evaluation Factor Table

Evaluation factors	Weights	Indicator Grading	Indicator weights
Slope/(。)	0.20	<20	0.25
		[20, 45)	0.35
		[45, 60)	0.25
		≥60	0.15
Land use type	0.25	Agricultural Land	0.30
		Forests, grasslands and unutilized land	0.20
		Urban, rural, industrial, mining and residential land	0.30
		Water area	0.10
		Transportation Land	0.10
Vegetation cover	0.15	[-1, 0]	0.20
		(0, 0.2]	0.30
		(0.2, 0.4]	0.30
		>0.4	0.20
Slope type	0.10	Concave	0.40
		Linear	0.35
		Convex	0.25
Degree of terrain undulation/m	0.15	≤10	0.30
		(10, 20]	0.30
		(20, 30]	0.25
		>30	0.15

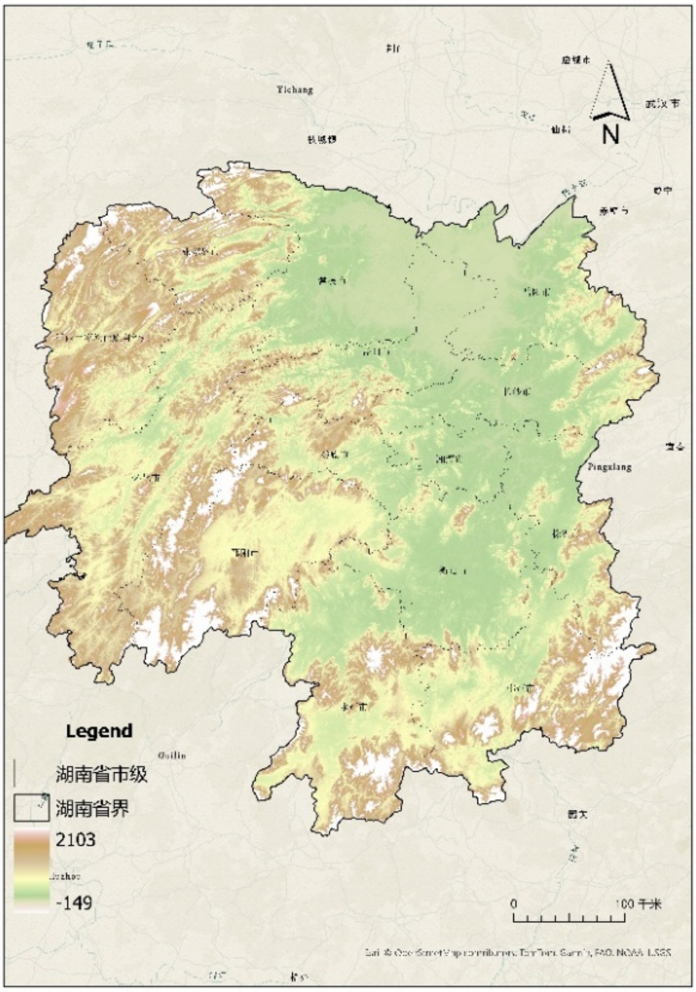

Figure 5 | Topography of Hunan Province

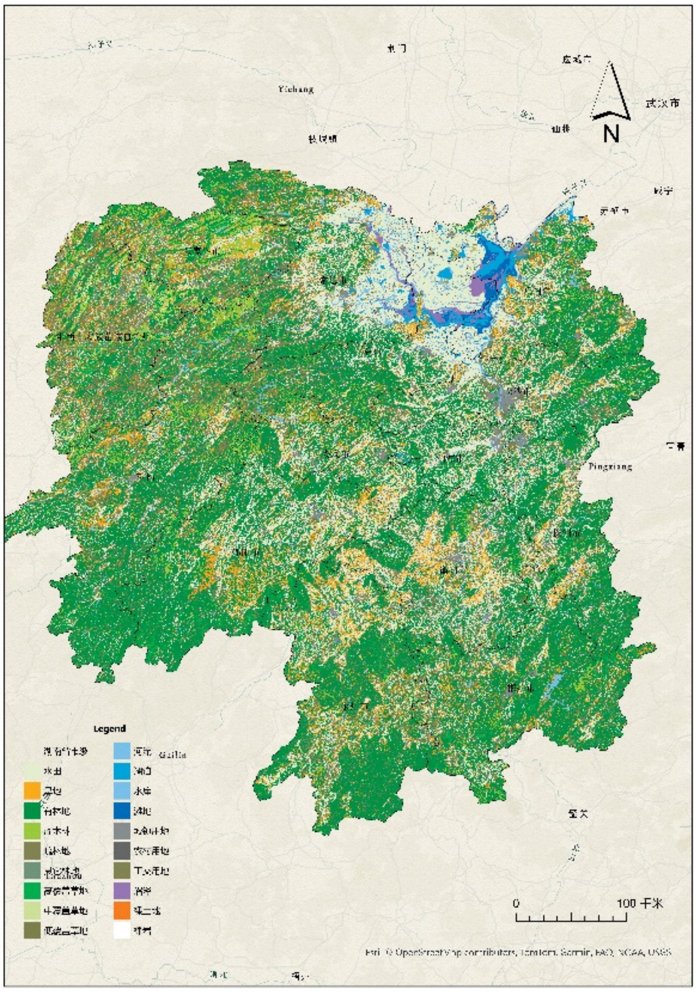

Figure 6 | Land use map of Hunan Province

ing the characteristics of the geologic environment and the types of disasters in Hunan Province. Firstly, according to the development pattern and geological conditions of geological disasters in Hunan Province, through the investigation and analysis of various factors affecting the occurrence of geological disasters, a number of influencing factors were selected as indicators of susceptibility assessment (see Table 4).

Using the information quantity method and GIS spatial analysis tools, the spatial analysis and information quantity calculation of each evaluation factor were carried out, and finally the evaluation layer of geohazard susceptibility in Hunan Province was generated. According to this evaluation layer, combined with the proportion and frequency of various types of geohazards, the geohazard susceptibility was divided into three levels: high, medium and low susceptibility areas. After filtering and denoising, the susceptibility evaluation map was further optimized and finally formed the geohazard susceptibility zoning map of Hunan Province (see Figure 7).

4.2. Hazard Evaluation

Geological disaster risk mainly reflects the probability of occurrence of a specific type and scale of geological disaster in a certain area within a certain time frame under the effect of specific triggering factors. According to the research and analysis, most of the geohazards in Hunan Province occur during the rainy season, and precipitation is the main triggering factor for the occurrence of geohazards. Based on the foundation of geohazard susceptibility evaluation, combined with the monthly average precipitation data, the risk coefficient is introduced to carry out the geohazard risk assessment.

On the basis of the susceptibility evaluation, the hazard coefficient was introduced in combination with the monthly mean precipitation distribution (see Fig. 8) to carry out the

Table 5 | Hazard secondary evaluation factor weights

	Vulnerability results	Average monthly precipitation	Wi
Vulnerability results	1	2	0.6667
Measured quantity of rain	1/2	1	0.3333

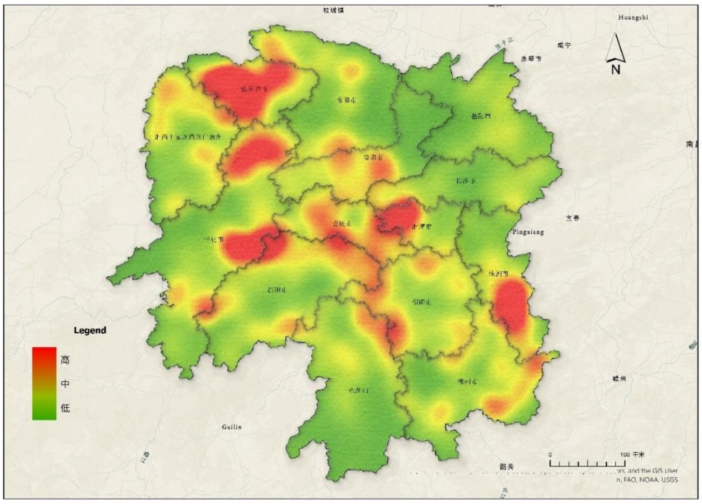

Figure 7 I Geological hazard susceptibility zoning map of Hunan Province

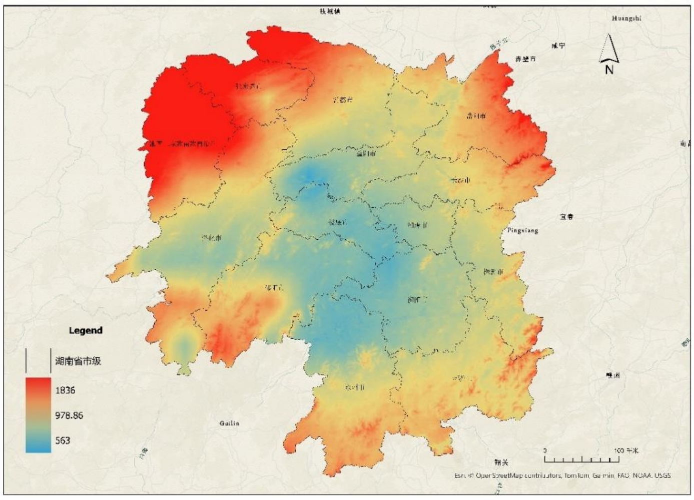

Figure 8 I July mean precipitation in Hunan Province (2022)

hazard assessment of geologic hazards in . A hierarchical analysis model of geologic hazards was constructed using Matlab software, and the judgment matrix of the susceptibility evaluation results and monthly mean precipitation in the hazard evaluation was set on this basis (see Table 5). The weighting factors of the susceptibility evaluation results and average monthly precipitation were calculated as (0.6667, 0.3333), respectively.

Through the hierarchical analysis method and combined with the evaluation standard of geologic hazards, the weights of the average monthly precipitation and the evaluation result of susceptibility were determined, and the precipitation and susceptibility evaluation results of Hunan Province were superimposed and analyzed to derive the geologic hazard risk evaluation map of Hunan Province.

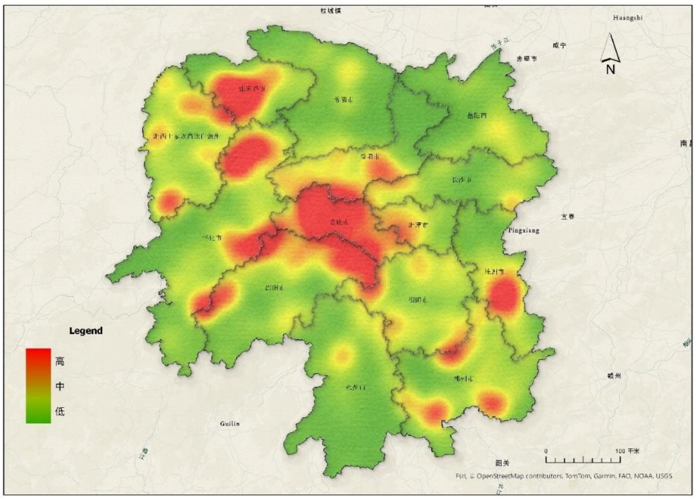

Figure 9 I Geologic Hazard Risk Evaluation Map

Using the natural discontinuity method in ArcGIS software, the results of the hazard evaluation were categorized into three types, namely, low-hazard zone, medium-hazard zone, and high-hazard zone, and the geohazard hazard zoning map of Hunan Province was drawn (see Fig. 9).

4.3. Geologic Hazard Risk Areas

Geological disaster risk reflects the possibility of losses caused by geological disasters to different types of disaster-bearing bodies in a specific region and period of time. The final geohazard risk evaluation results are obtained by combining the results of the evaluation of the danger and the susceptibility of geohazards, and by classifying the risk level based on the matrix judgment method, and integrating the data by using focal statistical tools. The risk evaluation of geohazards can be expressed by the product of hazard evaluation and susceptibility evaluation, risk = hazard⊠susceptibility.

Matrix analysis method is used for specific evaluation. The results of the evaluation of the risk of geologic hazards in the study area are superimposed on the results of the evaluation of the susceptibility to geologic hazards to obtain a table of the classification of the risk of geologic hazards in the study area (see Table 6), and the calculation and analysis is carried out by using the formula of the risk to obtain the results of the evaluation of the risk of geologic hazards in the study area, and the results of the evaluation are classified into three levels of intervals, and the evaluation map of the risk of geologic hazards in the study area is obtained (see Fig. 10)

The percentage of each risk zone is derived by statistically analyzing the results of hazard risk evaluation in Hunan Province. Low-risk zone, medium-risk zone and high-risk zone account for 58.25%, 30.45% and 11.3% of the total area respectively. High-risk zones are mainly concen-

Table 6 I Geologic hazard risk classification table

Vulnerability/hazard	high Hazard	Medium Hazard	low Hazard
Low susceptibility	medium risk	high risk	high risk
Medium Vulnerability	high risk	medium risk	high risk
High Vulnerability	high risk	high risk	medium risk

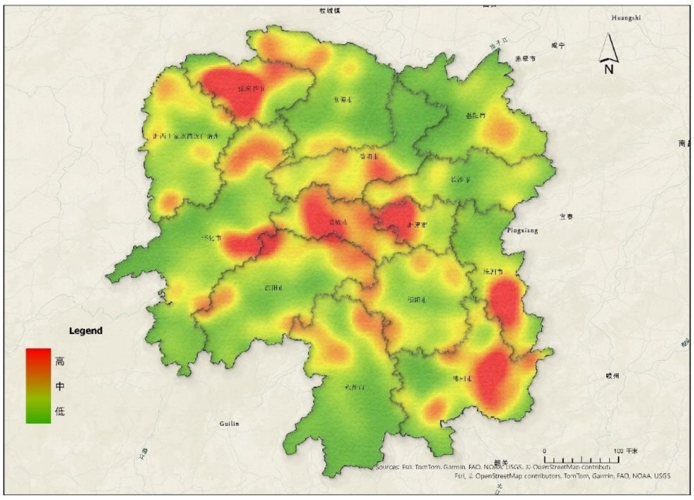

Figure 10 | Geologic hazard risk zoning map

trated in central Hunan, northwestern Hunan and southern Hunan mountainous areas, especially in the central area of Loudi City, the northern area of Zhangjiajie City, and the western mountainous area of Chenzhou City, with an area of about 23,900km². Medium-risk zones are mainly distributed in the central and southern low-hill areas of Hunan Province, covering an area of about 64,500km². The low-risk zone is mainly concentrated in the plains and river alluvial areas in the province, with the largest area of about 123,400km². Overall, the distribution of low-risk areas in Hunan Province is wide, and mainly concentrated in the central and southern plains; the area of very high-risk areas is the smallest, and mainly distributed in mountainous areas with complicated terrain. In terms of the distribution of geohazard risk, the mountainous areas in the east-central part of Hunan Province have higher geohazard risk, the central and western parts are medium-risk zones, and the plains in the south and east are low-risk zones.

5. Flood Risk Zoning

5.1. Evaluation of Susceptibility

Disaster-causing factor is the external condition that triggers flood disaster, and it is the key factor indispensable to the occurrence of disaster, and the disaster-causing factor and the environment that breeds disaster work together to constitute the conditions for the occurrence of flood disaster. By determining the disaster-causing factors, the weighted comprehensive evaluation method is used to analyze the influence of each factor on the overall disaster, and the influence degree of each specific index is summarized, so that the strengths and weaknesses of the overall evaluation object are reflected centrally through the quantitative indexes. In this study, the weighted comprehensive evaluation method is used to construct a risk assessment model for heavy rainfall and flooding in Hunan Province.

Disaster susceptibility refers to the environment and conditions affecting the occurrence of disasters, which can, to a certain extent, exacerbate or weaken the occurrence of disasters and their consequences. In Hunan Province, the terrain is complex and hilly, and water in low-lying areas is difficult to discharge, making it easy to form waterlogging. At the same time, there are many rivers running from northeast to southwest in Hunan Province, and continuous precipitation can easily lead to a rapid rise in water level, which in turn triggers flooding. Therefore, the average annual precipitation, topographic relief and river network density were mainly selected as indicators to measure the susceptibility to pregnant disasters, and the corresponding weight values were assigned to combine the degree of influence of each factor on flooding.

Table 7 | Flood vulnerability evaluation factor table

Evaluation factors	Weights	Indicator Grading	Indicator weights
DEM/m	0.25	> 1200	0.05
		(500, 800]	0.15
		(200, 500]	0.25
		(50, 200]	0.35
		≤50	0.20
Density of river network/（m / m²）	0.25	(0.03, 0.05]	0.40
		(0.01, 0.03]	0.35
		≤0.01	0.25
Average annual precipitation (mm)	0.35	(400, 800]	0.25
		(800, 1200]	0.40
		> 1200	0.35
Slope/(。)	0.15	<20	0.25
		[20, 45)	0.35
		[45, 60)	0.25
		≥60	0.15

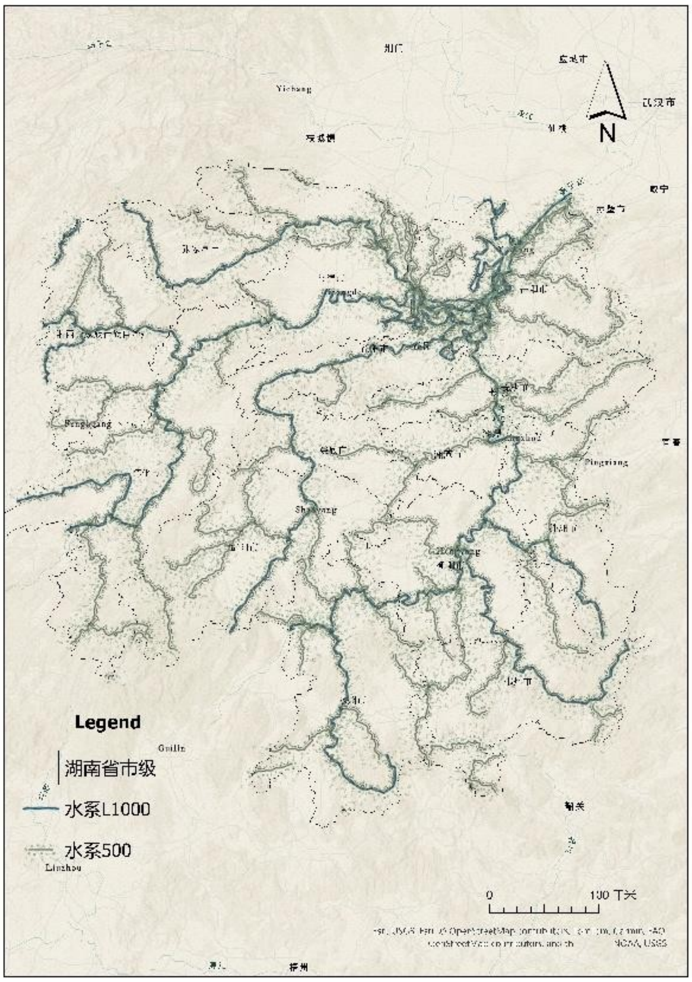

Figure 11 | Density map of water systems in Hunan Province

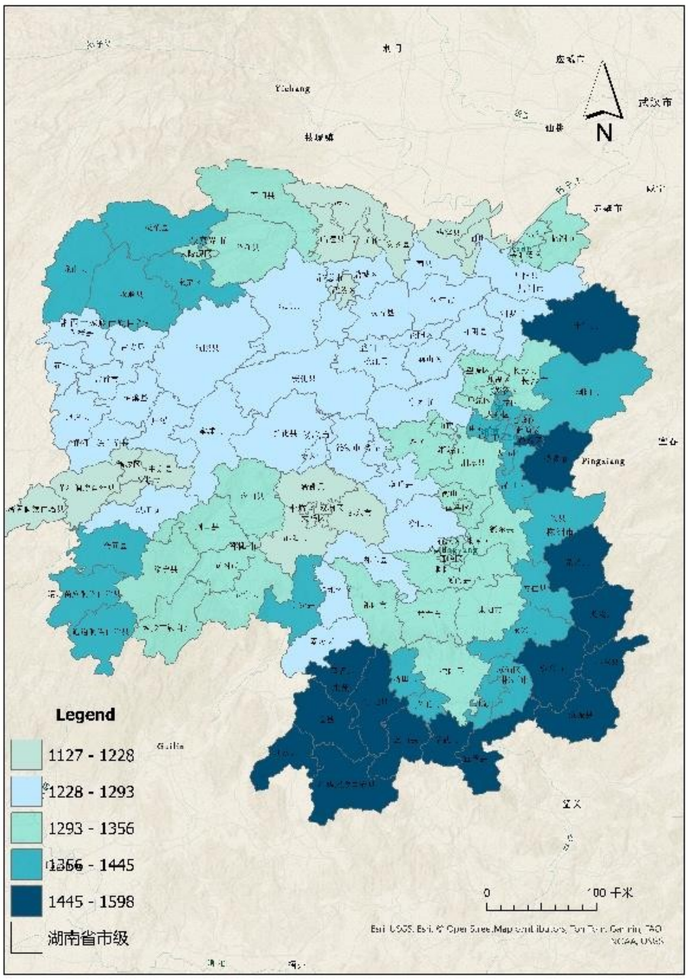

Figure 12 | Average annual precipitation statistics for Hunan Province

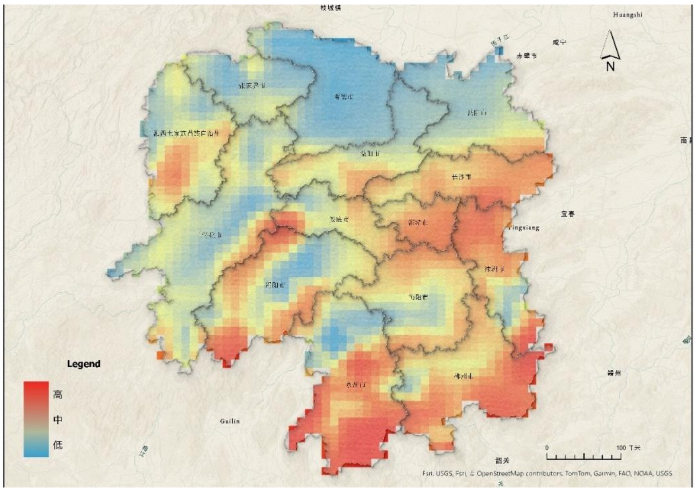

Figure 13 | Flood vulnerability zoning map of Hunan Province

In ArcGIS, the raster data of flood disaster susceptibility in Hunan Province were obtained by assigning different amounts of information to the influencing factors in each interval and spatially overlaying them using a raster calculator. The natural discontinuity method can effectively reflect the spatial distribution status of each influence factor when flooding occurs. Therefore, the natural discontinuity method is used in the ArcGIS reclassification tool to divide the total value of information into three grade intervals, which are low susceptibility zone, medium susceptibility zone, and high susceptibility zone (see Figure 13). Based on this, the distribution map of flood disaster susceptibility assessment in Hunan Province was obtained.

5.2. Hazard Evaluation

Hunan Province is located in the monsoon climate zone, and precipitation characteristics show long duration, high intensity and obvious seasonality. Especially in the summer, heavy rainstorms are frequent, and precipitation is concentrated and of significant intensity. In order to study the risk of flooding in Hunan Province, the heavy rain days in Hunan are defined as daily precipitation ≥ 50 mm, which is used as one of the evaluation factors of flooding risk. The intensity and frequency of heavy rainfall are closely related to the occurrence of floods, so evaluating the risk of heavy rainfall is of great significance for predicting and preventing floods.

In order to quantify the risk of flooding, two key factors, the daily maximum rainfall and the annual average number of days of heavy rainfall, were selected. The daily maximum rainfall reflects the extreme intensity of precipitation on a single day, which is an important factor in the degree of flood hazard. Based on the collected meteorological data for Hunan Province in 2022, the daily maximum rainfall was categorized into four classes: (86.20, 122.06]mm,

Table 8 | Flood Hazard Evaluation Factor Table

Evaluation factors	Weights	Indicator Grading	Indicator weights
Maximum daily rainfall/mm	0.48	(86.20, 122.06]	0.35
		(62.99, 86.20]	0.30
		(38.90, 62.99]	0.20
		(0, 38.90]	0.15
Average annual number of days of heavy rainfall/(d)	0.52	(5, 8]	0.40
		(3, 5]	0.35
		(1, 3]	0.20
		(0, 1]	0.05

(62.99, 86.20]mm, (38.90, 62.99]mm, and (0, 38.90]mm, which were assigned a weight of 0.35, 0.30, 0.20, and 0.15, respectively, and the annual average number of days of rainstorms reflects the frequency of heavy rainfall in Hunan Province, and this factor is important for the prediction of flooding.

Statistically, the annual average number of days of heavy rainfall was categorized into four intervals: (5, 8] days, (3, 5] days, (1, 3] days, and (0, 1] days, which were assigned weights of 0.40, 0.35, 0.20, and 0.05, respectively. Higher frequency of heavy rainfall days implies a more severe risk of flooding occurrence, and thus higher weights are given to high frequency heavy rainfall areas. By combining the evaluation weights of the two factors of daily maximum rainfall and annual average number of days of heavy rainfall, the risk of flooding in Hunan Province can be described more comprehensively.

Based on the statistical data of the number of days of heavy rainfall and the maximum rainfall in each county of Hunan Province in 2022, the spatial analysis and informativeness calculation of each evaluation factor were carried out by the informativeness method and the GIS spatial analysis tool. Through the calculation of these data, the results of the evaluation of the risk of flooding in each region of Hunan Province were obtained. According to the calculation results, the regions were divided into high, medium and low danger zones from high to low (see Figure 16).

5.3. Flood Risk Areas

The risk of flooding reflects the likelihood of flood damage suffered by different types of bearers in a given area and time period. By combining the results of flood hazard and susceptibility evaluation, and using the matrix judgment method to classify the risk level of (see Table 6), and integrating the data with the Focus Statistical Tool, the risk assessment results of flood hazard are finally derived. Based on the flood disaster risk evaluation model of Hunan Province, combined with the evaluation results of danger and susceptibility obtained from the above calculation, the risk formula was used to calculate and substitute the corresponding evaluation index weights, i.e., risk = Dangerousness× Susceptibility.

The specific evaluation also adopts the matrix analysis method. The results of the evaluation of flood hazard risk in the study area are superimposed on the results of the evaluation of flood hazard susceptibility to obtain the classification of flood hazard risk in the study area, which is calculated and analyzed by using Equation 4-3 to obtain the results of the evaluation of flood hazard risk in the study area, which is divided into three grade intervals to obtain the evaluation map of flood hazard risk in the study area (see Fig. 17).

According to the results of the flood risk assessment in Hunan Province, the flood risk in Hunan Province shows obvious spatial distribution differences and is mainly divided into three risk zones: low, medium and high. The high-risk zones are usually located in the low-lying areas around South Hunan, West Hunan and Dongting Lake, especially in Yueyang, Changde, Zhangjiajie and Chenzhou. These areas have low topography, well-developed water systems, frequent and intense rainstorms, and are prone to waterlogging, so the risk of flooding is high, and severe flooding often occurs during heavy rains. Medium-risk areas are mainly located in hilly and low-mountain areas in central and southern Hunan Province, in cities like Changsha, Hengyang, and Loudi. These areas have moderate precipitation and moderate frequency of heavy rainfall, and although they do not have the dense water systems of the high-risk zones, they are also at risk of poor flood drainage due to the relatively gentle topography. The low-risk areas are concentrated in the mountainous and higher terrain areas of Hunan Province, including parts of northern and eastern Hunan. These areas have relatively low precipitation and steep topography, which makes water flow faster and floodwaters easier to discharge, so they are at lower risk of flooding. The natural drainage capacity of these regions is high, which avoids the occurrence of floods. Overall, flood riskiness in Hunan Province shows different levels from south to north and from low-lying to upland areas, with high- risk areas mainly concentrated in the south and

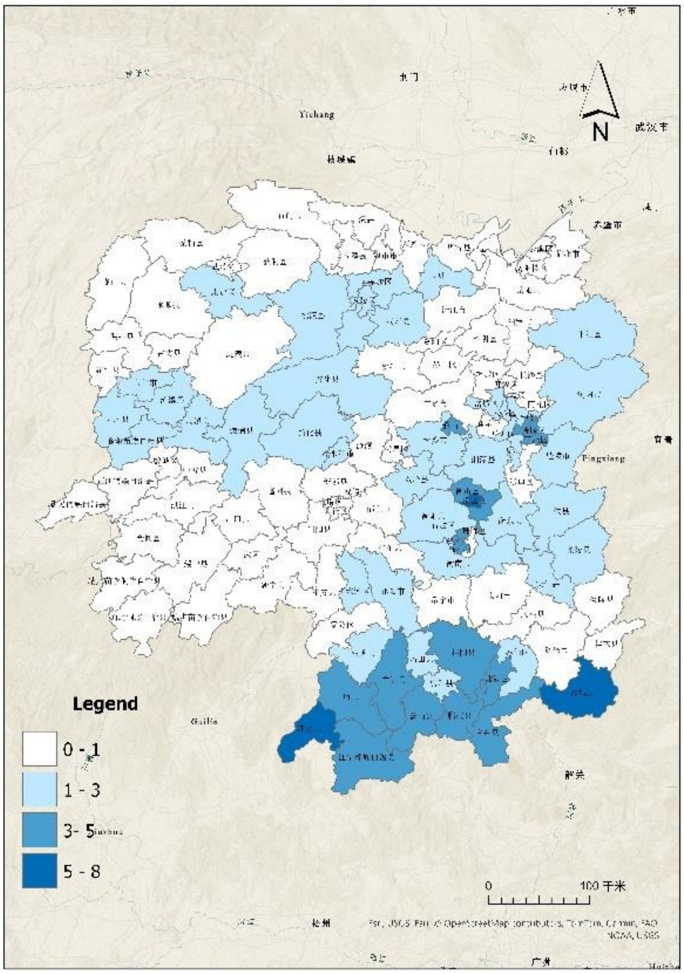

Figure 14 | County-level storm days statistics

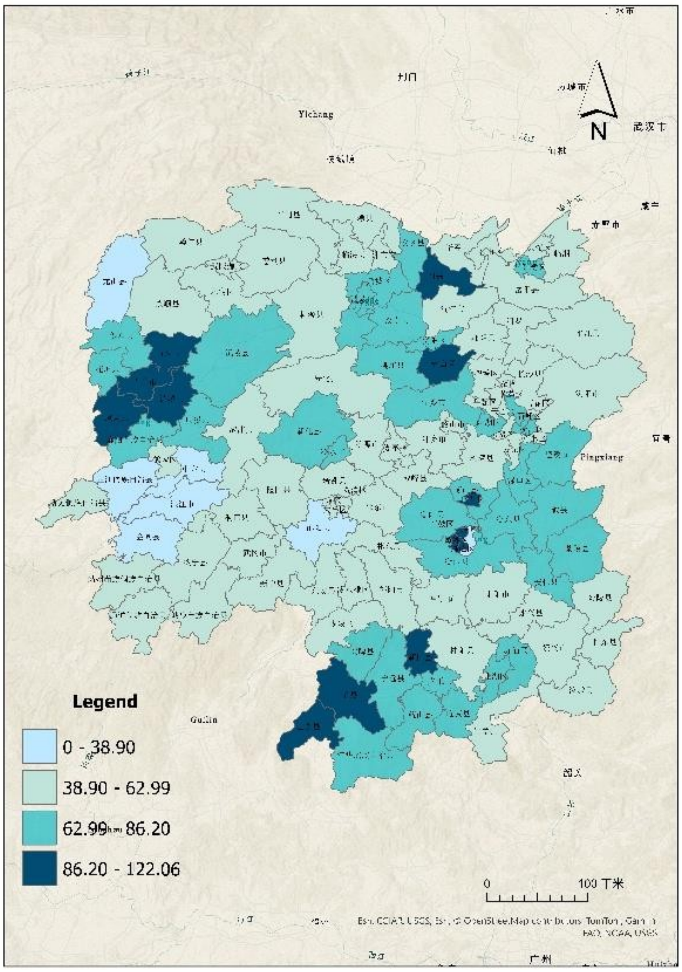

Figure 15 | County-level maximum rainfall statistics

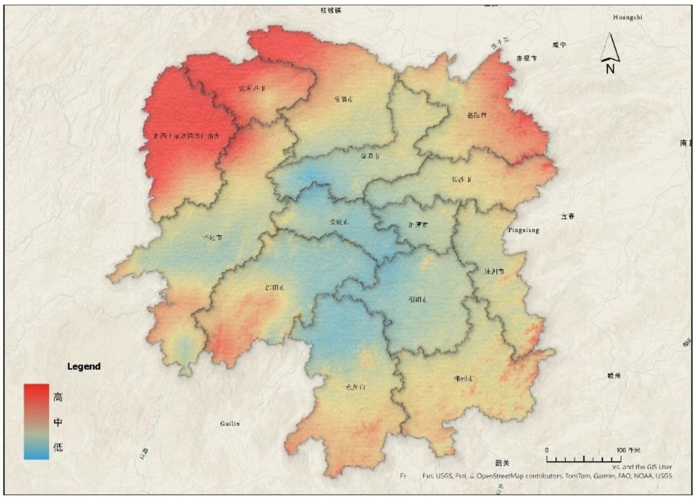

Figure 16 | Flood Hazard Evaluation Map

lowlands, while low-risk areas are distributed in mountainous areas and upland zones.

6. Control Zoning and Countermeasures

6.1. Disaster Prevention and Control Zoning

According to the results of the flood risk assessment of the ancient stage in Hunan Province, combined with the natural environment of the region, the distribution characteristics of geological hazards and the need for protection of cultural heritage, based on the distribution of the 72 ancient stages in the medium- and high-risk areas, and through the optimization of cold hot spot analysis of GIS-Pro, the 72 ancient stages in the risk area are divided into three levels of key prevention and control areas, sub-priority prevention and control areas, and general prevention and control areas, to form the Geological disaster prevention and control zoning map of Hunan Province.

The map of geohazard prevention and control zones is shown in Figure 18, and the key prevention and control areas are mainly located in places with frequent geologic activities, such as high mountainous areas and low hilly areas. The area is about 10,640,000 square kilometers, accounting for 4.99% of the province's area. Most of the ancient theaters in Hunan Province are located in these key prevention and control areas, and the probability of disasters is high. Protective measures should be focused on strengthening. The sub-priority prevention and control areas are mainly located in the valleys or fringes of Hunan Province, covering an area of 61,400 square kilometers, accounting for 28.89% of the province's area. The risk of geologic hazards in these areas is relatively low, but there

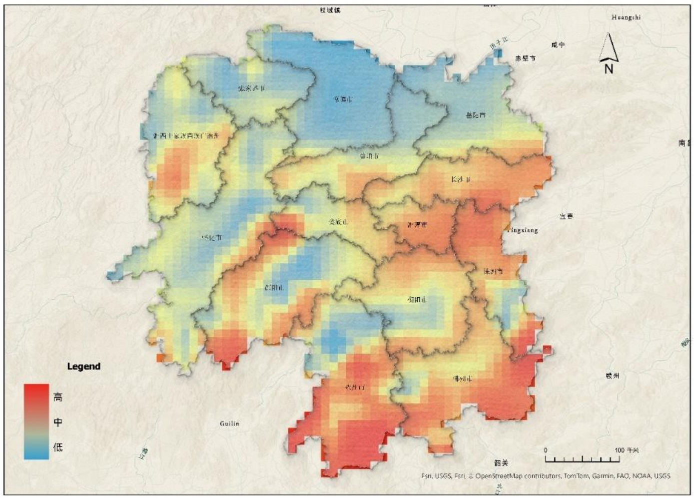

Figure 17 | Flood risk zoning map of Hunan Province

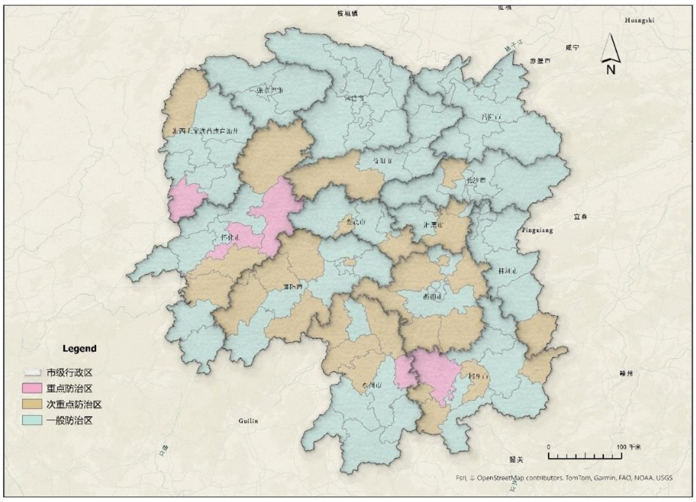

Figure 18 | Geologic Hazard Prevention and Control Zone Map

are still potential disaster threats, which may also cause a large impact in case of occurrence. Therefore, ancient theaters in the sub-priority prevention and control zones should develop moderate protection strategies and conduct routine safety inspections and maintenance.

Similarly, based on the flood risk assessment results of the ancient theaters in Hunan Province, combined with the geographic environment, historical disaster data and potential threat of flooding in each region, and also based on the distribution of 169 ancient theaters in the medium- and high-risk areas, the 169 ancient theaters in the risk area are divided into three levels: key prevention and control area, sub-priority prevention and control area, and general prevention and control area, through the optimization of the cold hotspot area analysis by ArcGIS Pro. The 169 ancient theaters in the risk area were divided into three levels: priority control area, sub-priority control area and general control area through ArcGIS Pro optimized cold-hot spot area analysis.

The flood hazard control zoning map is shown in Figure 19, and the key control zones are mainly concentrated in the localized low hills and river valleys in southern Hunan Province, covering an area of about 0.64 million square kilometers, or 3.01% of the province's area. These areas have a higher degree of vulnerability to flooding and are low-lying and densely populated, and therefore have a higher risk. The sub-priority prevention and control areas are mainly located in the southern and western low mountainous areas in the north and the low mountainous areas in the center of Hunan Province, with an area of 98,900 square kilometers, accounting for 46.73% of the total area of the province. These areas are moderately prone to flooding, with a relatively low disaster density and a relatively decentralized population. Although such areas face a certain degree of flood risk, the frequency and impact of disasters is relatively limited because of the moderate importance of the disaster-bearing body, and prevention and control efforts should focus on strengthening flood management and infrastructure development in order to mitigate the risks that may be posed.

6.2. Recommendations for Prevention Strategies

6.2.1. Strengthening Disaster Risk Assessment and Zoning Management

The ancient theaters in Hunan Province are located in a number of areas with high incidenceof geologic hazards; therefore, it is necessary to first conduct a disaster risk assessment and divide different risk prevention and control zones based on the potential impacts of geologic hazards and flooding. The results of the risk assessment for each zone will provide the basis for the development of targeted prevention and control measures, ensuring that the safety management of each ancient theater is accurately assessed.

6.2.2. Improvement of Disaster Early Warning and Emergency Response Mechanisms

The establishment of a sound disaster warning and emergency response mechanism is crucial in the disaster risk control of the ancient theater. Through the Meteorological Bureau, the Geological Hazard Monitoring Center and other institutions, disaster warning information is issued on a regular basis to warn of possible disasters in advance and ensure that the Government and relevant management departments can respond quickly.

6.2.3. Promoting Digital Preservation and Monitoring of Cultural Heritage

With the development of modern science and technology, digital technology has been widely used in cultural heritage protection. The implementation of digital protection is an indispensable part of the disaster risk control of ancient opera stages in Hunan Province. Intelligent monitoring equipment, such as geological sensors and meteorological monitoring systems, are installed in conjunction with the Internet of Things technology to monitor the structural condition of the ancient theater in real time and discover potential risks in a timely manner.

6.2.4. Enhancement of Public and Local Government Awareness of Disaster Prevention and Management

Disaster risk management in ancient theaters does not only depend on the efforts of the government and profes-

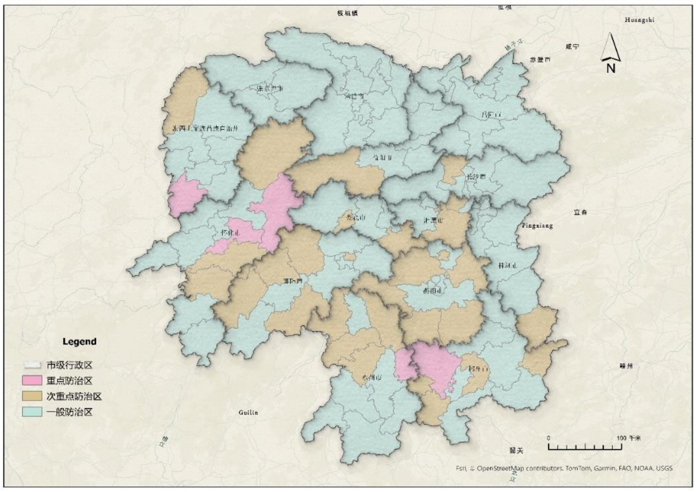

Figure 19 | Flood control zoning map

sional organizations, but also requires the active participation of local communities and the public. By raising the awareness of local residents on disaster control, the risk in case of disaster can be effectively reduced.

6.2.5. Enhancement of Financial Support and Policy Guarantees

Disaster risk control requires strong financial support and policy guarantee. Hunan Province should ensure the smooth progress of disaster prevention and control of the ancient theater through diversified funding channels such as government investment, social financial support, and international assistance. In terms of policy, local governments can introduce relevant regulations to provide legal protection for disaster prevention and control.

7. Conclusion

In this study, the spatial distribution characteristics of ancient stage and its disaster risk pattern in Hunan Province are systematically investigated by combining the GIS spatial analysis technology and disaster risk assessment model with the ancient stage in Hunan Province. The results show that the distribution of ancient stage in Hunan Province has significant regional differences, and its disaster risk pattern is closely related to the natural geographic environment, climate conditions and human activities.

The distribution of ancient stage in Hunan Province presents a spatial pattern of "built along the water and built on the mountain", with obvious local aggregation characteristics. Through kernel density analysis, nearest-neighbor index and standard deviation ellipse analysis, it is found that in terms of spatial distribution type, the overall distribution of ancient opera houses in Hunan Province shows a discrete distribution (nearest-neighbor index R=1.86), but in the south and west of Hunan Province, there is a significant agglomeration, especially in the western part of Chenzhou and the central part of Huaihua, where the kernel density value is higher, and the number of ancient theaters reaches 12-20 per 100 square kilometers. In the spatial distribution trend from the Ming and Qing Dynasties to the Republic of China, the distribution range of ancient opera houses gradually expanded from southern Hunan to central and western Hunan, showing a diffusion trend of "from south to north, from the center to the periphery". The southern Hunan region is always the core area of the distribution of ancient stage, while the western and central Hunan regions became new distribution areas in the late Qing and Republic of China periods. In terms of the distribution of continuous areas, the high-density continuous area of ancient stage in Hunan Province is mainly concentrated in the south of Hunan, such as Guiyang County, Xintian County, etc. The distribution density of ancient stage in these areas is significantly higher than the average level of the whole province (1.14/thousand km²), which is of high centralized and continuous conservation value.

The disaster risks faced by ancient theaters in Hunan Province mainly include geological disasters (landslides, mudslides) and floods. Through the information quantity method, weighted comprehensive evaluation method and GIS spatial analysis, the study concludes that the high-risk areas of geologic hazards in Hunan Province are mainly concentrated in the mountainous areas of central Hunan, northwest Hunan and south Hunan, accounting for 11.3% of the province's area. These areas have complex topography and concentrated precipitation, and the ancient theater faces high threats of landslides and mudslides. The medium-risk area accounts for 30.45%, mainly located in the low hills of central and southern Hunan; the low-risk area accounts for 58.25%, mainly located in the plains of northern Hunan and the highlands of eastern Hunan. The high-risk areas of flooding in Hunan Province are mainly located in the low-lying areas around Hunan South, Xiangxi and Dongting Lake, accounting for 3.01% of the province's area. These areas have well-developed water systems and frequent heavy rainfall, and the ancient theater is vulnerable to flooding. The medium- risk area accounts for 46.73%, mainly located in the low mountainous areas of central and southern Hunan; the low-risk area accounts for 50.26%, mainly located in the highlands of northern and eastern Hunan.

Based on the results of disaster risk assessment, the study divides the ancient stage in Hunan Province into key prevention and control areas, sub-priority prevention and control areas and general prevention and control areas, of which the key prevention and control areas are mainly located in the high-risk areas of geologic hazards and floods, such as Guiyang County, south Hunan Province, Huaihua City, west Hunan Province, and other places. It is recommended to strengthen the construction of the disaster early warning system, implement the structural reinforcement project of the ancient theater, and establish a digital monitoring platform. The sub-priority prevention and control zones are mainly located in medium-risk zones, such as Loudi City in central Hunan and Yongzhou City in southern Hunan. It is recommended to improve the drainage facilities, carry out regular safety inspections of the ancient stage, and promote community participation in the protection work. General prevention and control zones are mainly located in low-risk areas, such as Yueyang City in northern Hunan and Changsha City in eastern Hunan. It is recommended to strengthen daily maintenance, raise public awareness of disaster prevention and control, and develop emergency plans.

This study combines GIS spatial analysis and disaster risk assessment model for the first time,

and systematically reveals the spatial distribution pattern of ancient stage and its disaster risk pattern in Hunan Province, which provides a scientific basis for "preventive protection" of cultural heritage. This study is mainly based on the existing data, and in the future, the field research

Journal of Sustainable Built Environment

https://doi.org/10.70731/b3b1q080

Spatiotemporal Characteristics of Built Environment Impacts on Street Vitality in Central Nanchang: A Multiscale Geographically Weighted Regression Approach

Zheng Gong [a], Qiyang Zhao [a,*], Wentao Song [a], Zhiling Jian [a]

[a] *School of Earth Sciences, East China University of Technology, Nanchang 330013,China*

KEYWORDS

Street Vitality;
Built Environment;
Multiscale Geographically Weighted Regression (MGWR);
Street View Imagery;
Nanchang City

ABSTRACT

Exploring the impact of the built environment on street vitality is essential for enhancing urban public spaces. Using the central urban area of Nanchang City as a case study, multi-temporal street vitality is measured with population heat data. A multi-dimensional built environment indicator system is developed based on macro-scale neighborhood composition and micro-scale street characteristics, using street view imagery, POI data, and OSM road network data. The spatiotemporal variations in the influence of built environment factors on street vitality are examined through a multiscale geographically weighted regression (MGWR) model. Results reveal that: (1) Street vitality is most prominent between 10:00 and 20:00, with a spatial pattern of "eastern core, western belt, and multiple clustered points" across all time periods. (2) Macro-scale neighborhood composition generally has a stronger impact on street vitality than micro-scale street characteristics. (3) The influence of various built environment factors on street vitality exhibits significant spatiotemporal heterogeneity. Factors like sky view openness and parking lot density show robust spatiotemporal variations, while connectivity, facility densities, walkability, street ratio, and green view index have localized spatiotemporal effects.

1. Introduction

Streets, as multifunctional aggregators within urban landscapes, not only facilitate the city's daily transportation needs but also serve as vital public spaces for social interaction and leisure activities among residents. Street vitality, perceived through the lens of human activity within these spaces, reflects the concentration of people in streets and stands as a significant indicator of urban vibrancy[1].Influenced and constrained by the built environment that accommodates human spatial activities, street vitality is shaped by the continuous organization and succession of urban functions. Both the aggregation of resources at the macro neighborhood level and the composition of the spatial environment at the micro street level contribute to the temporal and spatial distribution differences of vitality within urban street spaces[2]. Against the backdrop of high-quality urban development aimed at creating desirable living environments, the quality of urban public spaces has garnered increasing attention from residents. Investigating the impact mechanisms of the built environment on street vitality across multiple scales is crucial for fostering human-centered public spaces and enhancing urban living environments.

* Corresponding author. E-mail address: 2124566697@qq.com

Received 18 March 2025; Received in revised form 24 March 2025; Accepted 29 March 2025; Available online 31 March 2025.

Existing research has predominantly focused on uncovering the effects of the built environment on street vitality, considering both macro neighborhood characteristics and micro street compositions, and has constructed multi-element indicators from perspectives such as location, interface accessibility, functionality, and facilities[3-5]. Early small-scale case studies based on field research delved into observing interface characteristics, facility arrangements, and landscape compositions within micro street spaces[4-5]. Subsequently, the advent of the new data wave has expanded the research scale of street vitality through the integration of multi-source big data, with POI and road network data widely applied to measure the density distribution of neighborhood resources and the accessibility of transportation and facilities at the urban scale[6-7]. However, compared to the detailed measurements at the neighborhood scale that focus on micro street characteristics, the large-scale measurements at the urban scale are limited by data collection and analysis methods, often remaining at the two-dimensional material space level and seldom addressing the micro three-dimensional street space characteristics from the perspective of human subjective perception and experience. Recent advancements in machine learning and image segmentation within the computer science field have provided new methodologies for the large-scale measurement of three-dimensional built environment indicators of streets[8]. Related studies, based on image semantic segmentation and large-scale image recognition technologies, have automated the extraction of elements such as sky, buildings, and roads from street view images to form three-dimensional built environment indicators of streets, applying these to the measurement and evaluation of street quality[9-10], urban functional area identification[11], and urban spatial perception[12].

In exploring the relationship between the built environment and street vitality, existing research has predominantly employed linear regression models[13], analyzing the impact differences of various built environment elements on street vitality based on the linear distribution trends of sample values among variables. However, traditional linear regression analysis focuses on exploring the effect of variables on vitality at a global scale through the linear distribution differences of indices, neglecting the spatial distribution patterns of variables at the meso and macro scales. For streets within a city, the similarity of their regional environment and their inherent attractiveness determine a certain degree of similarity and dependency in attracting people among nearby streets[14], thereby forming a differentiated distribution of vitality and the built environment in space. Recently, scholars have utilized the multi-scale geographically weighted regression model (MGWR) to explore neighborhood vitality[14], housing prices[15], the proportion of public transport commuting[16], and their influencing mechanisms, preliminarily validating its applicability in studying the differentiation of spatial characteristics at the urban scale. This method addresses the lack of consideration for spatial heterogeneity in traditional linear regression models by setting differentiated bandwidths for each variable to form different spatial action scales, thereby providing a more realistic explanatory power to the overall spatial model[17-18].

In summary, this paper takes the central urban area of Nanchang as a case study, utilizing POI data and OSM road network data to measure the two-dimensional material space environment, and further employs street view data to measure the micro three-dimensional space environment from the perspective of human subjective perception and experience. Finally, the multi-scale geographically weighted regression model (MGWR) is introduced to explore the temporal and spatial differences in the impact of various built environment elements on street vitality, offering insights and references for the differentiated creation of urban vitality and the enhancement of public space quality.

2. Research Object and Data Sources

2.1. Research Object

The case study area is selected as the central urban area of Nanchang, Jiangxi Province, with its spatial scope defined as the area within the Dongxi Lake District and the Honggutan New District of Nanchang City, which is the concentrated construction area and highly populated area of Nanchang City, covering a total area of approximately 114 km². For convenient comparative analysis, the road network within the research scope is divided into 651 street segments, serving as the basic units for this study (Figure 1). As the traditional core area of the city, the central urban area of Nanchang is the political, economic, and cultural center of Wuhan City, with a large concentration of population, commercial, office, residential, educational, and ad-

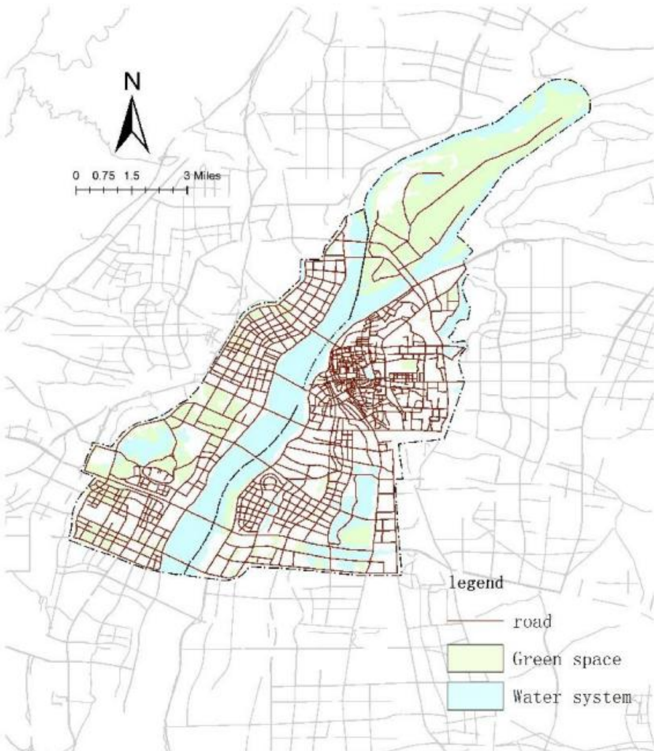

Figure 1 | Distribution of streets in the central urban area of Nanchang

ministrative facilities, forming differentiated urban spatial built environments and human activity distribution characteristics within the region.

2.2. Data Sources and Processing

The basic data of this paper mainly include four categories: road network data, population heat data, street view image data, and POI data:

Road Network Data: The road network data of the central urban area of Nanchang is sourced from the OpenStreetMap website (www.openstreetmap.org). Based on the ArcGIS 10.8 platform, the road network data is cleaned and topologically processed, and then interrupted at intersections. Subsequently, road buffers are constructed based on the road centerline with a buffer distance of 55 meters. This range basically includes the road red line range and its surrounding shops, open spaces, and other areas that may affect street vitality.

Population Heat Data: The population heat data is sourced from the Baidu Map Huiyan Big Data Platform (https://huiyan.baidu.com). Using Python to access the server's open port, location service data of the central urban area of Nanchang is collected continuously for 24 hours from May 5, 2025, to May 11, 2025, with the data format being "longitude_latitude_value". Since the activity state of people when using mobile devices is mostly walking or staying, the instantaneous positioning data generated in this state can effectively reflect the real location information of people at specific times[19].

Street View Data: The street view data is obtained from the Baidu Street View Application Programming Interface (http://bsyun.baidu.com). First, based on the vector road network of the central urban area of Nanchang, a sampling point coordinate is obtained every 100 meters, and a Python program is written to call the server interface to obtain panoramic images of the sampling points. A total of 35,687 panoramic street view images are collected starting from May 2024. Then, the PSPNet model pre-trained on the MIT ADE20K dataset is used to semantically segment the panoramic images, identifying and calculating the area proportion of street built environment elements such as sky, green plants, buildings, and roads in the street view images. PSPNet, as a commonly used method in street view image semantic segmentation, effectively reduces the probability of misidentification by applying a pyramid pooling module to extract and fuse multi-layer features of images, and is one of the current image recognition algorithms with high data classification accuracy[20].

POI Data: The POI data is sourced from Tencent Maps, with the acquisition time being June 2024. The data covers 16 major categories including food, corporate enterprises, hotels, tourist attractions, and infrastructure, and has advantages in describing the functional diversity of streets and the spatial distribution of stations. Considering the spatial layout forms on both sides of roads of different grades, a total of 132,316 POI points are obtained after intersecting with the street buffers within the research scope through the ArcGIS 10.8 platform.

3. Research Methods and Technical Path

3.1. Indicator Construction

3.1.1. Measurement of Street Vitality Intensity

Referring to existing research on the scale measurement of street vitality, this paper quantifies street vitality as the aggregation intensity of people staying or walking slowly in space. First, based on the acquired location service data, population heat points are visualized on the ArcGIS 10.8 platform according to coordinate information and value values. Second, through kernel density analysis, population heat points are generated into heat grids with a search radius of 200 meters and a cell size of "20 meters x 20 meters", totaling 128 images. Using the natural breakpoint mean of each grid as the division standard, the reclassification tool is used to divide the heat grid values into 7 levels, and then the raster to polygon tool is used to vectorize the graded heat grids. Finally, the vector grids are intersected with each road buffer, and based on the face data with vitality intensity levels within the intersected buffer and the buffer area, a weighted average is performed to obtain the vitality intensity value of each road segment. The specific calculation formula is as follows:

$$Q = \frac{\sum_{i=1}^{n} A_i Q_i}{\sum_{i=1}^{n} A_i} \tag{1}$$

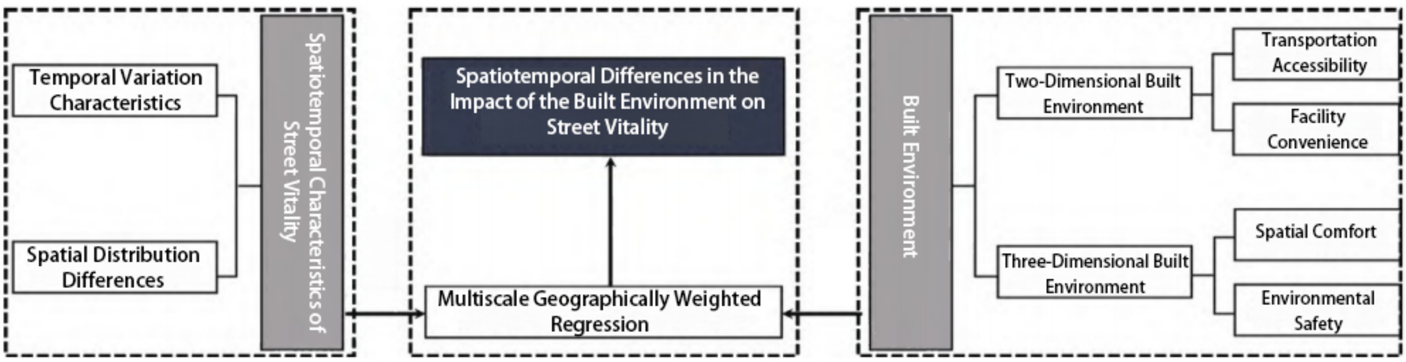

Figure 2 | Technical Path

Table 1 | Calculation statistics of the built environment elements

Built environment	Evaluation level	Evaluation metrics	Quantification of metrics
Two-dimensional built environment	Traffic convenience	The nearest distance to a transportation station	Using the Nearest Facility Point Analysis tool in ArcGIS 10.8 software, the actual distances from the midpoint of streets to the nearest bus stops and subway stations were calculated to reflect the accessibility of the streets
		Parking lot density	The number of parking lots within a 55-meter buffer zone on both sides of the street centerline
		Convenience	The accessibility of a street to nearby streets was analyzed by calculating the ratio of the number of street intersections to the length of the street.
	facility convenience	Functional mixing degree	The location entropy of major points of interest (POIs) within the street buffer zone reflects the diversity of facilities
		Catering function	The ratio of the number of catering facilities within a 55-meter buffer zone on both sides of the street centerline to the length of the street was calculated using the ArcGIS Spatial Join tool
		Entertainment function	The ratio of the number of Entertainment within a 55-meter buffer zone on both sides of the street centerline to the length of the street was calculated using the ArcGIS Spatial Join tool
		Shopping function	The ratio of the number of accommodation hotels within a 55-meter buffer zone on both sides of the street centerline to the length of the street was calculated using the ArcGIS Spatial Join tool
Three-dimensional built environment	Space comfortability	Sky openness	The average proportion of sky elements in street view images within the street unit reflects the degree of spatial openness
		Green light rate	The average proportion of vegetation elements in street view images within the street unit reflects the level of greenery
		Architectural Continuous Process	The standard deviation of the building-to-space ratio within a street reflects the degree of continuity of the building interface.
		Enclosure degree	The ratio of buildings, walls, columns, fences, and trees within street view images reflects the degree of enclosure in the street space
	environmentl safety	Road surface feasibility	The average ratio of pedestrian walkways to roadways within the street reflects the scale of pedestrian space
		Relative pedestrian width	The average ratio of pedestrian pathways to roadways within a street reflects the scale of pedestrian space.
		Traffic safety	The proportion of the midpoint of the street to traffic safety facilities, along with the average ratio of railings and columns within the street, reflects the level of traffic safety, as well as the distance to the nearest subway entrance

Where Q isthe street vitality intensity, Q_i is the vitality intensity level corresponding to the i-th unit within the street, A_i is the area of unit i, and n is the number of face data of each level within the road buffer. The built environment indicators that meet the conditions are used as independent variables to construct the MGWR model with street vitality at each time period to explore the temporal and spatial differences in the impact of different built environment elements on street vitality .

3.1.2. Measurement of Built Environment Indicators

Referring to the existing indicator composition of street vitality influencing factors[21-22], 14 built environment elements are preliminarily selected for measurement from four levels: transportation accessibility, facility conveuilt environment includes 8 indicators such as sky openness, enclosure degree, and green view rate, reflectinnience, spatial comfort, and environmental safety, including two-dimensional spatial environment indicators focusing on macro neighborhood characteristics and three-dimensional spatial environment indicators focusing on micro street composition. Among them, the three-dimensional bg the micro street spatial composition environment from the perspective of human subjective perception and experience at the three-dimensional level. These indicators can provide references for the design of local street spaces and the improvement of human settlements. The composition and calculation rules of each indicator are shown in Table 1.

3.2. Analysis Methods

This paper adopts the multi-scale geographically weighted regression model to explain the temporal and spatial differences in the impact of two-dimensional and three-dimensional built environments on street vitality. The multi-scale geographically weighted regression model (MGWR) improves on the classic geographically weighted regression model (GWR) by addressing the limitation that variables can only choose the same bandwidth.

The model sets different bandwidths for each variable to present different scale characteristics. The smaller the bandwidth selected for a variable, the smaller its impact on the overall spatial scale and the stronger its spatial heterogeneity. Conversely, the larger the bandwidth selected for a variable, the more stable it is on the global scale[23]. The calculation formula is as follows

$$y_i = \sum_{j=1}^{k} \beta_{bwj}(u_i, v_i)x_{ij} + \epsilon_i \tag{2}$$

Where X_{ij} is the j-th predictor variable, (U_i, U_v) are the centroid coordinates of street segment i, and β_{bwj} represents the bandwidth of the regression coefficient for the j-th variable. This study uses MGWR 2.2 software for model calculation and completes visual analysis based on the ArcGIS 10.8 platform

3.3. Technical Path

First, Baidu Huiyan population heat data is used to measure and deconstruct the temporal and spatial variation characteristics of street vitality in the central urban area of Nanchang at different times of the day. Second, POI data, OSM road network data, and Baidu street view data are used to measure the two-dimensional and three-dimensional built environment. Finally, spatial autocorrelation analysis and linear regression analysis are used to screen variables.

4. Temporal and Spatial Variation Characteristics of Street Vitality in the Study Area

4.1. Temporal Variation Characteristics of Street Vitality Intensity

To intuitively reflect street vitality, the calculated average heat value of streets is represented as a line chart. The statistical results are shown in Figure 3: The fluctuation situation can be roughly divided into four stages: the morning period from 7:00 to 11:00, the noon period from 11:00 to 15:00, the afternoon period from 15:00 to 19:00, and the night period from 19:00 to 23:00. During different times of the day, there are multiple transient heat peaks. Street vitality reaches its first peak at 12:00, consistent with the rapid gathering of people during the morning peak period. From 12:00 to 14:00, it gradually decreases. After that, entertainment and commercial activities in the central urban area gradually become active. Due to the influence of the evening peak and nightlife activities, the number of people in the streets reaches a peak around 20:00, but after that, gathering activities gradually decrease, leading to a rapid decline in street vitality.

The Baidu heat data is divided into 6 levels using the natural breakpoint method, with levels 1-2 classified as low vitality areas, levels 3-4 as medium vitality areas, and levels 5-6 as high vitality areas. The Baidu heat data obtained through vectorization processing is used to count the area proportion of each level, and the proportion of streets with different vitality levels is studied. The statistical results are shown in the table.

Analyzing the proportion of streets with different vitality levels, it can be seen that during the morning peak from 7:00 to 9:00, the proportion of high vitality streets and medium vitality streets is low, and they start to rise with

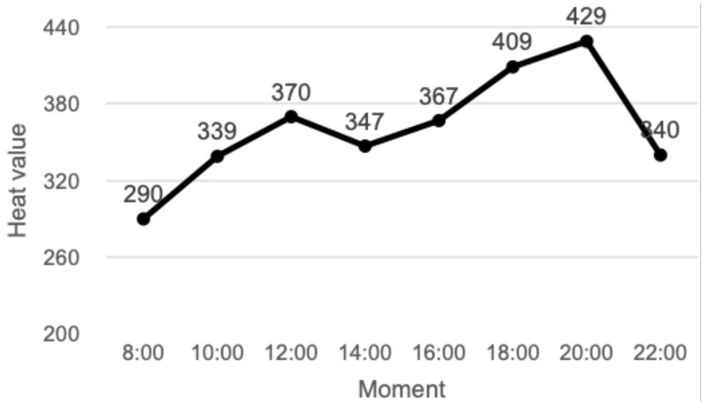

Figure. 3 | Variation of Overall Street Vitality in the Central Urban Area of Nanchang

Table. 2 | Statistics of Instantaneous Vitality Intensity Proportion in Streets of Central Urban Area of Nanchang

Time period	Type of fluctuation	Heat value	Volatility
07:00-11:00	Rapid rise	290-339	0.17
11:00-13:00	Slowly rising	339-370	0.09
13:00-15:00	Slow descent	370-347	-0.06
15:00-17:00	Slowly rising	347-367	0.06
17:00-19:00	Rapid rise	367-409	0.11
19:00-21:00	Slowly rising	409-429	0.05
21:00-23:00	Fast descent	429-340	-0.21

roughly the same trend. Due to the relatively dispersed distribution of people during lunch time, the proportion of high vitality streets and medium vitality streets shows a slow downward trend from 11:00 to 13:00. At 18:00 in the afternoon, the proportion of medium vitality streets is relatively high, reaching a vitality peak. At 20:00 at night, the proportion of high vitality streets is relatively high, reaching a vitality peak, while the proportion of medium vitality streets is relatively low. This phenomenon can be attributed to the further gathering of people's activities in the central urban area at night. It can be inferred that the intensity of people's activities in the morning is usually higher than that during the noon period. The density of people in the neighborhood gradually increases after lunch time, indicating that the leisure activities of neighborhood people usually reach a peak from after lunch time to the evening.

4.2. Spatial Differentiation Characteristics of Street Vitality Intensity

To further explore the spatial differentiation characteristics of street vitality at different times of the day, especially during the main activity periods, the average vitality of streets during four time periods: 7:00-11:00 (morning), 11:00-15:00 (noon), 15:00-19:00 (afternoon), and 19:00-23:00 (night) is visualized. The analysis results in the spatial distribution map of the comprehensive heat value of streets on weekdays (Figure 4). From Figure 4, it can be seen that the overall street vitality in the central urban area of Nanchang shows a spatial differentiation pattern of "east core, west belt, multi-point aggregation", with medium and high value areas forming differentiated distributions with time changes. It can be seen that high vitality streets and medium vitality streets on weekdays are mostly concentrated in the central part of the old city, and the vitality of streets in the north is significantly higher than that in the south. Specifically, high vitality streets are mainly con-

Table 3 | Statistics of Instantaneous Vitality Intensity Proportion in Streets of Central Urban Area of Nanchang

	8:00		10:00		12:00		14:00	
	Quantity	Ratio	Quantity	Ratio	Quantity	Ratio	Quantity	Ratio
High-energy street	10	1.54%	30	4.61%	45	6.91%	33	5.07%
Mid-energy street	96	14.75%	123	18.89%	118	18.13%	112	17.20%
Low-energy street	545	83.72%	498	76.50%	488	74.96%	506	77.73%
	16:00		**18:00**		**20:00**		**22:00**	
	Quantity	Ratio	Quantity	Ratio	Quantity	Ratio	Quantity	Ratio
High-energy street	44	6.76%	55	8.45%	71	10.91%	48	7.37%
Mid-energy street	136	20.89%	147	22.58%	102	15.67%	95	14.59%
Low-energy street	471	72.35%	449	68.97%	478	73.43%	508	78.03%

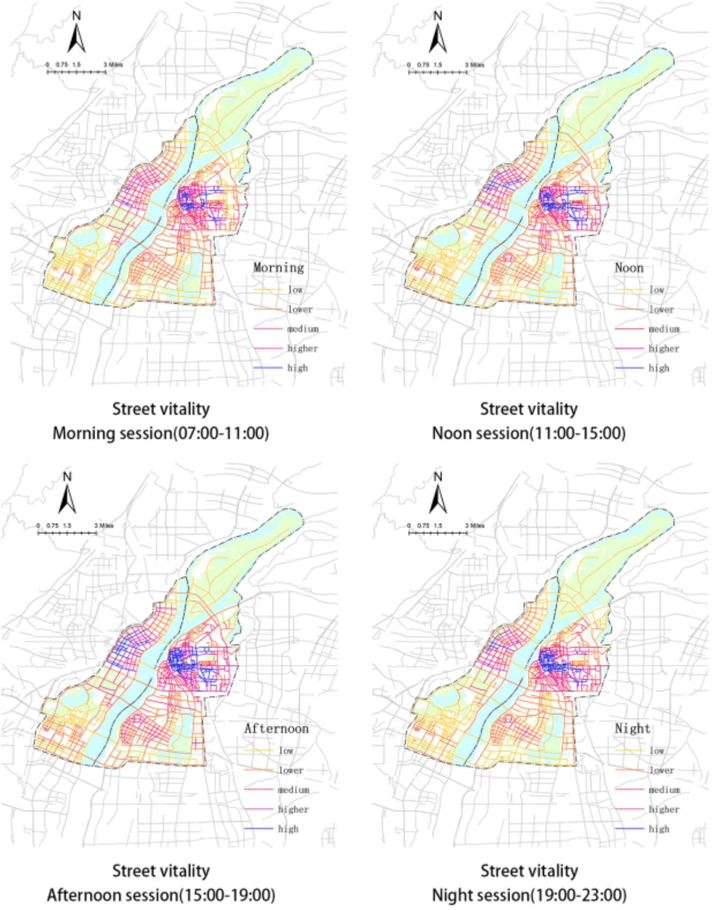

Figure 4 l Spatial Variation of Street Vitality Intensity Across Different Time Periods

centrated in the cultural and tourism integration area within the Wanshou Palace historical urban area and the traditional commercial center area of Zhongshan Road-Shengli Road Pedestrian Street. Although this area is an old city, it has a large concentration of shopping, dining, and accommodation resources, rich tourism resources, complete public service functions, and well-equipped living facilities. Secondly, the central area of Honggutan, centered on Central Financial Street, also has high street vitality, including CBD, Qiushui Square, etc. This area has well-equipped commercial facilities and high transportation accessibility, making it easy to gather vitality. It can be seen that the street vitality in the central urban area shows a trend of decreasing from the central area on both sides of the Gan River to the suburbs, and a distribution of central aggregation and stronger north than south.

5.Spatiotemporal Heterogeneity in the Impact of Street-Level Built Environment on Urban Vitality Intensity: a Multiscale Analysis

5.1.Analytical Framework for MGWR Model Results

5.1.1.Screening of Built Environment Indicators

First, spatial autocorrelation analysis is conducted on the 14 built environment indicators, and the results show that all variables have obvious clustering characteristics in space. From the global Moran's index statistics, the nearest distance to comprehensive shopping malls, proximity, and the nearest distance to transportation stations have very strong clustering characteristics (Table 4). Then, ordinary least squares (OLS) is further used to perform regression analysis with the 14 multi-dimensional built envi-

Table 4a l Results of Spatial Autocorrelation and Multicollinearity Diagnostics for the Built Environment

First-level indicators		Two-dimensional built environment						
		Traffic convenience			facility convenience			
Secondary indicators		Transportation distance	Parking lot density	Connectivity	Functional mixing degree	Catering function	Entertain-ment function	Shopping function
Space-time self-correlation	Global Moran's index Numeric	0.440341	0.334867	0.682102	0.252610	0.167312	0.297193	0.777576
	Variance	0.000004	0.000004	0.000004	0.000004	0.000004	0.000004	0.000004
	Z score	171.765156	225.414225	348.521286	129.080649	85.559826	152.102850	397.443716
	P-value	0.000000	0.000000	0.000000	0.000000	0.000000	0.000000	0.000000
Collinearity Diagnosis	Variance inflation factor	1.563141	1.494003	1.590602	1.645913	1.385783	1.747346	1.505872

Table 4b | Results of Spatial Autocorrelation and Multicollinearity Diagnostics for the Built Environment

First-level indicators		**Three-dimensional built environment**						
		Space comfortability				environmentl safety		
Secondary indicators		Sky openness	Green light rate	Architectural Continuous Process	Enclosure degree	Road surface feasibility	Relative pedestrian width	Traffic safety
Space-time self-correlation	Global Moran's index Numeric	0.144728	0.235639	0.089482	0.317182	0.084996	0.089482	0.112461
	Variance	0.000004	0.000004	0.000004	0.000004	0.000004	0.000004	0.000004
	Z score	171.765156	162.072935	45.788505	129.080649	45.194476	185.559826	57.571604
	P-value	0.000000	0.000000	0.000000	0.000000	0.000000	0.000000	0.000000
Collinearity Diagnosis	Variance inflation factor	1.252827	1.371032	1.420298	3.133947	1.065539	1.385783	1.058528

ronment elements as independent variables and the street vitality values at each time period as dependent variables. The results show that the VIF values of all independent variables are far below 75 (Table 4), indicating that there is no multicollinearity problem among the variables. However, the probability p-values of relative pedestrian width and building continuity are greater than 0.01 in all time periods, indicating that their impact on street vitality is not significant and needs to be excluded. Finally, the remaining 12 built environment indicators participate in the subsequent model construction.

5.1.2. Model Regression Results

According to the temporal variation characteristics of street vitality intensity, the street vitality and built environment indicators of the four time periods are introduced into the multi-scale weighted regression model for analysis (Table 5). The results show that the average adjusted R^2 of the MGWR model in each time period is 0.844, indicating that its overall explanation degree of street vitality changes in the central urban area of Nanchang is as high as 84.4% on average. Subsequently, based on the regression coefficients, variable interpretability, and spatial action scale (bandwidth), the temporal and spatial effects of different built environment elements on street vitality in each time period are further analyzed. The regression coefficients of the three-dimensional built environment indicators are relatively high overall, but there are differences in variable influence and interpretability in different time periods.

5.2. Spatiotemporal Differences in the Impact of Two-Dimensional Built Environment on Street Vitality

5.2.1. Temporal Differences in the Two-Dimensional Built Environment

(1) Transportation Accessibility

Parking lot density showed a positive correlation with street vitality across all time periods, with higher significance overall. Its influence was stronger in the morning and midday compared to the afternoon and evening, indicating that the capacity for vehicle parking in street spaces positively promotes vitality. Connectivity also demonstrated a positive impact on vitality, particularly during daytime hours when pedestrian accessibility attracts natural travel choices. However, the average distance to the nearest transportation hub exhibited a negative correlation with street vitality across all periods, though its explanatory power was negligible. This may be due to the relatively balanced distribution of transportation hubs in Nanchang's central urban area[25], resulting in minimal differences in accessibility between streets (Figure 5).

Facility Accessibility

The explanatory power of dining facilities on street vitality (37.79%-68.97%) remained consistently high across all periods. This is primarily because dining facilities cater to various needs throughout the day, including breakfast, lunch, afternoon tea, dinner, and late-night snacks, ensuring a steady flow of people and sustaining street vitality. Shopping facilities had the highest absolute regression coefficients (0.159-0.234) across all periods, with their positive influence peaking during the evening. Their explanatory power (51.31%-70.20%) was also consistently high, highlighting the strong promotional effect of commercial activities on street vitality. However, the localized clustering

Table 5 | Statistical Summary of Regression Results from the Multiscale Geographically Weighted Regression (MGWR) Model

Variable	07:00-11:00			11:00-15:00			15:00-19:00			19:00-23:00		
	Bandwidth	Average value	Variable interpret ability	Bandwidth	Average value	Variable interpret ability	Bandwidth	Average value	Variable interpret ability	Bandwidth	Average value	Variable interpret ability
The nearest distance to a transportation station	221	-0.053	0	189	-0.012	0	650	-0.041	0	650	-0.023	0
Parking lot density	646	0.082	100	650	0.081	100	507	0.075	73.58	650	0.057	57.93
Convenience	650	0.181	80.65	650	0.133	57.31	252	0.136	57.30	268	0.118	56.99
Functional mixing degree	650	-0.065	0	650	-0.066	0	650	-0.067	0	650	-0.115	0
Catering function	650	0.070	37.79	650	0.072	58.06	650	0.093	58.06	650	0.074	68.97
Entertainment function	650	0.002	14.75	650	0.010	17.97	650	0.011	51.77	650	0.009	39.63
Shopping function	257	0.159	62.83	236	0.158	70.20	249	0.195	51.31	236	0.234	70.20
Sky openness	650	-0.348	100.00	650	-0.073	100.00	650	-0.327	77.57	650	-0.338	100
Green light rate	338	0.605	0	198	-0.227	0	439	0.571	0	447	0.787	0
Enclosure degree	431	-1.313	0	650	0.108	0	431	-1.244	0	419	-1.568	0
Road surface feasibility	295	0.011	74.50	650	0.001	64.71	650	0.003	59.91	650	0.011	35.94
Traffic safety	650	0.216	53.92	650	0.032	54.84	650	0.205	36.71	148	0.257	14.13
Adjusted R-squared		0.835			0.843			0.852			0.846	

Note: Variable interpretability represents the percentage of the total sample size with significant coefficients ($p \leq 0.05$) for explanatory variables.

of commercial facilities led to spatially significant variations in their explanatory power.

Entertainment facilities showed an increasing positive correlation with street vitality as the day progressed, peaking in the evening. This indicates that the impact of leisure and entertainment facilities on street vitality is more pronounced at night due to their primary usage times. Functional mix exhibited a negative correlation with street vitality across all periods, suggesting that streets with lower functional mix tend to concentrate vitality more effectively. Specifically, streets dominated by single-use commercial activities are more likely to attract consumer behavior, with clear travel purposes for various facilities, especially at night.

5.2.2. Spatial Differences in the Two-Dimensional Built Environment

To explain the spatial heterogeneity of the influencing factors, ArcGIS 10.8 was used to visualize the coefficients of significant factors during the main activity periods. The spatial patterns of some variables are shown in Figures 6 and 7. Overall, connectivity, as a global variable, exhibited the most stable spatial influence on street vitality, followed by parking lot density. Entertainment and dining facilities showed significant spatial heterogeneity, while shopping facilities displayed distinct spatial differentiation.

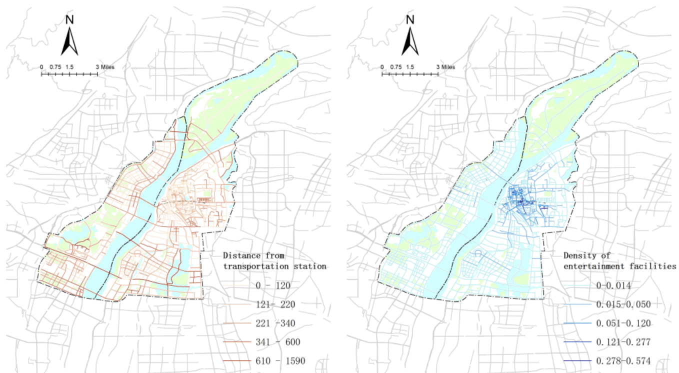

Distance from transportation station

Density of entertainmen

Figure 5 | Distribution of the Nearest Distance to Transportation Stations and Density of Entertainment Facilities in Streets

Specifically, the impact of connectivity on street vitality showed minimal spatial variation, with its positive influence gradually increasing from north to south throughout the day. High-value areas were concentrated in Jiuzhou and Chaonong streets in Xihu District, where parks and educational facilities are abundant, facilitating pedestrian activi-

Figure 6 | Spatial Distribution of Regression Coefficients forTraffic convenience

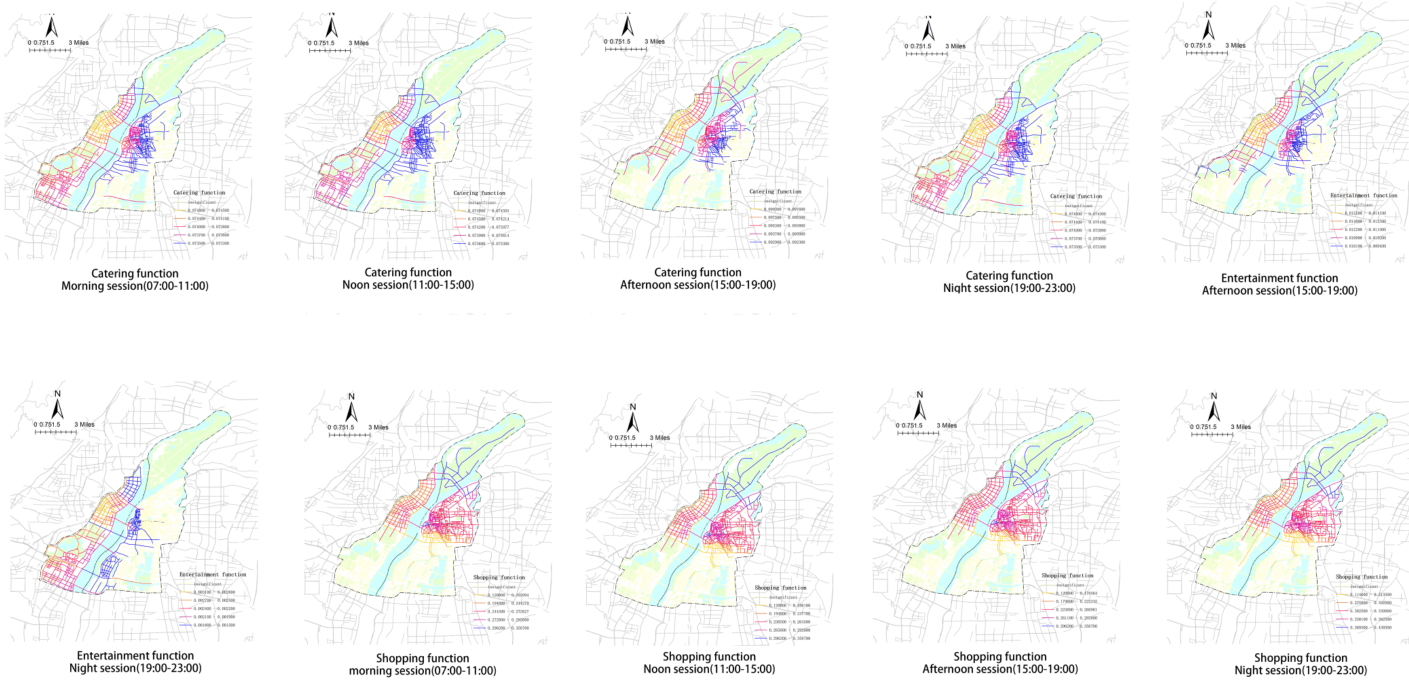

Figure 7 | Spatial Distribution of Regression Coefficients for Facility Convenience

ties such as sightseeing and commuting. In contrast, areas like Honggutan District's Hongjiaozhou and Jiulonghu streets, as well as Baihuazhou Street in the historical district, showed no significant impact due to the high density of transportation and educational facilities, which attract purpose-driven pedestrians unaffected by street connectivity.

The positive impact of parking lot density on street vitality generally increased from the central to the western areas. High-value areas were clustered in Dinggong Road and Pengjiaqiao streets in Donghu District, where limited

Figure 8 | Distribution of Green View Index and Enclosure Rate

Figure 9 | Spatial Distribution of Regression Coefficients for Spatial Comfort

vehicle access in the historical district necessitates parking before entering, enhancing the influence of parking density on vitality. In other areas, the availability of public transportation, such as subways and buses, reduced the reliance on parking facilities.

Dining facilities exhibited a positive influence on street vitality that decreased from the central to the western areas. High-value areas were concentrated in Dinggong Road and Shengjin Tower streets in Donghu District, where local cuisine in the old town enhances street attractiveness. Entertainment facilities showed positive correlations and significance in the afternoon and evening, with their influence decreasing from the central to the western areas. High-value areas were mainly located in the historical districts of Donghu and Xihu Districts, where abundant tourism and leisure resources attract visitors and sustain high street vitality.

Commercial facilities displayed localized clustering in their positive influence on street vitality, with high-value areas concentrated in Tengwang Pavilion Street in Xihu District and Shajing Street in Honggutan District. These areas feature a mix of traditional and chain commercial establishments, attracting both local residents and tourists and enhancing street vitality.

5.3. Spatiotemporal Differences in the Impact of Three-Dimensional Built Environment on Street Vitality

5.3.1. Temporal Differences in the Three-Dimensional Built Environment

As shown in Figure 8, the regression coefficients of the built environment indicators across the four time periods were generally low, with significant variations in influence and explanatory power across different periods.

Spatial Comfort

The explanatory power of green view ratio and enclosure degree was negligible. This may be due to the dispersed distribution of greenery along roads and the relative clustering of vegetation around natural landscapes, rendering the green view ratio ineffective in explaining vitality. High pedestrian flow streets may not be significantly affected by enclosure degree, as the existing foot traffic is sufficient to sustain street vitality. Sky view openness exhibited a negative correlation and was significant across all four periods. Its negative influence gradually increased during the daytime, peaking in the afternoon. This is likely because streets with high sky view openness often lack building or tree cover, leading to functional monotony and a lack of commercial, cultural, or social activities that attract pedestrians. In the afternoon, people tend to gather in work areas, amplifying the impact of sky view openness on street vitality.

Environmental Safety

The average regression coefficient of walkability ratio showed a positive correlation with street vitality across all periods, with high explanatory power (35.94%-74.50%). Its positive influence was stronger in the morning and afternoon, as these periods involve commuting activities. A well-maintained pedestrian environment supports walking, cycling, and other modes of transportation, increasing street usage and attracting more customers, thereby promoting commercial activity. In contrast, traffic safety facilities had lower explanatory power (14.13%-54.84%), with their positive influence peaking in the afternoon when commuting demand is high. Properly designed traffic facilities can optimize traffic flow, reduce congestion, and enhance street attractiveness.

5.3.2. Spatial Differences in the Three-Dimensional Built Environment

As shown in Figure 9, sky view openness, as a global negative correlation variable, exhibited a spatial pattern of higher influence in peripheral areas and lower influence in central areas. High negative impact areas were concen-

Figure 10 | Spatial Distribution of Regression Coefficients for Traffic Safety

trated in Hongjiaozhou and Jiulonghu streets in the southwestern part of the central urban area, where large transportation and entertainment facilities dominate, and pedestrian activities are more purpose-driven. In contrast, Taohua Street and Shengjin Tower Street in the southern historical district showed relatively lower impacts on street vitality. These areas feature scenic landscapes and iconic buildings, where high sky view openness does not significantly affect pedestrian destinations or street activities.

As shown in Figure 10, the positive influence of walkability ratio on street vitality exhibited a spatial pattern of higher values in the west and lower values in the east. High-value areas were concentrated in Hongjiaozhou and Jiulonghu streets in the Honggutan New District, with additional clustering in Shajing Street during midday. This may be due to the presence of large commercial and office facilities in these areas, where pedestrians primarily use sidewalks for dining and commuting activities during lunchtime. The influence of traffic safety facilities on street vitality was concentrated near the historical district during midday and afternoon periods. This is because these periods involve diverse pedestrian activities, and the historical district's commercial vibrancy, combined with fewer vehicle lanes, enhances the pedestrian environment, attracting more customers and promoting commercial activities.

6. Conclusions and Discussion

This paper takes the central urban area of Nanchang as a case study, uses population heat data to measure and deconstruct the temporal and spatial differences of street vitality, uses OSM road network data and POI data to measure the two-dimensional material space environment, further uses street view images to measure the micro three-dimensional street space environment based on human subjective perception and experience, and uses the multi-scale geographically weighted regression model to explore the differentiation characteristics of multi-dimensional built environment and urban street vitality in time and space. The main conclusions are as follows.

The temporal and spatial distribution differences of street vitality in the central urban area of Nanchang are obvious. In terms of time, residents' activities on the streets are mostly concentrated from 6:00 to 23:00, with the highest proportion of medium and high vitality streets from 9:00 to 18:00. In terms of space, the spatial structure of street vitality generally shows a differentiation pattern of "east core, west belt, multi-point aggregation", and the aggregation characteristics are most obvious in the afternoon.

The impact of the two-dimensional built environment on street vitality is generally more significant than that of the three-dimensional built environment. Specifically, among the two-dimensional built environment indicators, parking lot density, connectivity, and shopping facility density have high interpretability for street vitality in all time periods, while catering facility density and entertainment function have high interpretability in some time periods. Among the three-dimensional built environment indicators, only sky openness and road surface feasibility have high interpretability for street vitality in most time periods.

The temporal and spatial heterogeneity of the impact of each built environment element on street vitality is obvious. In terms of transportation accessibility, the positive influence of connectivity on street vitality generally increases from north to south in space in all time periods

Data availability: Data will be made available on request.

Competing Interests: The authors declare that they have no known competing financial interests or personal relationships that could have appeared to influence the work reported in this paper.

1. Long Y ,Zhou Y, Study of chengduQuantitative Evaluation on Street Vibrancy and its impact Factors: A Case [J]. New Construction ,2016(1):52- 57.
2. Wu W J, Wu L Y, Shi X D, et al. Human Settlements and High-quality Development [J]. Urban Planning,2020,44(1):99-104.
3. Wang B L, Spatial impact of the built environment on street vitality: a case study of the Tianhe district, Guangzhou[J]. Frontiers in environmental science, 2022, 10: 966562.
4. Jiang L, Quantitative Assessment and Shaping Strategies for Urban

Street Vitality [D]. Dalian : Dalian University of Technology ,2013.
5. Huang D, DAI D H, Effect of Living Street's Elements on Vitality—Taking Typical Streets in Shenzhen as an Example [J]. Chinese Landscape Architecture ,2019,35(9):89-94.
6. Huang S H, WANG C S, Street Urbanism : Street Urbanism:Quantitative Evaluation on Wuhan Street Vibrancy and Its Impact Factors [J]. Shanghai Urban Planning Review ,2020(1):105-113.
7. Wang P, Long Y, Shi M, et al. Street Vibrancy of Beijing: Measurement, Impact Factors and Design Implication [J]. Shanghai Urban Planning Review ,2016(3):37-45.
8. Long Ying , Tang J X, Large-Scale Quantitative Measurement of the Quality of Urban Street Space: The Research Progress [J]. City Planning Review ,2019,43(6):107-114.
9. Guo X, Lai J D,Ma Z f, et al. Consistency analysis between virtual evaluation and on-site survey methods for street quality: A case study of streets in Shenzhen’s core transit areas. [J]. Planners ,2022,38(6):70-78.
10. Chen C, Chen Q J, Jia Z M, et al . Large-scale Measurement of the Quality of Urban Street Space Based on Physical Disorder Theory: A Case Study of Area within the Second Ring of Hefei City [J]. Southern Architecture ,2020(2):10- 18.
11. Wan J Q, Fei T. "ProductionLiving-Ecological Spaces" recognition method based on street view images[J]. Journal of Geo-information Science, 2023,25(4):838- 851.
12. Wu C, Ye Y, Gao F, et al. Using street view images to examine the association between human perceptions of locale and urban vitality in Shenzhen, China[J]. Sustainable cities and society, 2023, 88: 104291.
13. Niu X Y, Wu W S, Li M. LBS Positioning Data Influence of Built Environment on Street Vitality and Its Spatiotemporal Characteristics Based on [J]. Urban Planning International ,2019,34(1):28-37.
14. Fan L: Zhang D Y . Research on the Influence Mechanism and Spatial Heterogeneity Characteristics of Block Vitality in Beijing: Based on Multi-Scale Geographically Weighted Regression[J]. City Planning Review ,2022,46(5):27-37.
15. Shen T，Yu H C，Zhou L, et al. On Hedonic Price of Second-Hand Houses in Beijing Based on Multi-ScaleGeographically Weighted Regression:Scale Law of Spatial Heterogeneity [J]. Economic Geography ,2020,40(3):75-83.
16. An R, Wu Z, Tong Z, et al. How the built environment promotes public transportation in Wuhan: a multiscale geographically weighted regression analysis[J]. Travel behaviour and society, 2022, 29: 186-199.
17. Lao X, Gu H, Unveiling various spatial patterns of determinants of hukou transfer intentions in China: a multi-scale geographically weighted regression approach[J]. Growth and change, 2020, 51(4): 1860-1876.
18. Wu C, Ren F, Hu W, et al. Multiscale geographically and temporally weighted regression: exploring the spatiotemporal determinants of housing prices[J]. International journalofgeographicalinformationscience,2019,33(3):489-511.
19. WU Z Q, YE Z N, Research on Urban Spatial Structure Based on Baidu Heat Map: A Case Study on the Central City of Shanghai[J].City Planning Review,2016,40(4):33-40.
20. ZHAO H, SHI J, QI X, et al. Pyramid scene parsing network[C]//Proceeding of IEEE Conference on Computer Vision and Pattern Recognition. New York: IEEE, 2017.
21. Si R, Lin Y Y, Xiao Z P, et al. Spatio-temporal analysis of built environment and street vitality relationship based on street-level imagery: A case study of Futian District, Shenzhen. Scientia Geographica Sinica,2021,41(9):1536-1545.
22. MA0 Z R, CHEN X K, XIANG Z H, et al. Research on the Measurement and influencing Factors of Street Vigour in HistoricDistricts: A Case Study of Wenming Street Historic District in Kunming[]. South Architecture, 2021 (4):48-55.
23. FOTHERINGHAMA,YANGW,KANGW.Multiscalegeographicallyweightedregression(MGWR)[J].AnnalsoftheAmericanAssociationofGeographers,2017,107(6):1247-1265.
24. WANG Lucang.Central Areas of Wuhan City Spatial-temporal Characteristics of Urban Population Aggregation Based on Baidu Heat Map in[J].J. Sustain. Habitat West. China,2018,33(2):52-56.
25. Ren P, Peng J D, Yang H, et al. Relationship between jobs-housing balance and built environment in areas around urban rail transit stations of Wuhan[J]. Journal of Geo-information Science, 2021,23(7):1231-1245.

Journal of Sustainable Built Environment

https://doi.org/10.70731/3na6hj45

Investigating the Impact of Emotional Perception on Low-carbon Urban Travel: A Case Study of Wuhan Metro

Xuan Qin [a], Xiaoran Wu [a], Haining Tang [a], Ran Peng [a,*]

[a] *School of Civil Engineering and Architecture, Wuhan Institute of Technology, Wuhan 430074, China*

KEYWORDS

Metro Travel;
Emotional Perception;
Structural Equation Modeling (SEM);
Multi-Group Structural Equation Modeling (MSEM)

ABSTRACT

As urban metro systems play an increasingly vital role in public transportation, passengers' emotional perception has become increasingly crucial for enhancing their travel experience and quality of life. This study establishes a theoretical relational model for whole-process perception during metro travel. Structural Equation Modeling (SEM) was employed to validate the significant relationships between travel experience perceptions and passenger emotions throughout metro journeys. Furthermore, Multi-group Structural Equation Modeling (MSEM) was utilized to analyze group differences in emotional perception among populations with varying genders and travel frequencies. The findings reveal: (1) The impact mechanism demonstrates that metro passengers' travel emotions are positively influenced by pre-boarding/post-alighting perceptions, accessibility perception, and in-carriage perception, with accessibility perception exhibiting the strongest effect. (2) Group effect analysis indicates significant differences in metro travel emotional perception across gender groups and travel frequency subgroups.

1. Introduction

At the 75th United Nations General Assembly, China pledged to peak its carbon emissions by 2030 and achieve carbon neutrality by 2060. Given that transportation is a significant source of carbon emissions, the transportation sector needs to develop low-carbon transportation facilities and encourage the public to adopt green travel modes[1-2]. As a low-carbon transportation mode with large capacity, low emissions, and the ability to effectively alleviate traffic congestion, the metro has been favored by many cities. According to statistics from the Ministry of Transport of China[3] , as of September 2024, 54 cities in China have opened 313 urban rail transit lines, with an operational mileage of 10,440.5 kilometers and a monthly passenger volume of 2.58 billion.

With the continuous development of metro systems and the increase in passenger numbers, urban transportation management agencies face a dual challenge: on the one hand, they need to meet the growing basic transportation demands, and on the other hand, they need to provide high-quality and personalized travel experiences [4]. Although Chinese transportation authorities are working together to enhance the transportation service capacity of urban hubs to meet the diverse needs of the population, there are still challenges in meeting passengers' psychological and emotional needs during travel [5].

In 2019, China launched the "Healthy China Action (2019-2030)," which set a goal of raising the level of public mental health literacy to 30% by 2030 [6]. Mental health is not only of great significance to individual development but also plays a key role in the overall well-being of society. Studies have shown that more than 70% of diseases are related to negative emotions (e.g., depression, anxiety, and stress) [7]. Moreover, frequent negative emotions (such as depression, irritability, anxiety, and stress) can also lead to

* Corresponding author. E-mail address: pengran@wit.edu.cn

Received 14 February 2025; Received in revised form 14 March 2025; Accepted 22 March 2025; Available online 31 March 2025.

many social problems [8]. Emotions not only reflect the current psychological state and feelings but also reflect the psychological demand for a better urban environment and public services [9]. Given this, it is particularly urgent and important to explore the impact of emotional perception in urban metro travel and to enhance positive emotions in people's daily travel to promote sustainable transportation development.

This study first constructs a theoretical model of the entire process of metro travel perception. Subsequently, the study uses Structural Equation Modeling (SEM) to analyze the impact mechanism of each stage of the metro travel process on passengers' travel emotions. Meanwhile, Multi-group Structural Equation Modeling (MSEM) is employed to analyze differences among different groups, with a focus on the differences in emotional perception during metro travel among groups with different genders and travel frequencies.

In the following sections of this study, Section 2 is the literature review; Section 3, "Theoretical Research and Hypotheses," introduces the theoretical and methodological approaches and proposes the hypotheses; Section 4, "Research Design and Data Analysis," describes the sources and methods of data collection; Section 5, "Model Construction and Analysis," introduces the Structural Equation Modeling and Multi-group Structural Equation Modeling, using SEM to analyze the impact mechanism and MSEM to analyze group effects; Section 6 summarizes the results and main findings of this study, and discusses the limitations and future research prospects.

2. Literature Review

Passenger travel emotions have become a prominent research topic in the field of urban transportation. Numerous studies have explored factors influencing passenger travel emotions, including environmental perception, service quality, mode choice, and travel time, purpose, and companions.

In terms of environmental perception, Yazdanpanah and Hosseinlon [10] found that adverse weather conditions can increase passengers' negative emotions. Balaban et al. [11] demonstrated that passengers experience varying emotions when navigating public transit spaces, depending on their perception of these spaces. Cox et al. [12] revealed a significant correlation between crowding and negative emotions among UK railway passengers, while Mahudin et al. [13] developed a scale to measure railway passenger crowding and investigated its psychometric properties. Meenar et al. [14], based on a survey of bike-transit users (CTUs) in Philadelphia, USA, found that negative emotions were more prevalent than positive emotions during travel, often linked to specific geographic locations or operational management issues. Chen and Yan et al. [15] used SEM and MGWR models to show that urban architectural design, layout, and surrounding public spaces directly influence passengers' psychological states.

Regarding service quality, Delaplace and Dobruszkes [16], using France as a case study, identified fare, convenience, and speed as key service attributes affecting passenger emotions. Alberto et al. [17] highlighted the correlation between service disruptions and negative passenger emotions. Zhai et al. [18] found that proximity to metro stations significantly enhanced passengers' positive emotions, whereas greater distances increased the likelihood of negative emotions.

In terms of mode choice, St-Louis et al. [19] demonstrated in Canada that slower modes such as walking and cycling tend to elicit more positive emotions. Páez and Whalen[20], also in Canada, found that walking and cycling commuters experienced more positive emotions compared to car and bus users. Le and Carrel [21] revealed that public transit users generally experience more negative emotions than car users but feel slightly less stress and frustration.

Concerning travel time, purpose, and companions, Morris and Guerra [22]found in the US that travel duration had little impact on passengers' emotional states. Watkins et al. [23] noted that uncertainty in travel time can cause psychological stress and irritability. Olsson et al. [24], in Sweden, found that social and recreational activities can enhance positive emotions and mitigate stress and boredom for long-distance commuters. Zhu et al. [25], using 2012–2013 US time-use survey data, explored the relationship between daily travel behavior and emotional well-being, particularly the effects of travel mode, duration, purpose, and companions. Their study showed that cycling is the most enjoyable mode, travel duration negatively correlates with happiness, dining-related trips generate the highest happiness, and traveling with family and friends enhances positive emotions. Zhang et al. [8], in China, found that the choice of travel companions influences individuals' emotional states during daily travel.

Existing literature confirms that environmental perception, service perception, mode choice, and travel time, purpose, and companions all influence passenger travel emotions. However, most studies focus on specific factors, with limited exploration of how the entire travel process affects passenger emotions. Additionally, research on the emotional impact of metro travel remains scarce. Furthermore, subjective perceptions and travel habits vary across groups due to individual differences and travel contexts, leading to diverse emotional perceptions.

To address these gaps, this study investigates the mechanisms influencing passenger travel emotions through perceptions before boarding, after alighting, accessibility, and in-carriage experiences during metro travel. It also examines group differences in emotional perception based on gender and travel frequency. By doing so, this research aims to explore the impact of metro travel on passenger emotions and promote the sustainable development of low-carbon transportation infrastructure.

3. Theoretical Analysis and Hypotheses

3.1. Theoretical Analysis

Arnold's theory of emotion posits that emotion is a "reaction to an object or situation"[26]. The necessary condition for the generation of emotion is the individual's perception of a specific stimulus event. Once perceived, the individual automatically evaluates the event, and this evaluation leads to an emotional response regarding the relevance of the stimulus to the individual's well-being, resulting in various needs and behaviors to approach or avoid the stimulus [27]. Based on Arnold's theory, we define metro travel as a "stimulus event." Passengers perceive the entire process of metro travel, and this perception automatically generates an evaluation, which in turn produces emotions.

The cognitive theory of emotion suggests that emotions and feelings are reactions to the relationship between objective reality and personal needs [28]. The person-environment fit theory indicates that an individual and their environment may achieve a state of mutual adaptation or may experience inconsistencies. When the external environment meets an individual's needs, it helps to elicit positive emotions; conversely, if the environment fails to meet these needs, it may lead to emotional problems and related negative impacts [29]. When an individual traverses a public transport space, they experience different feelings and emotions based on their perception of the space [30]. Therefore, in the perception process, we categorize the entire metro travel experience into pre-boarding and post-alighting perceptions, in-carriage perceptions, accessibility perceptions, and emotional perceptions. Since passengers' needs and environments before boarding and after alighting are essentially the same, we do not consider pre-boarding and post-alighting perceptions separately but include them together in our analysis. Thus, we measure metro travel emotions based on these four aspects of perception.

Based on Arnold's theory of emotion, we establish the path for the generation of metro travel emotions (Figure 1). By analyzing passengers' perceptions of the entire metro travel process using the cognitive theory of emotion and the person-environment fit theory, we identify the key factors. Following the path of emotion generation, we collect data on passengers' different perceptions and subjective emotions during travel through questionnaires. We then use Structural Equation Modeling (SEM) and Multi-group Structural Equation Modeling (MSEM) to analyze the collected data and explore the impact mechanisms of each stage of metro travel on passengers' travel emotions.

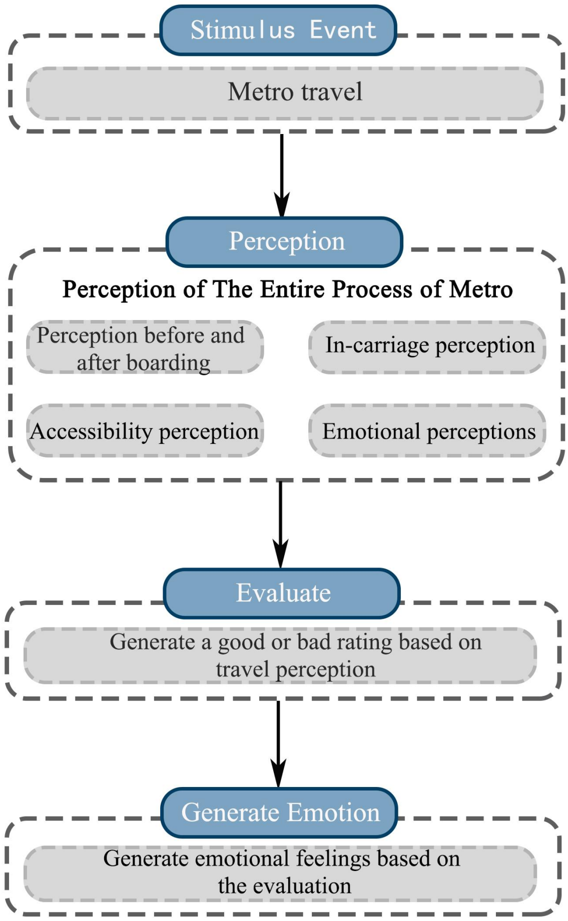

Figure 1 I Path Diagram of Metro Travel Emotion Generation

3.2. Variable Selection

Based on the cognitive theory of emotion and the person-environment fit theory mentioned in the methodology above, we consider the environment and needs of passengers before boarding and after alighting. The perceptions before boarding and after alighting include fare, station entry process, supporting facilities, waiting time, and environmental space. These factors are included as measurement variables to construct the evaluation framework for pre-boarding and post-alighting perception experiences.

Similarly, considering the environment and needs of passengers inside the carriage, the perceptions of passengers inside the carriage include crowding level, temperature, and carriage environment. These factors are included as measurement variables to construct the evaluation framework for in-carriage perception experiences.

Considering the need for accessibility, the perceptions of accessibility include transfer convenience, connections with other transportation modes (e.g., shared bicycles, buses, walking), and detour (i.e., the distance traveled by metro is greater than that by car). These factors are included as measurement variables to construct the evaluation framework for accessibility perception experiences.

For travel emotion perception, emotional state, satisfaction, and willingness to use are included as measurement variables to construct the evaluation framework for emotional perception experiences. The specific measurement items are shown in Table 1.

In addition, descriptive variables were also established. Descriptive variables measured a range of socio-demographic attributes and travel situations, which help to understand the travel patterns of different groups of people. These attributes include gender, age, number of times taking the metro per week, and purpose of travel. The number of times taking the metro per week is measured in four aspects: 1. Daily, 2. 3–5 times per week, 3. 1–2 times per week, 4. Very rarely. The purpose of travel is measured in seven aspects: 1. Commuting to work, 2. Going to school, 3. Tourism, 4. Shopping, 5. Visiting friends, 6. Entertainment, 7. Others. All other socio-demographic data are continuous variables.

Thus, the questionnaire design includes five dimensions, namely descriptive variables, emotional perception, pre-boarding and post-alighting perceptions, accessibility perception, and in-carriage perception. Except for the descriptive variables, a 5-point Likert scale was used to rate the statements, ranging from 1 (Strongly Disagree) to 5 (Strongly Agree).

3.3. Research Hypotheses

3.3.1. Hypotheses on Impact Mechanisms

The perception before boarding and after alighting refers to the experiences that passengers have before they start their metro journey and after they finish it. This process involves a series of procedures, such as purchasing tickets, undergoing security checks, passing through turnstiles, perceiving the station space environment, and using the supporting facilities within the station. Studies have shown that when the environment, services, ticketing, and supporting facilities in the metro station are well-man-

Table 1 | Measurement Variable Settings

Divisor	Quantity	Content
Emotional Perceptions	3	On this subway ride, I felt comfortable emotionally. During this subway trip, I felt satisfied with all kinds of objective conditions. I would like to keep taking the Wuhan subway.
Preboarding/Post-alighting Perceptions	5	I feel satisfied with the fare of this subway trip. I am satisfied with the process of entering the subway station (including ticket purchase, security check, passing the gate, etc.). I am satisfied with the facilities (toilets, waiting seats, vending machines, etc.) at the subway station. I am satisfied with the waiting time for this trip. I felt comfortable with the environmental hygiene in the station during this trip.
Accessibility Perception	3	I am satisfied with the convenience of transferring to other routes during this trip. I was satisfied with the convenience of connecting the subway station with other modes of transportation (shared bikes, buses, etc.). The detour (the distance traveled by subway is greater than the distance traveled by car) was acceptable to me.
In-carriage Perception	4	I am satisfied with the safety of the subway during this trip. I found the congestion in the subway car acceptable during this trip. The temperature of the carriage made me feel comfortable. I felt comfortable with the sanitary conditions of the carriage this time.

aged, passengers' positive emotions are enhanced [16,31]. Therefore, we propose Hypothesis H1: The perception before boarding and after alighting has a positive effect on passengers' emotions. Reasonable travel costs, convenient station entry procedures, well-equipped supporting facilities, and appropriate waiting times can lead to more positive emotions among passengers.

Accessibility perception refers to an individual's subjective feeling about the ease of reaching a destination. The quality of accessibility depends on the convenience with which people can experience services and activities [32]. Studies have indicated that during transfers, transfer areas often cause more negative emotions [30].Good accessibility can enhance passengers' overall sense of well-being [33]. Therefore, we propose Hypothesis H2: Accessibility perception is positively correlated with passengers' travel emotions. When passengers feel that transfers are inconvenient, connections with other modes of transportation (such as shared bicycles, buses, etc.) are poor, and the travel distance by metro is greater than that by car (i.e., detour), they are likely to experience more negative emotions.

In-carriage perception involves passengers' emotional experiences inside the carriage. Studies have shown that when facing crowded carriages, delays, or uncomfortable environments, passengers' emotions tend to become negative [30]. The environmental conditions of the vehicle, such as crowding level, noise level, and temperature, can affect passengers' psychological feelings [32]. Therefore, we propose Hypothesis H3: In-carriage perception is positively correlated with passengers' travel emotions. When passengers have a positive evaluation of the environment and conditions inside the carriage, their travel emotions are also more likely to be positive.

3.3.2. Hypotheses on Group Differences

Existing research has demonstrated significant differences in travel emotion perception among different groups. Regarding gender, Fong and Shaw [34] found that women's emotional responses during travel experiences differ from those of men. Other studies have shown that women's emotional response mechanisms during travel may be more complex, influenced by various factors such as travel purpose, personal emotional state, and social relationships [35]. In terms of travel frequency, Ma and Chen [36] found that increased travel frequency is generally positively correlated with emotional well-being. Frequent travelers tend to experience more positive emotions, which is closely related to their improved quality of life. Travel provides an opportunity to escape daily stress, thereby enhancing travelers' emotional states. Additionally, some studies have identified an interaction effect between gender and travel frequency. The impact of travel frequency on emotional benefits varies between genders. Although both men and women can derive emotional benefits from travel, women's motivations for psychological relaxation and cultural learning during travel may make their emotional experiences more positive with increased travel frequency [37].

Therefore, the following hypotheses are proposed:

H4: There are significant differences in metro travel emotion perception between genders and travel frequencies.

H5: There are significant differences in metro travel emotion perception among different travel frequencies.

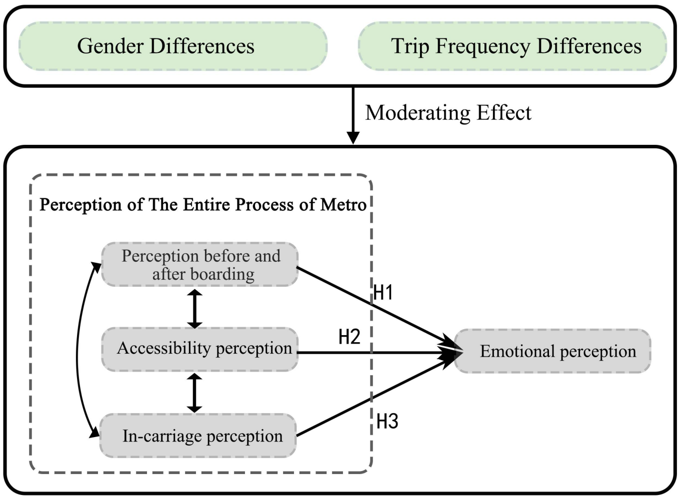

Figure 2 | Theoretical Model Diagram

Based on the research hypotheses presented in this section, a theoretical model is constructed as shown in Figure 2.

4. Research Design and Data Analysis

4.1. Research Design and Data Collection

Data were collected through offline questionnaires distributed in Wuhan City in July 2024. Wuhan, the central city of China's central region and an important comprehensive transportation hub nationwide, is a rapidly developing city with a permanent population of 12.3265 million (according to the 7th National Population Census of Wuhan). It is also the capital city of Hubei Province. As of June 2024, Wuhan Metro had 12 operational lines with a total operating mileage of 486 kilometers. On June 24, 2024, the total passenger volume of Wuhan Metro's network exceeded 10 billion.

The 12 operational lines of Wuhan Metro were selected as the research subjects. Random sampling surveys were conducted among passengers on these 12 lines, with small gifts (valued at less than 5 Chinese yuan) provided as incentives for participation. A total of 500 questionnaires were distributed. After preliminary processing of the 500 returned questionnaires, including the removal of incomplete responses and those with contradictory answers, 402 valid datasets were obtained.

4.2. Variables

4.2.1. Descriptive Statistics of the Sample

Table 2 reflects the socio-demographic attributes and travel situation data. In terms of gender distribution, male respondents slightly outnumber females. Regarding age

Table 2 | Statistics of Socio-Demographic Attributes and Travel Situations

Sample Information	Options	Quantity	Percentage
Gender	Man	241	60
	Woman	161	40
Age	Ages 0-14	7	1.7
	Ages 15-24	241	60.0
	Ages 25-34	108	26.9
	Ages 35-44	26	6.5
	Ages 45-54	10	2.5
	Ages 55-64	7	1.7
	Aged 65 and above	3	0.7
Number of Times Taking the Metro per Week	Daily use	41	10.2
	3-5 times per week	126	31.3
	1-2 times per week	158	39.3
	Very rarely	77	19.2
Purpose of Travel	Visiting friends	32	8.0
	Shopping	36	9.0
	Traveling	28	7.0
	Commuting to work	72	17.9
	Going to school	83	20.6
	Entertainment	115	28.6
	Other	36	9.0

distribution, young people aged 15–34 are the main force in metro travel, accounting for 60% of the total sample. Passengers in this age group are usually more active and have higher travel demands, including commuting to school, work, and social activities. Fewer passengers are aged 0–14 and 65 and above, which may be related to the relatively lower travel demands and activity ranges of these age groups. In terms of metro usage frequency, passengers who travel 1–2 times per week are the most numerous, accounting for 39.3%. This indicates that the metro is a regularly used mode of transportation for many passengers. Passengers who travel 3–5 times per week also constitute a significant proportion, highlighting the important role of the metro in urban transportation. Regarding travel purposes, commuting to work and school are the main purposes, accounting for 38.5% of the total sample. This emphasizes the key role of the metro in urban daily commuting. The data analysis results reveal a balanced distribution of the survey sample across various basic attributes, effectively avoiding sample bias and ensuring the representativeness and diversity of the statistical results.

4.2.2. Reliability and Validity Testing

The reliability of the questionnaire was assessed using Cronbach's alpha coefficient, with the analysis conducted using SPSS. As shown in Table 3, the overall reliability coefficient of the questionnaire scale is 0.954, indicating a high level of reliability for the entire questionnaire. Typically, a Cronbach's alpha coefficient greater than 0.7 is considered acceptable, while a value greater than 0.8 is regarded as good. The Cronbach's alpha coefficients for each dimension of the scale range from 0.865 to 0.921, all exceeding the standard value of 0.6. Therefore, the internal consistency reliability of the survey questionnaire is good, and its reliability is strong.

To assess the structural validity of the data, Bartlett's test of sphericity and the KMO (Kaiser-Meyer-Olkin) test were employed to evaluate the suitability of using factor analysis. The KMO value is an indicator of the correlation between variables; the closer it is to 1, the stronger the correlation between variables, and thus the more suitable for factor analysis. As shown in Table 4, the KMO value of the scale is 0.949 (>0.7), and Bartlett's test of sphericity yields a p-value of 0.000 (<0.01). This indicates that the correlations between variables are significant and suitable for exploratory factor analysis.

Excluding the items of descriptive variables in the sample, the principal component analysis method of exploratory factor analysis was used. According to the total variance explained, the first four principal components cumulatively accounted for 78.543% of the total variance, a proportion significantly higher than the minimum acceptable standard (at least 50%). This indicates that most of the data variation can still be explained, and they have a strong explanatory power over the data as a whole. Therefore, four common factors can be extracted, which correspond exactly to the four dimensions in the questionnaire, proving the rationality of the questionnaire's setting of four dimensions. In the factor analysis, the factor loadings of each item ranged from 0.611 to 0.798, exceeding the threshold of 0.5. Thus, the model data also performed well in terms of structural validity, and the quality of the model data passed the test.

4.2.3. Correlation Analysis

The correlation between travel emotions, pre-boarding and post-alighting perceptions, accessibility perceptions, and in-carriage perceptions was examined using Pearson's correlation coefficient method. As shown in Table 5, all correlation coefficients were statistically significant (p<0.001), indicating that the relationships between these variables are significant.

Table 3 | Reliability Test of the Questionnaire

Total *alpha*	Dimension *alpha*
0.954	α_1=0.875
	α_2=0.921
	α_3=0.885
	α_4=0.865

Note: Dimension 1: Travel Emotion is denoted as α_1; Dimension 2: Pre-boarding and Post-alighting Perception is denoted as α_2; Dimension 3: Accessibility Perception is denoted as α_3; Dimension 4: In-carriage Perception is denoted as α_4.

Table 4 | KMO and Bartlett's Test of Sphericity for the Scale

KMO		**0.949**
Bartlett's Test of Sphericity	Approximate Chi-Square	4881.833
	Degrees of Freedom	105
	Significance	0.000

Table 5 | Correlation Analysis

Correlation	Emotional perception	pre-boarding/post-alighting perceptions	Accessibility perception	In-carriage perception
Emotional perception	1	0.749**	0.767**	0.716**
pre-boarding/post-alighting perceptions	0.749**	1	0.755**	0.679**
Accessibility perception	0.767**	0.755**	1	0.688**
In-carriage perception	0.716**	0.679**	0.688**	1

Note: ** indicates ***p*<.001**, the correlation is significant.

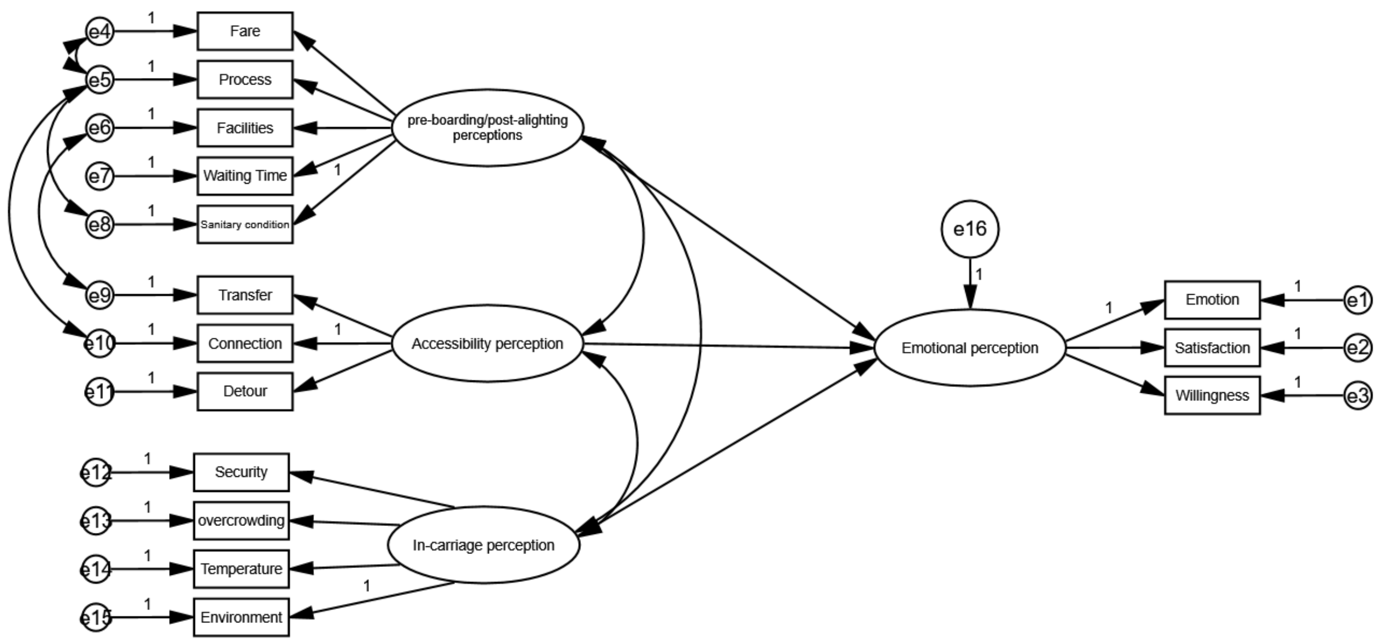

Figure 3 | Path Diagram of the SEM Model

5. Model Construction and Analysis

5.1. Construction of Structural Equation Modeling (SEM)

This study employs Structural Equation Modeling (SEM) for data analysis. SEM is capable of simultaneously resolving the complex relationships between endogenous and exogenous variables and calculating the direct, indirect, and total effects of these variables. SEM is used to test a set of theory-driven hypotheses, aiming to measure the fit between the hypothesized conceptual model composed of observed indicators and latent constructs and the data[33] .

Based on existing literature and theoretical knowledge, we designed and constructed a theoretical conceptual model for the entire process of metro travel perception to explore the interrelationships among different variables. In this process, we first established the measurement models for latent variables, which are based on theoretical hypotheses and used for preliminary analysis of the correlations between latent variables. Subsequently, we conducted path analysis to further investigate the relationships between these variables and constructed the Structural Equation Model accordingly.

The SEM model was constructed using AMOS 24.0 software, where ellipses represent latent variables and rectangles represent measurement indicators. We considered three exogenous latent variables—perception before boarding and after alighting, accessibility perception, and in-carriage perception—and one endogenous latent variable—travel emotion. The three measurement indicators for travel emotion, the five measurement indicators for perception before boarding and after alighting, the three measurement indicators for accessibility perception, and the four measurement indicators for in-carriage perception are

Table 6 | Goodness-of-Fit Test for the SEM Model

Statistical Test Metric	Standard or Critical Value for Fit	Test Result	Model Fit Judgment
Chi-Square(χ^2)	$p>0.05$（Not Significant）	348（$p<0.001$）	Fit Indices Reference Statistics
CMIN/DF	<5	4.139	Yes
RMR	<0.05	0.024	Yes
RMSEA	<0.08	0.088	No
GFI	>0.90	0.898	No
AGFI	>0.80	0.854	Yes
TLI	>0.90	0.932	Yes
IFI	>0.90	0.946	Yes
NFI	>0.90	0.930	Yes
CFI	>0.90	0.946	Yes

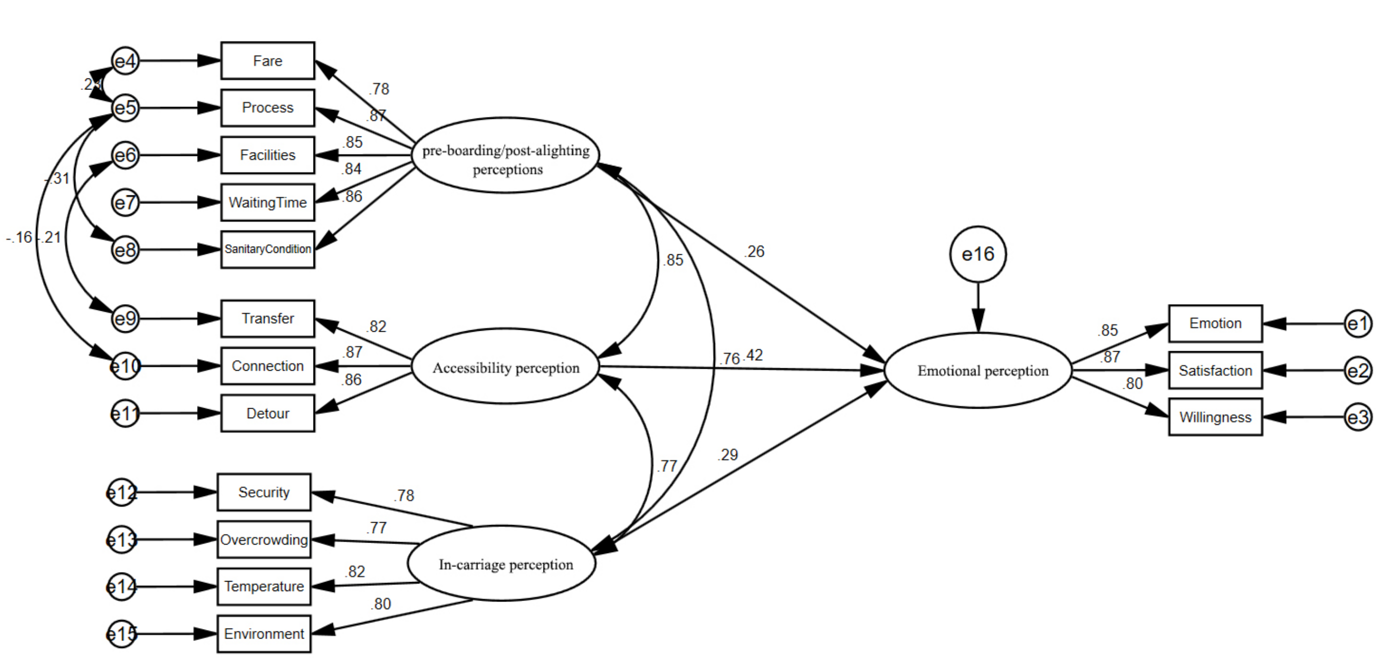

Figure 4 I Revised SEM Model and Path Diagram

shown in Figure 3. The circular e1 to e16 represent the measurement errors for each measurement indicator. In the constructed Structural Equation Model, the three exogenous latent variables and one endogenous latent variable are interconnected through three hypothesized paths. These paths represent our expected influences between the variables, and the model construction aims to verify whether these expectations align with the actual data.

A goodness-of-fit test was conducted on the constructed SEM model. The goodness-of-fit indices are shown in the table. Table 6 indicates that the Root Mean Square Error of Approximation (RMSEA) is 0.088, which exceeds the acceptable threshold of 0.08. Additionally, the Goodness-of-Fit Index (GFI) is 0.898, slightly below the standard value of 0.90. These results suggest that the constructed model requires further refinement.

When a model fails to meet the fit criteria, variables with high Modification Indices (MI) can be removed to refine the model. A high MI value (typically greater than 10) indicates a strong correlation,

suggesting the need to release paths with large MI values to improve the model's fit. In this study, the MI values between e4 and e5, e5 and e8, e5 and e10, and e6 and e9 were found to be significant. Therefore, correlation paths between these residuals were added to enhance the model's fit.

The revised SEM is shown in Figure 4. The results of the goodness-of-fit test after revision are shown in Table 7, and all fit indices indicate that the model fits well. Therefore, it can be concluded that the model is well-fitted overall.

Table 7 I Goodness-of-Fit Test for the Revised SEM Model

Statistical Test Metric	Standard or Critical Value for Fit	Test Result	Model Fit Judgment
Chi-Square(χ^2)	p>0.05（Not Significant）	280（p<0.001）	Fit Indices Reference Statistics
CMIN/DF	<5	3.498	Yes
RMR	<0.05	0.022	Yes
RMSEA	<0.08	0.079	Yes
GFI	>0.90	0.916	Yes
AGFI	>0.80	0.874	Yes
TLI	>0.90	0.946	Yes
IFI	>0.90	0.959	Yes
NFI	>0.90	0.944	Yes
CFI	>0.90	0.959	Yes

5.2. Structural Equation Modeling (SEM) Analysis and Hypothesis Path Testing

The relationships between model variables are determined by the signs of the standardized path coefficients, which indicate the positive or negative correlations between variables. The absolute values of the path coefficients are used to assess the strength of the influence between two variables; the larger the absolute value, the greater the impact one variable has on the other along the path. The standardized path coefficients for the revised SEM paths, as shown in Figure 3, are presented in Table 8.

The results reveal significant relationships between metro passengers' travel emotions and their perceptions of different travel stages. Specifically, accessibility perception has a significant positive impact on travel emotions (standardized path coefficient = 0.42); pre-boarding and post-alighting perceptions also have a positive impact on travel emotions (standardized path coefficient = 0.26); and in-carriage perception has a positive impact on travel emotions as well (standardized path coefficient = 0.29). The differences in the impact of pre-boarding and post-alighting perceptions and in-carriage perception on travel emotions are not significant. The standardized coefficients between accessibility perception and pre-boarding and post-alighting perceptions and in-carriage perception are 0.85 and 0.77, respectively, indicating a very significant influence.

Based on the above findings, accessibility perception has the most significant impact on travel emotions, reflecting contemporary residents' high emphasis on the accessibility of public transportation. A well-designed metro network can provide convenient connections, reduce the number of transfers and walking distances, thereby enhancing passengers' travel emotions. Wuhan, a densely populated and geographically extensive city, is divided into three main areas (Wuchang, Hanyang, Hankou) by the Yangtze River and the Han River. This unique geographical feature poses higher demands on transportation connectivity. In such an urban environment, the metro, as a key and rapid mode of public transportation, plays a decisive role in alleviating traffic congestion and improving travel efficiency. Therefore, residents are particularly sensitive to the accessibility of the metro, paying close attention to the connections between the metro and residential areas, commercial districts, educational institutions, and tourist attractions during their travels. These factors directly affect their travel convenience and time costs, which in turn influence passengers' travel emotions.

5.3. Multi-Group Structural Equation Modeling (MSEM) Analysis

The purpose of multi-group structural equation modeling (MSEM) is to evaluate whether the theoretical model proposed by researchers is equivalent across different sample groups or if there are significant differences [38]. This paper employs MSEM to conduct differential analysis on two dimensions: gender and travel frequency. In terms of gender, due to the interaction of physiological factors and socio-cultural influences, there are certain psychological differences between men and women, and these differences are also reflected in their experiences with public transportation. Regarding travel frequency, it is divided into frequent users and occasional users. Based on the samples collected in this study, individuals who use the metro daily or 3–5 times per week are categorized as frequent users, while those who use it 1–2 times per week or very rarely are classified as occasional users. Occasional users account for 58.5% of the total sample, which is close to the proportion of frequent users, making it suitable for multi-group analysis. On the other hand, frequent and occasional users of the metro have different focal points regarding the construction and services of the metro. For example, frequent users may place greater emphasis on the punctuality, crowding levels, and transfer convenience of the metro, while occasional users may be more concerned with the convenience of ticket purchasing and the clarity of station guidance. Therefore, this paper selects these two

Table 8 | Interpretation of the Paths in the Revised Model

Path	Hypothesis Explanation	Standardized Path Coefficient	p	Direction of Influence	Validation Result
H1	Perception before boarding and after alighting has an impact on travel emotions.	0.26	***	Positive	Valid
H2	Accessibility perception has an impact on travel emotions.	0.42	***	Positive	Valid
H3	In-carriage perception has an impact on travel emotions.	0.29	***	Positive	Valid

Note: *** indicates that the path significance level *P* value is less than 0.01.

representative dimensions to analyze the differences between groups.

The results of the multi-group analysis are shown in Table 9. In terms of the impact mechanism, the multi-group test results are basically consistent with the main model results, all showing positive impacts. However, the accessibility perception for women is not significant. The specific analysis is as follows:

In the gender dimension, the path coefficient for men regarding the impact of accessibility perception on travel emotions is 0.492, while it is not significant for women. This indicates that men place greater emphasis on the accessibility of the metro, and accessibility perception has a more significant impact on men's travel emotions. In daily travel and commuting, men tend to focus more on travel efficiency, and inefficient travel can lead to more negative emotions for them. The path coefficient for women regarding the impact of pre-boarding and post-alighting perceptions on travel emotions is 0.435, while for men, it is 0.208. This suggests that women pay more attention to pre-boarding and post-alighting perceptions, including ticket prices, station environmental hygiene, entry procedures, and supporting facilities and services. These perceptions have a more significant impact on women's travel emotions. The path coefficients for men and women regarding the impact of in-carriage perception on travel emotions are 0.302 and 0.259, respectively. The slightly higher path coefficient for men indicates that in-carriage perception has a more significant impact on men's travel emotions.

In the travel frequency dimension, for the group that frequently uses the metro, the path coefficient for the impact of accessibility perception on travel emotions is 0.459, which is higher than the path coefficient of 0.330 for the group that occasionally uses the metro. This suggests that frequent users place slightly more importance on accessibility perception, which has a more significant impact on their travel emotions. Frequent users, who mostly commute for work or school, tend to focus more on the accessibility and efficiency of the metro. The path coefficients for the impact of pre-boarding and post-alighting perceptions and in-carriage perception on travel emotions are 0.257 and 0.269 for frequent users, and 0.325 and 0.313 for occasional users, respectively. This indicates that occasional users are more affected by pre-boarding and post-alighting perceptions and in-carriage perception in terms of travel emotions. Occasional users tend to pay more attention to ticket purchasing, station guidance clarity, entry procedures, station environment, and supporting facilities.

6. Conclusion and Outlook

6.1. Conclusion

This study proposes a theoretical relational model for the entire process of metro travel perception. Through a questionnaire survey of metro passengers in Wuhan, relevant data were collected and analyzed using Structural Equation Modeling (SEM) to explore the impact mechanism of different stages of metro travel on passengers' travel emotions. Additionally, Multi-group Structural Equation Modeling (MSEM) was employed to investigate differences among different groups. The following conclusions were drawn:

(1) The impact mechanism results show that passengers' travel emotions are positively influenced by pre-boarding and post-alighting perceptions, accessibility perception, and in-carriage perception. Among these, accessibility perception has the greatest impact on travel emotions and is a key factor in enhancing passengers' travel emotions.

(2) The group effect results indicate significant differences in travel emotion perception between different genders and travel frequencies. In terms of gender, male passengers' travel emotions are more influenced by accessibility perception, while female passengers' travel emotions are more affected by pre-boarding and post-alighting perceptions. Regarding travel frequency, passengers who frequently use the metro are more influenced by accessibility perception, while occasional users are more affected by

Table 9 | Results of Multi-group Analysis

Path	Gender				Trip Frequency			
	Man		Woman		Frequent Travelers		Occasional Travelers	
	Std	P	Std	P	Std	P	Std	P
pre-boarding/post-alighting perceptions →Emotional perception	0.208	**	0.435	**	0.257	**	0.325	**
Accessibility perception →Emotional perception	0.492	***	0.252	0.229	0.459	***	0.330	**
In-carriage perception →Emotional perception	0.302	***	0.259	**	0.269	**	0.313	***

Note: ***、**、*indicate significance at the 0.01 0.05, and 0.1 levels, respectively.

pre-boarding and post-alighting perceptions and in-carriage perception.

6.2. Limitations and Future Work

This study has provided some insights into the impact of the entire metro travel process on passengers' emotions, but there are still several limitations. The current study has focused on analyzing the differences in gender and travel frequency groups, and future research should incorporate other group differences such as age, income level, travel time, and travel purpose to enhance the explanatory power of the model. Moreover, the geographical location of metro stations may affect passengers' accessibility perception and travel experience. Metro stations located in the city center often have better accessibility than those in peripheral areas. Additionally, different metro stations may bring different perceptions to passengers. These differences may moderate the significance of the relationships among the variables examined in this study. Therefore, future research needs to further explore the impact of these factors to more comprehensively reveal the mechanisms that affect travel emotions and to provide more targeted strategies for improving passenger experience.

1. Chen, Q., Yan, Y., Zhang, X., & Chen, J. (2022). Impact of subjective and objective factors on subway travel behavior: Spatial differentiation. International Journal of Environmental Research and Public Health, 19(23), 15858. https://doi.org/10.3390/ijerph192315858.
2. Tang, B., Li, R., Yu, B., An, & Wei, Y. (2018). How to peak carbon emissions in China's power sector: A regional perspective. Energy Policy, 120, 365–381. https://doi.org/10.1016/j.enpol.2018.04.067
3. https://www.mot.gov.cn/jiaotongyaowen/202410/t20241016_4157852.html
4. Song, R.; Shi, W.; Qin, W.; Xue, X.; Jin, H. Exploring Passengers' Emotions and Satisfaction: A Comparative Analysis of Airport and Railway Station through Online Reviews. Sustainability 2024, 16(5), 2108. https://doi.org/10.3390/su16052108.
5. Lai, X.; Teng, J.; Ling, L. "Evaluating Public Transportation Service in a Transit Hub Based on Passengers' Energy Cost." In Proceedings of the IEEE 23rd International Conference on Intelligent Transportation Systems (ITSC), Rhodes, Greece, 20–23 September 2020; pp. 1–7.
6. https://www.gov.cn/xinwen/2019-07/15/content_5409694.htm
7. Cheng, P. P., & Liu, L. (2009). Five elements of music therapy research on the influence of emotion and meridian. Studies in health technology and informatics, 146, 818-9.Indexed.
8. Zhang, L., Zhou, S. H., & Kwan, M. P. (2023). The temporality of geographic contexts: Individual environmental exposure has time-related effects on mood. Health & Place, 79, 102953. https://doi.org/10.1016/j.healthplace.2022.102953
9. Zhang, L., Zhou, S., Kwan, M.-P., Chen, F., & Dai, Y. (2020). The threshold effects of bus micro-environmental exposures on passengers' momentary mood. Transportation Research Part D: Transport and Environment, 84, 102379. https://doi.org/10.1016/j.trd.2020.102379)
10. Yazdanpanah, M., & Hosseinlou, M. H. (2016). The influence of personality traits on airport public transport access mode choice: A hybrid latent class choice modeling approach. Journal of Air Transport Management, 55, 147-163. https://doi.org/10.1016/j.jairtraman.2016.04.010
11. Balaban, C.Z., Karimpur, H., Röser, F., & Hamburger, K. (2017). Turn left where you felt unhappy: how affect influences landmark-based wayfinding. Cognitive Processing, 18(2), 135–144.
12. Cox, T., Houdmont, J., & Griffiths, A. (2006). Rail passenger crowding, stress, health and safety in Britain. Transportation Research Part A: Policy and Practice, 40(3), 244-258.
13. Mahudin, N. D. M., Cox, T., & Griffiths, A. (2012). Measuring rail passenger crowding: Scale development and psychometric properties. Transportation Research Part F: Traffic Psychology and Behaviour, 15(1), 38-51.
14. Meenar, M.; Flamm, B.; Keenan, K. Mapping the Emotional Experience of Travel to Understand Cycle-Transit User Behavior. Sustainability 2019, 11, 4743. doi:10.3390/su11174743.
15. Chen, Q., Yan, Y., Zhang, X., & Chen, J. (2022). Impact of subjective and objective factors on subway travel behavior: Spatial differentiation. International Journal of Environmental Research and Public Health, 19(23), 15858. https://doi.org/10.3390/ijerph192315858. PMID: 3649793; PMCID: PMC9739888
16. Delaplace, M., & Dobruszkes, F. (2015). From low-cost airlines to low-cost high-speed rail? The French case. Transport Policy, 38, 73–85. https://doi.org/10.1016/j.tranpol.2014.12.006
17. Alberto, M., & Tim, J. R. (2015). The impact of extreme weather conditions on long-distance travel behaviour. Transportation Research Part A: Policy and Practice, 77, 305-319. https://doi.org/10.1016/j.tra.2015.04.025
18. Zhai, J., Wu, W., Yun, J., J. Sun, & Wang, Q. (2021). Travel satisfaction and rail accessibility. Transportation Research Part D: Transport and Environment, 100, 103052. https://doi.org/10.1016/j.trd.2021.103052
19. St-Louis, E., Manaugh, K., van Lierop, D., & El-Geneidy, A. (2014). The happy commuter: a comparison of commuter satisfaction across modes. Transportation Research Part F: Traffic Psychology and Behaviour, 26, 160–170. https://doi.org/10.1016/j.trf.2014.07.004
20. Páez, A., & Whalen, K. (2010). Enjoyment of commute: A comparison of different transportation modes. Transportation Research Part A: Policy and Practice, 44(7), 537-549.
21. Le, H. T. K., & Carrel, A. L. (2019). Happy today, satisfied tomorrow: Emotion—satisfaction dynamics in a multi-week transit user smartphone survey. Transportation Research Part A: Policy and Practice, 118, 360–373. https://doi.org/10.1016/j.tra.2019.01.002
22. Morris, E. A., & Guerra, E. (2015). Are we there yet? Trip duration and mood during travel. Transportation Research Part F: Traffic Psychology and Behaviour, 33, 38-47.
23. Watkins, K. E., Ferris, B., Borning, A., Rutherford, G. S., & Layton, D. (2011). Where Is My Bus? Impact of mobile real-time information on the perceived and actual wait time of transit riders. Transportation Research Part A: Policy and Practice, 45(8), 839-848. https://doi.org/10.1016/j.tra.2011.06.010
24. Olsson, L. E., Gärling, T., Ettema, D., et al. (2013). Happiness and satisfaction with work commute. Social Indicators Research, 111(1), 255-263.
25. Zhu, J., & Fan, Y. (2018). Daily travel behavior and emotional well-being: Effects of trip mode, duration, purpose, and companionship. Transportation Research Part A: Policy and Practice, 118, 360–373. https://doi.org/10.1016/j.tra.2018.09.019
26. Reisenzein, R. (2006). Arnold's Theory of Emotion in Historical Perspective. PsychArchives. https://doi.org/10.23668/psycharchives.10895
27. Qiao Jianzhong. Arnold's Theory of Emotion in the Current Perspective of Emotion Research [J]. Advances in Psychological Science, 2008, (02): 302-305. (in Chinese)
28. Wei Xintong, Zou Guangtian, Shao Jianwei. A Study on the Design Strategies for Happy Community Built Environment Based on Emotional Cognitive Theory [J]. Contemporary Architecture, 2023, (02): 122-124. (in Chinese)
29. Zhang Lin, Zhou Suhong, Guan Meibao. The Impact of Activity Space Geographic Environment on Residents' Immediate Emotions: The Moderating Effect of Activity Characteristics [J]. Geographical Research, 2024, 43(09): 2479-2492. (in Chinese)
30. Ferri, A., & Popp, M. (2022). 'Wayfeeling': Navigating through emotional and sensorial responses in public transit. Wellbeing, Space and Society, 3, 100104. https://doi.org/10.1016/j.wss.2022.100104
31. Li, X., Wang, Y., Tang, J., Shi, L., Zhao, T., & Chen, J. (2022). Emotional wellbeing in intercity travel: Factors affecting passengers' long-distance travel moods. Frontiers in Public Health, 10, 1046922. https://doi.org/10.3389/fpubh.2022.1046922
32. Jamei, E., Chan, M., Chau, H. W., Gaisie, E., & Lättman, K. (2022). Perceived Accessibility and Key Influencing Factors in Transportation. Sustainability, 14(17), 10806. https://doi.org/10.3390/su141710806
33. Yin, J. B., Cao, X. Y., & Huang, X. Y. (2021). Association between subway and life satisfaction: Evidence from Xi'an, China. Transportation Research Part D: Transport and Environment, 96, 102869.

https://doi.org/10.1016/j.trd.2021.102869
34. Fong, A. Z., & Shaw, F. A. (2024). Well-being implications of mobility of care: Gender differences among U.S. adults. Transportation Research Part D: Transport and Environment. https://doi.org/10.1016/j.trd.2024.104109
35. Pourhashem, G., Malichová, E., Piscova, T., & Kováčiková, T. (2022). Gender difference in perception of value of travel time and travel mode choice behavior in eight European countries. Sustainability, 14(16), 10426. https://doi.org/10.3390/su141610426
36. Ma, Y., Chen, S., Khattak, A. J., Cao, Z., Zubair, M., Han, X., & Hu, X. (2022). What affects emotional well-being during travel? Identifying the factors by maximal information coefficient. International Journal of Environmental Research and Public Health, 19(7), 4326. https://doi.org/10.3390/ijerph19074326
37. Vespestad, M. K., & Mehmetoglu, M. (2015). Gender differences in vacation behavior. Tourism Review International, 19(3), 147-161. https://doi.org/10.3727/154427215X14430967453670
38. Deng, L., & Yuan, K.-H. (2015). Multiple-Group Analysis for Structural Equation Modeling With Dependent Samples. Structural Equation Modeling: A Multidisciplinary Journal. https://doi.org/10.1080/10705511.2015.1028919

Acknowledgments Funding by Graduate Innovative Fund of Wuhan Institute of Technology (Grant CX2024521), Wuhan Social Science Fund (Grant 2023004) and Key Laboratory of Road and Traffic Engineering of the Ministry of Education, Tongji University (Grant K202407).

Journal of Sustainable Built Environment

press

https://doi.org/10.70731/nyqqqt55

Exploring the Pathways To Enhance the Resilience Performance of Prefabricated Medical Buildings

Yue Chen [a], Liang Ma [b,*], Sitong Li [c], Yonghui Jiang [d], Siyang Shi [e]

[a] *Beijing Advanced Innovation Center for Future Urban Design, Beijing,100044, China*
[b] *China Light Industry International Engineering Co., Ltd. , Beijing, 100026, China*
[c] *Peking University First Hospital, Beijing, 100034, China*
[d] *Beijing Polytechnic College, Beijing, 100042, China*
[e] *Peking University Third Hospital, Beijing, 100096, China*

KEYWORDS

Prefabricated Medical Buildings;
Seismic Resilience;
Resilience Performance

ABSTRACT

This paper explores strategies to enhance the seismic resilience of prefabricated medical buildings, particularly in China, where urbanization has led to increasingly stringent seismic performance requirements for newly constructed hospitals. Prefabricated hospital buildings, utilizing green construction methods with healthy, age-friendly, and easily maintainable components, have become the primary model for the construction and renovation of emergency medical facilities. The study addresses the current limitations in seismic resilience, exploring paths to improve the structural toughness of medical buildings. It covers the application of precast concrete in hospital construction, a comparison of the economic benefits of precast concrete versus steel structures, seismic performance at varying levels of prefabrication, and the overall integrity of precast concrete structures. Additionally, the paper examines the synergy of concrete structures with seismic isolation and damping technologies. The findings underscore the importance of integrating advanced seismic isolation and vibration reduction technologies to maintain the functionality of medical buildings during and after seismic events, ensuring operational continuity in times of crisis.

1. Introduction

With the continuous advancement of urbanization in China, the requirements for the seismic performance of newly constructed hospitals are increasingly stringent. The "Regulations on Seismic Fortification Management of Construction Projects" clearly stipulate that new hospitals in high-intensity fortification areas should adopt seismic isolation and vibration reduction technologies to ensure that they do not lose their functional capabilities during the design-basis earthquake events in their regions[1]. Hospital buildings play an extremely crucial role in earthquake disasters, serving as a core component of the urban disaster prevention and mitigation system. They are responsible for critical functions such as post-earthquake casualty treatment, epidemic prevention and control, and public health services[2][3]. The continuity of their functions directly affects the life safety of the affected population and the stability of society. The ability of a hospital to quickly engage in rescue operations after an earthquake depends on the damage sustained by the hospital building and its internal medical equipment during the earthquake. Prefabricated hospital buildings, which utilize green construction methods and

* Corresponding author. E-mail address: maliang@sinolight.cn

Received 19 March 2025; Received in revised form 25 March 2025; Accepted 28 March 2025; Available online 31 March 2025.
2759-7318 /

select healthy, age-friendly, and easily maintainable building components, are undergoing a revolution in construction technology and design philosophy. Since the outbreak of the COVID-19 pandemic in 2020, prefabricated construction has fully demonstrated its advantages of rapid construction and high quality, becoming the primary model for the construction and renovation of emergency medical facilities in various regions. Therefore, in-depth research on seismic isolation and vibration reduction technologies for medical buildings, and the enhancement of hospitals' seismic resilience, hold extremely important practical significance.

2. The Significance of Enhancing the Resilience Performance of Medical Buildings

2.1. The Key Role of Medical Buildings in Post-Earthquake Emergency Rescue

China is a country prone to frequent earthquakes, and each major earthquake has caused substantial economic losses and casualties. The urban medical system, as one of the critical subsystems within the urban system, serves as a vital node in the urban lifeline and an essential carrier for medical services. Under normal conditions, it is responsible for basic medical treatment, but after a disaster, it immediately participates in medical rescue operations[4]. The safe and stable operation of medical buildings during an earthquake is crucial for ensuring the continuity of medical services. Any interruption in the functionality of medical buildings directly threatens the efficiency of post-earthquake emergency response. Hospitals need to quickly initiate the treatment of casualties, diagnosing, treating, and nursing various types of injured individuals. They provide basic medical care for affected populations, which is essential for stabilizing social order in the disaster area, reducing casualties, and lowering the disability rate[5].

2.2. The Complexity and Vulnerability of Medical Buildings

The seismic capacity of medical buildings directly affects the regional disaster recovery capability[6] and is also a core indicator[7] for the restoration of social order after an earthquake. However, medical buildings themselves are complex system projects. A large number of high-precision, high-value, and vibration-sensitive medical devices, such as Magnetic Resonance Imaging (MRI) and Computed Tomography (CT) equipment, face severe threats during earthquakes. In the 2011 Great East Japan Earthquake, many hospital buildings suffered structural damage, with walls cracking and collapsing. Non-structural components, such as ceilings falling and doors and windows deforming, were also affected. Numerous medical devices were damaged by violent shaking, not only rendering the hospital's internal facilities unusable but also severely impeding the hospital's medical service functions and significantly affecting the post-earthquake rescue operations. In the 2008 Wenchuan earthquake in China, many hospital buildings suffered heavy damage and even collapsed due to the imperfections of their structural systems and insufficient seismic measures. In the 2022 Luding earthquake of magnitude 6.8, medical buildings with unverified seismic design, such as those made of wood and masonry structures, were severely damaged, and the destruction of non-structural components directly led to the paralysis of hospital functions[3].

3. The Limitations of Current Seismic Resilience in Medical Buildings

3.1. The Limitations of Traditional Seismic Design in Medical Buildings

Traditional seismic design follows the principle of "minor earthquakes cause no damage, moderate earthquakes cause repairable damage, and major earthquakes do not cause collapse." This approach primarily focuses on ensuring the safety of the building structure during an earthquake to prevent casualties from structural collapse. However, this philosophy falls short of meeting the modern medical building's demand for functional continuity. Medical buildings designed according to current regulations often suffer significant damage to non-structural components during rare but severe earthquakes, leading to functional interruptions[6]. Under the action of high intensity earthquakes, although the traditional seismic design of medical buildings can ensure that the structure will not collapse, the excessive inter-story displacement angle and floor acceleration may lead to the damage of precision medical equipment[8]. There are fewer studies on the susceptibility of non-structural components such as flexible ducts and enclosures[9]. Comparison of seismic, damping, and isolation techniques reveals that traditional seismic strengthening can only maintain the original design objectives, but cannot effectively reduce the impact of floor acceleration on equipment[10].

In recent years, seismic resilience has become an important research direction in the field of earthquake engineering, with its core being the ability of buildings to "rapidly restore functionality" after an earthquake[13][14]. The seismic resilience of medical buildings not only relies on structural safety but also needs to achieve rapid post-earthquake functional recovery through seismic isolation, vibration reduction technologies, and non-structural protection strategies. Ma[4] have proposed constructing a resilience framework for urban medical systems from three aspects: robustness (R1), redundancy (R2), and efficiency (R3), to ensure that medical facilities do not interrupt their treatment functions during earthquakes and that personnel can more quickly enter a state of rescue. Seismic isolation technology can keep the upper structure elastic under rare earthquakes and reduce the floor acceleration to 1.69 m/s², significantly reducing the risk of equipment tipping over[9].

by using liquid viscous dampers, the structural displacement damping rate is increased to 20% - 40%, verifying the effectiveness of vibration reduction technology in high-intensity areas (Zhang Xinzhi, 2022). Therefore, traditional seismic design can no longer meet the needs of medical buildings to ensure structural safety and normal

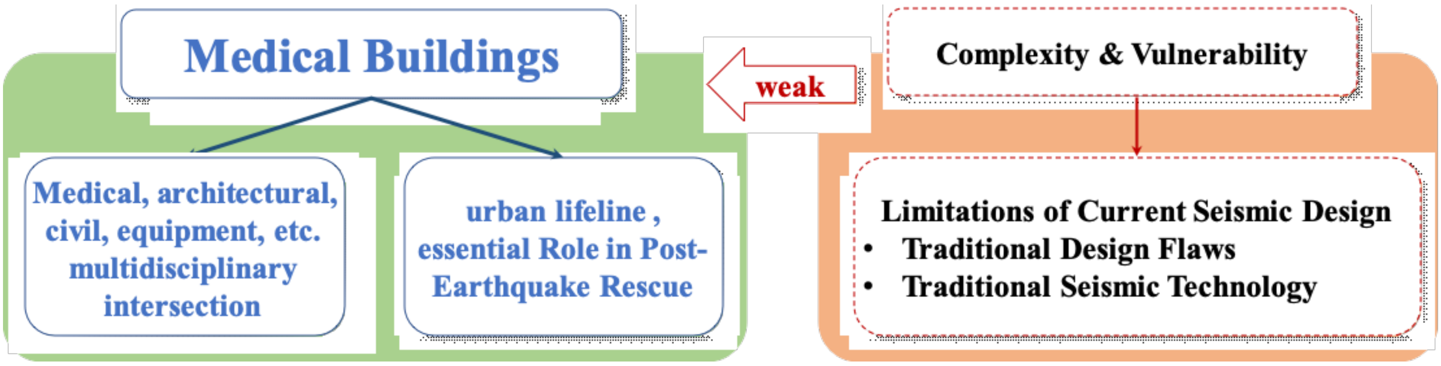

Figure 1 | Mismatch between level of seismic toughness and needs in healthcare buildings

operation of equipment during earthquakes, and there is an urgent need to explore new seismic isolation and vibration reduction technologies to enhance the seismic performance of medical buildings. The structural displacement damping rate was increased to 20-40% by liquid viscous dampers, which verified the effectiveness of the damping technology in high intensity zones[1]. Therefore, traditional seismic design can no longer meet the needs of medical buildings to ensure structural safety and normal operation of equipment during earthquakes, and there is an urgent need to explore new seismic isolation and vibration reduction technologies to enhance the seismic performance of medical buildings.

3.2. The Limitations of Traditional Seismic Technology in Medical Buildings

Due to the particularity of their functions, medical buildings impose higher demands on the seismic performance of their structures. Current seismic design for medical buildings still faces issues such as insufficient multidisciplinary collaboration and difficulties in data integration. Research on the structural systems of medical buildings and their seismic isolation and vibration reduction implementation plans not only helps enhance the seismic capacity of medical buildings but also provides new ideas and methods for the development of seismic technology in the entire building structure field. Cheng[12] proposed a multi-level functional assessment model based on BIM, which integrates component vulnerability data with functional logical relationships to achieve department-level functional coupling analysis. Ning[13] developed an evaluation method for seismic safety and resilience, providing a quantitative basis for the performance grading of medical buildings. Zhai[14] presented a basic approach for seismic resilience design of buildings through resilience concept design and computational design methods, constructing a five-step process for seismic resilience design of buildings, which includes determination of resilience targets, structural safety design, seismic resilience concept design, post-earthquake functional verification of buildings, and rapid functional recovery strategies. Fang[15] demonstrated that point layout can improve the post-earthquake treatment efficiency of the emergency department through the optimization of spatial combination patterns.

4. Path to Improved Toughness Performance in Medical Buildings

4.1. Research on Precast Concrete Structures and Technical and Economic Comparative Analysis With Steel Structures

4.1.1. Current Application Status of Precast Concrete Structures in Hospital Construction

A comprehensive survey of domestic and international hospital projects that have adopted precast concrete structures is conducted. Design drawings, construction records, cost data, and user feedback are collected. First, the characteristics of precast concrete structures used in hospitals of different regions and scales are analyzed, including types of precast components, production processes, transportation, and installation methods. Second, a classification of medical buildings into large general hospitals, specialized hospitals, and primary healthcare centers is established based on their categories, functions, and volumes, forming a case library for medical buildings. The advantages and shortcomings of precast concrete structures in meeting the functional demands of hospitals are studied to provide a practical basis for technical and economic comparisons and optimized design.

4.1.2. Economic Comparison of Precast Concrete Structures and Steel Structures

4.1.2.1. Construction Cost Comparison

Cost Calculation: Detailed cost calculations are performed for the construction costs of precast concrete structures and steel structures in hospital construction projects. Differences in material costs, labor costs, and equipment rental costs between the two structural forms are analyzed. Management costs during the construction process, including temporary facility costs and construction management fees, are also compared. Based on the case library of medical buildings, a cost model is established to predict the construction cost range for hospitals of different scales and functional requirements using precast concrete structures and steel structures.

4.1.2.2. Lifecycle Operation and Maintenance Cost Comparison

Lifecycle Cost Analysis: The operational, maintenance, and demolition costs of precast concrete structures and steel structures over the lifecycle of hospitals are studied.

Given the long service life of hospital buildings, maintenance and operational costs account for a significant proportion of the total lifecycle costs. The cost of adaptability and functionality changes in medical buildings to meet new medical demands is also investigated. The convenience of construction modifications to meet new medical requirements is analyzed, considering the need for adjustments in ventilation, fire protection, and vibration-sensitive control in existing medical areas.

The comprehensive construction costs and lifecycle cost benefits are synthesized to provide an economic basis for investment decisions in hospital construction projects.

4.2. Research on Seismic Performance of Structures Under Different Prefabrication Rates

4.2.1. Establishment of Structural Models With Different Prefabrication Rates

According to relevant standards and practical engineering requirements, a series of concrete precast structural models with different prefabrication rates (30%, 50%, 70%) and different structural forms (frame structures, frame-shear wall structures, etc.) are designed and established. The impact of changes in prefabrication rates on the seismic performance of different structural forms is investigated through numerical simulation and experimental research.

4.2.2. Seismic Performance Analysis of Structures Under Earthquake Actions

4.2.2.1. Seismic Response Analysis

Using seismic isolation and vibration reduction techniques, dynamic characteristic analysis is conducted on structural models with different prefabrication rates and structural forms. Parameters such as the natural vibration period, frequency, and mode shapes of the structures are calculated. The influence of prefabrication rate changes on the dynamic characteristics of structures is studied, and the differences in vibration characteristics under different prefabrication rates are analyzed. Different seismic waves are input to perform seismic response analysis on the established structural models. Response parameters such as inter-story drift angle and floor acceleration of the structures under earthquake actions are calculated. The seismic performance of models with different prefabrication rates and structural forms is evaluated. The damage patterns and injury distribution under earthquake actions are analyzed, revealing the impact of prefabrication rates on structural damage mechanisms.

4.2.2.2. Seismic Resilience Indicator Assessment

Based on the evaluation method of building seismic performance using full probability theory, the calculation methods for measurement standards such as repair costs, repair time, casualties, and environmental impact are clarified. The seismic resilience levels of medical buildings with different prefabrication rates are analyzed. A vulnerability database for precast concrete medical buildings is established. Combined with the three-star resilience grading standard proposed in the "Standard for Seismic Resilience Evaluation of Buildings" (GB/T38591-2020), a seismic resilience indicator evaluation system for precast concrete medical buildings that is compatible with China's seismic fortification standard system is proposed.

4.2.3. Research on Rational Design and Connection Construction

4.2.3.1. Design Optimization for High Prefabrication Rate Structures

Combining the functional requirements and seismic demands of hospital buildings, seismic isolation and vibration reduction techniques that match the medical functions are selected to improve the seismic resilience level of medical buildings. The dimensions and shapes of precast components are optimized to enhance their load-bearing and deformation capacities. Considering the overall requirements of the structure, the cast-in-place parts are reasonably arranged to strengthen the collaborative work between precast components and cast-in-place parts.

4.2.3.2. Connection Construction Measures Research

The key parts of the connection nodes in precast medical building structures are determined. Through experimental research and numerical simulation, indicators such as the strength, stiffness, ductility, and energy dissipation capacity of the connection nodes are analyzed. Key factors affecting the seismic performance of high prefabrication rate structures, such as the construction form of connection nodes, dimensions, and shapes of precast components, are analyzed. Rational connection construction design methods and structural optimization measures are proposed, such as increasing constraints on connection nodes and using high-performance connection materials, to ensure the seismic resilience safety of precast medical buildings.

4.3. Research on the Integrity of Precast Concrete Structures

4.3.1. Impact of Connection Nodes on Structural Integrity

This research investigates the influence of connection nodes on the collaborative performance of components during the overall force transmission process of the structure. By establishing comprehensive structural models and simulating the force distribution under various connection node properties, the study quantitatively assesses the extent to which nodes affect the overall structural behavior. Based on these findings, optimized design methods for connection nodes are proposed to enhance the structural integrity and performance of precast concrete structures.

4.3.2. Role and Optimization of Cast-in-Place Concrete Areas

This section examines the impact of the location, size, and construction techniques of cast-in-place concrete areas on the structural integrity of precast concrete buildings. A rational layout scheme for cast-in-place concrete areas is developed, which includes scientifically determining the critical locations, dimensions, reinforcement details, and high-performance cast-in-place concrete materials for post-pour strips. Through the optimization of these cast-in-place concrete areas, the study aims to further improve the overall integrity and seismic performance of precast concrete structures.

4.4. Research on the Impact of Assembly Construction Sequence and Construction Accuracy on Structural Seismic Performance

4.4.1. Impact of Assembly Construction Sequence on Structural Seismic Performance

4.4.1.1. Construction Process Simulation Analysis

Finite element analysis software is utilized to simulate the assembly construction process of precast concrete structures. Structural models that account for the construction sequence are established, with prefabricated components added incrementally in accordance with the actual construction process, and the connection processes between components are simulated. The force states and deformation of the structure under different construction sequences are analyzed, and the redistribution patterns of internal forces and the stability of the structure during the construction process are investigated. Through construction process simulation analysis, a rational assembly construction sequence is determined to ensure the safety of the structure during construction and to provide a foundation for subsequent seismic performance analysis.

4.4.1.2. Long-term Impact of Assembly Construction Sequence on Seismic Performance

The long-term impact of the assembly construction sequence on the seismic performance of the structure after completion is examined. The internal force changes and deformation of the structure during long-term use due to factors such as concrete shrinkage and creep, temperature variations, etc., under different construction sequences are analyzed. Long-term monitoring and numerical simulation are employed to assess the long-term impact of the assembly construction sequence on the seismic performance of the structure, providing a basis for the development of rational construction plans to ensure good seismic performance throughout the structure's lifecycle.

4.4.2. Potential Impact of Construction Accuracy on Structural Seismic Performance

4.4.2.1. Determination of Construction Accuracy Indicators and Monitoring Methods

Construction accuracy indicators that affect the seismic performance of precast concrete structures, such as dimensional deviations of prefabricated components, installation position deviations, and construction accuracy of connection nodes, are identified. Effective real-time monitoring methods for construction accuracy indicators based on detection techniques such as ultrasonic waves and ground-based synthetic aperture radar (GB-SAR) are proposed to ensure precision control during the construction process. A construction accuracy database is established to record various accuracy indicator data during construction.

4.4.2.2. Impact Analysis of Construction Accuracy on Structural Seismic Performance

The impact of construction accuracy deviations on structural seismic performance is analyzed through experimental research and numerical simulation. Structural models considering construction accuracy deviations are established to simulate the force performance and failure modes of the structure under seismic actions under different accuracy deviation conditions. The influence patterns of construction accuracy deviations on seismic performance indicators such as displacement, internal forces, and inter-story drift angle of the structure are studied, and the potential risks of construction accuracy to structural seismic performance are assessed.

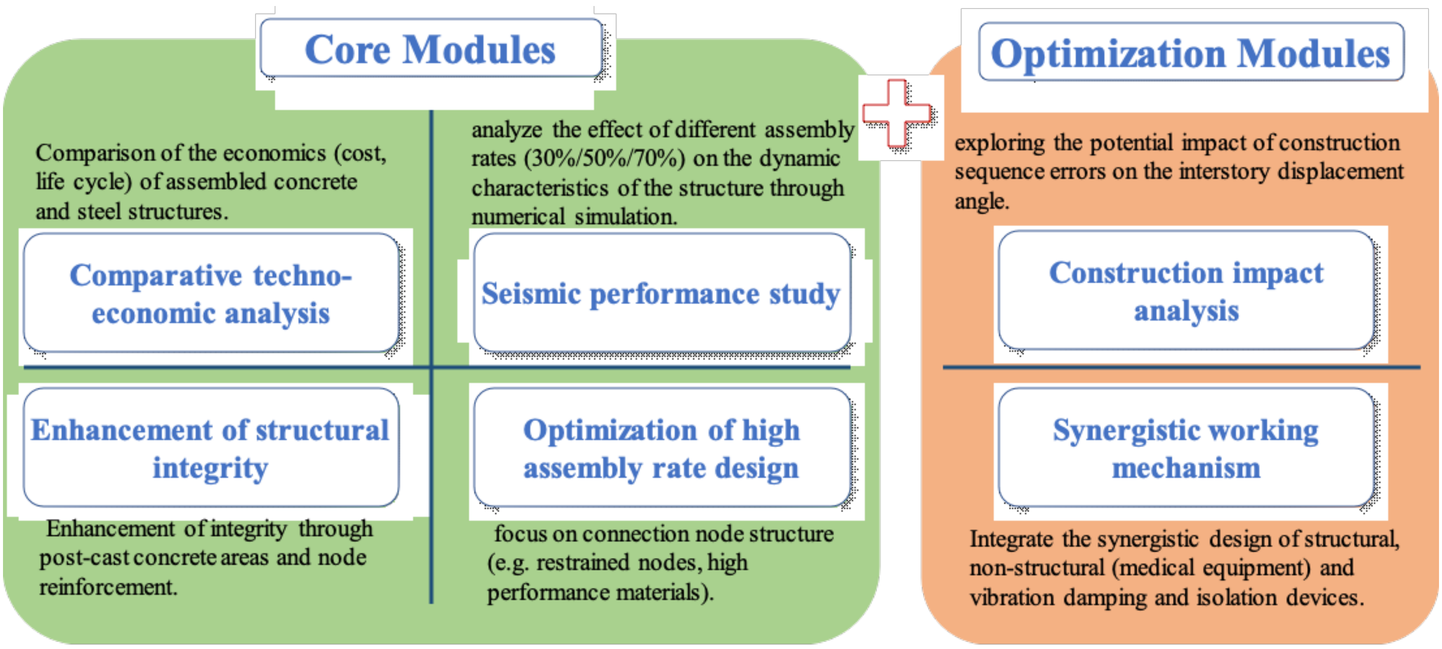

Figure 2 | Path to Improved Toughness Performance in Medical Buildings

4.5. Research on the Synergy of Concrete Structures and Seismic, Isolation, and Damping Devices

4.5.1. Research on the Synergy of Seismic, Isolation, and Damping Devices

This research focuses on the synergistic working mechanisms of seismic, isolation, and damping devices tailored to the functional demands of medical buildings. Through theoretical analysis, experimental testing, and numerical simulation, mechanical models for seismic isolation bearings (such as natural rubber bearings and lead-rubber bearings) and damping devices (such as viscous dampers and metallic dampers) are established. The study identifies key factors influencing the seismic control effectiveness of different devices and clarifies their mechanical characteristics under various loading conditions. A collaborative design method for precast medical building structures and seismic isolation and damping devices is proposed to enhance the overall seismic performance.

4.5.2. Research on the Synergy of Structural and Non-Structural Components

Based on the seismic and functional requirements of medical buildings, a performance-based collaborative design approach is adopted, fully considering the role and impact of non-structural components. The research explores the working synergy between non-structural and structural components, aiming to ensure the normal functionality of medical buildings under moderate seismic actions, with no impact on structural deformation and equipment operation. Under severe seismic actions, the structure should remain essentially intact, and the devices should effectively dissipate energy to ensure the continuation of medical services. Clear design parameter requirements for structures and devices under different performance targets are established, and a collaborative design process for precast structures and seismic isolation and damping devices is developed to provide specific design methods and recommendations for practitioners.

1. Chen G Y. Application Research on Viscous Fluid Dampers of a Medical Building in High Intensity Area [D]. Advisor: Zhang X Z; Li G T. North China University of Water Resources and Electric Power, 2022. DOI: 10.27144/d.cnki.ghbsc.2022.000305
2. Qingle Cheng, Linlin Xie, Zhencong Wang, Zixuan Liu, Xinzheng Lu, Xinyu Wang. Multilevel assessment method for post-earthquake functionality of medical buildings considering component–department–floor interdependencies[J].Reliability Engineering and System Safety, 2024, 251.
3. Pan Y, Peng X, Wang T, Shang Q, Wang T. Seismic damage investigation and analysis of hospital buildings in Ms 6.8 Luding earthquake [J]. Journal of Building Structures, 2024,45(05):14-29. DOI:10.14006/j.jzjgxb.2022.0853.
4. Meng J L. Study on Seismic Toughness Evaluation and Planning of Urban Medical System [D]. Advisor: Ma D H. Beijing University of Technology, 2020. DOI: 10.26935/d.cnki.gbjgu.2020.000123
5. An X Y. Seismic resilience assessment of medical buildings based on discrete event simulation [D]. Advisor: Wang T. Institute of Engineering Mechanics, China Earthquake Administration, 2023. DOI: 0.27490/d.cnki.ggjgy.2023.000089
6. Wu W. Study on The Seismic Resilience of RC medicalFrame buildings with Different SeismicFortification Levels [D]. Advisor: Zhang Y T. Huazhong University of Science and Technology, 2020. DOI: 10.27157/d.cnki.ghzku.2020.000452
7. Tao Q. Post-Earthquake Functionality Recovery Process Simulation andResilience Assessment for Urban Residential Communities [D]. Advisor: He Z. Dalian University of Technology, 2021. DOI: 10.26991/d.cnki.gdllu.2021.004751
8. Li A Q, Chen M, Zeng D M, Xie L L, Chen Y. Seismic Behavior Improvement of an Existing RC Frame Medical Building Based on Seismic Isolation and Energy Dissipation Technique [J]. Industrial Construction, 2019, 49(05): 184-188. DOI: 10.13204/j.-gyjz201905032
9. Lu J M. An High-efficiency Assessment Method for Seismic Resilience of Seismically Isolated Medical Buildings Considering the Vulnerability of Flexible Pipes [D]. Advisor: Li A Q; Xie L L; Liu X M. Beijing University of Civil Engineering and Architecture, 2020. DOI: 10.26943/d.cnki.gbjzc.2020.000380
10. Lu S. Aseismic Performance Improvement and Economic Analysis in Existing Medical Buildings [D]. Advisor: Li A Q; Zhang S L. Southeast University, 2018.
11. Qingle Cheng,Zixuan Liu,Linlin Xie,Zhencong Wang,Xinyu Wang. Post-earthquake medical functionality assessment methods and enhancement strategies for hospital inpatient buildings[J].International Journal of Disaster Risk Reduction,2024,110. DOI: 10.1016/j.ijdrr.2024.104639
12. Cheng Q , Xie L , Wang Z ,et al.BIM-based method for post-earthquake medical functionality assessment of hospital departments considering functional coupling[J].Journal of Building Engineering, 2024, 83. DOI: 10.1016/j.jobe.2023.108339
13. Ning X Q. Research on seismic safety and resilience evaluation methods for important buildings[J]. International Seismic Dynamics, 2019, (12): 73-74.
14. Zhai C H, Song Z R, Xie L L. A approach for seismic resilience design of buildings [J]. Journal of Building Structures, 2025, 46(01): 124-133. DOI: 10.14006/j.jzjgxb.2024.0038
15. Meng J L. Study on Seismic Toughness Evaluation and Planning of Urban Medical System [D]. Advisor: Ma D H. Beijing University of Technology, 2020. DOI: 10.26935/d.cnki.gbjgu.2020.000123
16. Kasai S. Research on the Effect of SpatialCombination of Emergency Departmenton Treatment Efficiency [D]. Advisor: Fang D P. Tsinghua University, 2016.

Funds

1. Industry-University Cooperation Collaborative Education Program, Ministry of Education (231100899210024), China.
2. BUCEA Postgraduate Education and Teaching Quality Improvement Project (J2025016), China.

Call for Papers

The Journal of Sustainable Built Environment (JSBE) invites researchers, scholars, and practitioners to submit original, high-quality research articles for publication. As a peer-reviewed, open-access academic journal, JSBE is committed to advancing interdisciplinary research and fostering innovative solutions for sustainable development across the built environment.

We welcome submissions that explore diverse aspects of sustainable development, including but not limited to:

Scope of the Journal

JSBE seeks contributions across a broad spectrum of topics in the social sciences, emphasizing interdisciplinary perspectives and global relevance. The journal welcomes submissions in areas including, but not limited to:

- **Built Environment and Infrastructure:**
  - Sustainable design, construction, and operation of buildings
  - Green building certification systems and resilient urban infrastructure
  - Integration of natural and built environments, including landscape planning
- **Urban and Regional Planning:**
  - Sustainable urbanization and rural-urban linkages
  - Compact city development and mitigation of urban sprawl
  - Sustainable spatial planning and land use
- **Transportation and Mobility:**
  - Energy-efficient and sustainable transportation systems
  - Promotion of public transit and active transportation
  - Sustainable urban freight and logistics planning
- **Environmental and Energy Systems:**
  - Renewable energy systems in the built environment
  - Climate change adaptation and mitigation strategies
  - Air quality management and sustainable ecosystems
- **Governance, Policy, and Economics:**
  - Institutional frameworks for sustainability
  - Stakeholder engagement and participatory urban governance
  - Financing mechanisms for sustainable development
- **Society and Communities:**
  - Social inclusion, equity, and resilience strategies
  - Community-driven sustainability approaches

- Cultural and historical preservation in urban planning

- **Emerging Technologies and Methodologies:**
  - Role of digital technologies in sustainable cities
  - Artificial intelligence, IoT, and big data applications in urban systems
  - Innovative research methodologies for sustainability analysis

We particularly value interdisciplinary perspectives that bridge architecture, urban planning, engineering, environmental sciences, public policy, and social sciences, offering holistic views on sustainable development.

Types of Submissions

- **Full-length Research Articles (6,000–9,000 words):** Original research or theoretical advancements.
- **Review Articles (5,000–8,000 words):** Comprehensive reviews and critical assessments of current literature.
- **Case Studies (4,000–6,000 words):** Analysis of specific projects or urban sustainability practices.
- **Viewpoints (1,500–2,000 words):** Short articles offering commentary or proposing new ideas.

**Note: Translations of articles originally published in another language will not be considered.*

Open Access and Peer Review

JSBE is committed to the principles of open access, ensuring all published research is freely available to readers worldwide. Articles undergo a rigorous double-anonymous peer review process to maintain academic integrity, objectivity, and fairness.

Submission Guidelines

Manuscripts must adhere to the Author Guidelines and be prepared in Microsoft Word or PDF format. Detailed formatting instructions are available on the journal's website. Submissions should be made via the online portal at: https://press.jandoo.ac/journals/jsbe. For inquiries, please contact the JSBE editorial team at **E-mail (**editorialoffice.jsbe@press.jandoo.ac).

Submission Deadline

Submissions are accepted on a rolling basis, ensuring timely review and publication.

We look forward to receiving your contributions and engaging in a shared effort to advance the field of social sciences.

Journal of Sustainable Built Environment (JSBE) is an interdisciplinary, fully open-access academic journal that publishes peer-reviewed original research articles, review papers, and case studies exclusively in English on sustainability issues in urban and regional development.

JSBE offers a platform for scholars, policymakers, and practitioners to exchange ideas and tackle the complex challenges facing built environments in a rapidly evolving world.

JOURNAL OF SUSTAINABLE BUILT ENVIRONMENT
VOLUME 2, NUMBER 2
(MARCH 2025)

Address:
1-53-13, Nishigahara
Kita City, Tokyo
114-0024
Japan

Tel: +81 (0)80-8515-9423

E-mail: editorialoffice.jgtss@press.jandoo.ac

Offical website: https://press.jandoo.ac/journals/jgtss

9 772759 731009